Energy System for a Data Center with 100% Hourly Renewable Utilization

A Techno-Economic and Environmental Impact Analysis

MSc SET Thesis project EEMCS

Carlo Truffino

Delft University of Technology

TU Delft

Energy System for a Data Center with 100% Hourly Renewable Utilization

A Techno-Economic and Environmental Impact Analysis

by

Carlo Truffino

Student Name	Student Number
Carlo Truffino	4692462

First Supervisor (University):	Prof.dr.ir. M.A. (Machteld) van den Broek
Second Supervisor (University):	Prof.dr. F.M. (Fokko) Mulder
Daily Supervisor (Company):	Jeroen Jansen
Project Duration:	November, 2023 - July, 2024
Faculty:	Faculty Electrical Engineering, Mathematics and Computer Science, Delft

TU Delft

Preface

This thesis was written by Carlo Truffino as part of my Master's program in Sustainable Energy Technology at the Faculty of Electrical Engineering, Mathematics & Computer Science, Delft University of Technology, Netherlands. The research focuses on finding the most cost-effective and feasible sustainable energy solutions for data centers, aiming to reduce carbon emissions.

I completed this thesis in collaboration with Repowered, where Jeroen Jansen was my daily supervisor during the research. I am deeply grateful to Repowered, and especially to Jeroen, for their excellent support and guidance throughout the project. Their expertise and resources were vulnerable to successfully completing this research.

I would also like to thank my primary supervisor, Prof. Dr. Ir. Machteld van den Broek, for her valuable feedback and continuous help during my research. Additionally, I am very thankful to my second supervisor, Prof. Dr. Fokko Mulder, for his feedback and input during the important meetings.

Personally, this journey has been both challenging and rewarding. It has improved my understanding of sustainable energy technologies and strengthened my commitment to making a positive impact in this field. I am excited about the potential applications of this research and hope it will serve as a foundation for further advancements.

This work was carried out from November 2023 to July 2024. I appreciate all the support and resources the Technical University of Delft and the Repowered provided.

Carlo Truffino
Delft, July 2024

Summary

The Paris Agreement aims to limit global warming to 2 degrees Celsius by reducing carbon dioxide emissions. Data centers are essential to the digital world and contribute approximately 1% to global electricity consumption. Major tech companies like Amazon, Microsoft, Google, and Meta are large contributors to this consumption. In countries like the Netherlands, this contribution is higher due to the Netherlands being a digital hub, accounting for 3% of the total national electricity consumption. Considering their significant energy usage, it is interesting to research how data centers can transition to using only renewable energy sources on an hourly basis so they can decrease their footprint.

This thesis aims to identify a feasible and cost-effective configuration for a 100 MW data center that operates 100% on renewable energy on an hourly basis. The research will assess the environmental impacts, focusing on CO_2 emissions (CO_2e) and land usage, with the main goal of achieving the lowest Levelized Cost of Electricity (LCOE).

First, an overview of potential energy storage technologies is provided to find suitable solutions. Based on different criteria, Lithium-ion (Li-ion), lead-acid, vanadium redox flow batteries (VRFB), zinc-bromide flow batteries (ZBFB), alkaline and PEM (proton exchange membrane) electrolyzers, storage tanks, and PEM fuel cells are chosen. With these technologies, eight different configurations are composed, combining various battery types and electrolyzer types with the storage tank and PEM fuel cell: Li-ion with alkaline (1), lead-acid with alkaline (2), Li-ion with PEM (3), lead-acid with PEM (4), VRFB with alkaline (5), ZBFB with alkaline (6), VRFB with PEM (7), and ZBFB with PEM (8).

An energy model is developed to identify the most feasible and cost-effective solution, using solar, wind, and load profiles as input. The assets are modeled based on their technical parameters and limitations. A 10-year simulation of the hourly energy flows is executed. In this simulation, the constraints, degradation, and replacement of the assets are taken into account. The costs are determined based on Capital Expenditures (CAPEX), Operating Expenses (OPEX), replacement costs, and residual costs of the asset after 10-year. The connection costs are also considered. The configuration dimensions are optimized based on the LCOE using the particle swarm optimization method. The two configurations with the lowest LCOE are evaluated for environmental impacts, including CO_2e and land usage.

The study shows that combining a Li-ion battery or VRFB with an alkaline electrolyzer is the most cost-effective and feasible configuration for a data center. The LCOE is 0.243 and 0.241 €/kWh, respectively. Additionally, this reduces kg CO_2e/kWh by 7-8 times compared to the current grid emissions in the Netherlands, which are approximately 0.037 and 0.032 kg CO_2e/kWh. However, the required land usage is approximately 20 km², and the LCOE of the configuration is about 2.5 times higher than the current power purchase agreement (PPA) price for a data center, which is 0.10 €/kWh.

Therefore, it is recommended to initially start with an 80% renewable scenario using only a Li-ion battery and renewable energy sources. This approach reduces the LCOE to 0.12 €/kWh, which is approximately the same as the current PPA price if an additional 0.01 €/kWh for the connection to the grid is included. Furthermore, kg CO_2e/kWh is three times lower compared to the current situation, which is 0.08 kg CO_2e/kWh. This strategy also mitigates the potential risks associated with the infancy of VRFB and the combination of intermittent renewable sources and an electrolyzer, as these are excluded in this scenario.

Contents

List of Figures

List of Tables

Nomenclature

Abbreviations

AEM	Anion Exchange Membrane
BMS	Battery Management System
BOP	Balance of Plant
CAES	Compressed Air Energy Storage
CAPEX	Capital Expenditure
CBS	Centraal Bureau voor de Statistiek
CO2	Carbon Dioxide
CRF	Capital Recovery Factor
DATAZERO	Data Center with Zero Carbon Emission
DC	Direct Current
EOL	End of Life
ESS	Energy Storage System
FC	Fuel Cell
FES	Flywheel Energy Storage
GA	Genetic Algorithm
GW	Gigawatt
GWP	Global Warming Potential
HHV	Higher Heating Value
IEA	International Energy Agency
IEEE	Institute of Electrical and Electronics Engineers
LCA	Life Cycle Assessment
LCOE	Levelized Cost of Electricity
LFP	Lithium Iron Phosphate
LHV	Lower Heating Value
NAS	Sodium-Sulfur
NMC	Nickel Manganese Cobalt
NREL	National Renewable Energy Laboratory
OPEX	Operational Expenditure
PB	Lead
PCM	Phase Change Material
PEM	Proton Exchange Membrane
PEMFC	Proton Exchange Membrane Fuel Cell
PHES	Pumped Hydro Energy Storage
PP	Power Plant
PPA	Power Purchase Agreement
PSO	Particle Swarm Optimization
PV	Photovoltaic
RES	Renewable Energy System
RFB	Redox Flow Battery
SC	Supercapacitor
SET	Sustainable Energy Technology
SMES	Superconducting Magnetic Energy Storage
SOC	State of Charge
ST	Solar Thermal
STES	Seasonal Thermal Energy Storage
TCS	Thermo-Chemical Storage
TES	Thermal Energy Storage
TRL	Technology Readiness Level
VRFB	Vanadium Redox Flow Battery
ZBFB	Zinc-Bromine Flow Battery

Symbols

Symbol	Description	Unit
C	capacity	[kWh]
C_{invest}	Investment cost	[€/kW]
$C_{O\&M}$	Operation and maintenance cost	[€/kW]
$C_{\text{replacement}}$	Replacement cost	[€/kW]
$E_{\text{char,max}}$	Maximum energy that can be charged into the battery at time	[kWh]
$E_{\text{char,avail}}$	Available energy for storage in the battery	[kWh]
E_{charge}	Energy available for charging the battery from renewable sources	[kWh]
$E_{\text{disc,max}}$	Maximum energy that can be discharged from the battery	[kWh]
$E_{\text{disc,avail}}$	Available energy for discharge from the battery	[kWh]
E_{disc}	Energy required to meet demand	[kWh]
E_{in}	Energy input into the battery	[kWh]
E_{out}	Energy output from the battery	[kWh]
L_{system}	System lifetime	[years]
L_{project}	Project duration	[years]
P_{battery}	Power supplied or absorbed by the battery	[kW]
$P_{\text{char,max}}$	Maximum charging power of the battery	[kW]
$P_{\text{disc,max}}$	Maximum discharging power of the battery	[kW]
$P_{\text{el,max}}$	Maximum operational power of the electrolyzer	[kW]
$P_{\text{el,min}}$	Minimum operational power of the electrolyzer	[kW]
$P_{\text{fc,max}}$	Maximum operational power of the fuel cell	[kW]
$P_{\text{fc,min}}$	Minimum operational power of the fuel cell	[kW]
P_{gen}	Power generated from renewable sources	[kW]
P_{load}	Power load of the data center	[kW]
$P_{\text{installed}}$	Installed capacity	[kW]
$P_{\text{compressor}}$	Power used by the hydrogen compressor	[kW]
r	Discount rate	[-]
Δt	Time step	[hours]
η_{charge}	Charging efficiency of the battery	[%]
η_{disc}	Discharging efficiency of the battery	[%]
η_{el}	Efficiency of the electrolyzer	[%]
η_{fc}	Efficiency of the fuel cell	[%]
$\eta_{\text{degradation}}$	Degradation rate of efficiency	[%]
m_{H2}	Mass of hydrogen produced	[kg]
HHV_{H2}	Higher heating value of hydrogen	[kWh/kg]
LHV_{H2}	Lower heating value of hydrogen	[kWh/kg]
SoC_{max}	Maximum state of charge of the battery	[%]
SoC_{min}	Minimum state of charge of the battery	[%]
V	Velocity	[m/s]
ρ	Density	[kg/m^3]

1

Introduction

The Paris Agreement, approved by 196 parties at COP21 in Paris on December 12, 2015, and effective from November 4, 2016, aims to limit global warming to 2 degrees Celsius to reduce climate change risks as highlighted by the Intergovernmental Panel on Climate Change [1]. This commitment addresses the acute need to counteract the rapid increase in carbon dioxide (CO_2) emissions, which reached 410 million tonnes in 2023 Globally [2]. The increase in CO_2 emissions is primarily due to industrialization, which heavily relies on fossil fuels and energy consumption. To reach the goal of the Paris Agreement, international collaboration across industry, transportation, and energy sectors is essential. The Agreement emphasizes adopting sustainable solutions and reducing emissions to secure the planet's future [3]. Data centers, which are important in our increasingly digitalized world, are a prime example. Despite their importance, the environmental impact of these centers is becoming a growing concern. The International Energy Agency (IEA) reported that data centers were responsible for approximately 1% of global electricity consumption in 2022 [4]. While 1% may seem like a small fraction, it represents a considerable amount. The electricity requirement for data centers is estimated to expand from 290 terawatt-hours (TWh) in 2022 to approximately 321 TWh by 2030 [4][5]. This consumption growth is primarily attributed to the rapid expansion of digital services. Key drivers are the rising reliance on cloud computing, the importance of big data analytics, and Internet of Things utilization. As these technologies become increasingly integral to daily life and business processes, the largest technology companies, such as Amazon, Microsoft, Google, and Meta, have become large contributors to global electricity consumption. For example, between 2017 and 2021, their combined electricity usage more than doubled, reaching approximately 72 TWh in 2021 [4]. For countries like the Netherlands, which serve as digital hubs, the increase in electricity consumption is even more pronounced. According to a report by the Centraal Bureau voor de Statistiek (CBS), data centers in the Netherlands consumed 1.65 TWh of electricity from the public grid in 2017 [6]. By 2021, this consumption had more than doubled, reaching 3.73 TWh. The report also showed that these data centers accounted for 3.3% of the total national electricity consumption in the Netherlands. The CBS based its findings on data provided by network operators.

There are multiple solutions for decreasing the energy consumption of data centers and increasing their reliance on renewable energy. The first approach focuses on minimizing energy consumption and maximizing efficiency to make data centers more environmentally sustainable. There are three strategies for improving the energy use of renewables. Firstly, technological advancements in specialized scheduling algorithms can reduce energy usage by 5% to 25%, thereby decreasing CO2 emissions and contributing to climate goals [7]. Secondly, the GreenSlot system, which increases renewable energy consumption and reduces reliance on non-renewable sources, predicts the upcoming availability of solar energy and schedules tasks to maximize the use of renewable energy while meeting job deadlines. Additionally, the GreenSlot system helps to reduce associated costs [8]. Thirdly, Crisan et al. presents a method to align data center energy use with local renewable energy availability. This method includes adjustments in electrical cooling systems, IT workloads, and energy storage [9]. Despite advancements in efficiency and scheduling leading to decreased energy

consumption in individual data centers, overall energy consumption in the sector has increased in recent years due to the growing demand for data centers.

The second approach focuses on contracts to increase the use of renewable energy. One of the most common methods to achieve this is through Power Purchase Agreements (PPAs). A PPA is a contract between a producer and a consumer, where the consumer agrees to buy electricity directly from the producer, often at predetermined prices, and typically involving renewable energy sources. In 2017, Google achieved a milestone by matching its annual electricity usage with an equivalent amount of renewable energy through a PPA [10]. Companies like Google claim to be fully powered by green sources. However, this does not mean that they use renewable energy exclusively. These companies utilize PPAs to contract an amount of renewable energy equivalent to their yearly electricity use. Because the consumption and purchase are balanced annually through the contract, they can claim to be 100% renewable. For example, during daylight hours, more solar power is often generated than needed, which is then sold back to the grid. At night, they purchase electricity from the traditional power grid, which may include fossil-fuel-generated electricity [11]. This system does not completely eliminate the use of electricity generated from fossil fuels. Therefore, while PPAs are a good step towards sustainable energy, they do not entirely eliminate reliance on fossil fuels [12].

In line with this, the Long Duration Energy Storage (LDES) Council report focuses on 24/7 clean energy power purchase agreements. It highlights that these PPAs are an improvement over traditional models. The traditional ”pay-as-produced” model, where energy is purchased as it is produced, often relies on fossil fuels for backup. In contrast, current PPAs, as described in the section above, achieve only 40 to 70 percent decarbonization of electricity consumption and expose buyers to market risks due to the variability of renewable energy sources. The report underscores the need for new PPA structures that provide more reliable clean energy. For example, PPAs could be structured to level energy consumption on a monthly or daily basis, which would necessitate the use of energy storage solutions. This approach would enhance the transition to a fully decarbonized energy grid [13].

In response to the challenges of energy consumption and renewable integration in data centers, various research groups and studies have explored multiple solutions.

Firstly, the DATAZERO research group, led by Pierson et al., has been dedicated to researching data centers that operate on renewable energy sources such as solar energy and wind energy. The research group also focuses on integrating energy storage solutions like batteries and hydrogen, alongside optimizing IT and energy management algorithms to adjust to energy supply and demand changes [14]. However, their research lacks details on the cost of storage solutions, their sizes, and capacities, which are essential for assessing economic viability and scalability [14].

Multiple studies have focused on the size and energy requirements of a combination of hydrogen, wind, solar energy, and batteries to address these gaps. For instance, a study by Haddad, Nicod, and Marion-Péra within the DATAZERO project calculates the specific energy requirements for a data center and 10 hybrid cars, emphasizing the important role of hydrogen for the data center’s power supply, as well as the necessary hydrogen storage and the utilization of solar and wind energy [15].

Furthermore, another paper by Haddad et al. explores the combination of wind turbines, solar panels, batteries, and hydrogen to achieve 100% reliance on renewable energy through simulation. However, this study does not account for the impact of aging on storage capacities or the associated costs of the system [16].

Additionally, Rostirolla et al. highlights the role of batteries for short-term energy needs and hydrogen for long-term storage, despite the high costs associated with these storage solutions [17].

Moreover, a paper by Iverson et al. focuses on optimizing the size of a hybrid power system incorporating wind, solar, and hydrogen to minimize energy costs and prevent power shortages. This paper demonstrates that a substantial portion of the total cost of the energy system is attributed to the hydrogen system, suggesting that integrating batteries could reduce overall expenses [18].

Furthermore, some studies focus on the costs and use of solar energy and batteries, emphasizing sizing and energy needs. For example, in the report by Vasconcelos et al., the research focuses on reducing a data center’s carbon footprint. This is performed by combining solar panels for electricity generation and batteries for storage, analyzing yearly weather patterns and energy needs. This study provides precise

sizing for solar panels and batteries and concludes that the best way to minimize carbon emissions is by using a hybrid approach that combines solar panels and batteries with conventional electricity from the grid. It also highlights that solar panels and batteries contribute to carbon emissions [19].

Lastly, an economic analysis by Gnibga, Blavette, and Orgerie of an energy storage system consisting of photovoltaic panels, lithium-ion batteries, solid polymer electrolyzers, and PEM fuel cells assesses the costs and economic feasibility of 100% renewable data centers across various sizes and workload types [20].

Research Question

The existing literature shows substantial research on renewable energy solutions for data centers. It is suggested that battery-hydrogen solutions could be a feasible option for achieving 100% renewable energy on an hourly basis. However, while most studies describe the operational aspects of these energy systems, only the work of Vasconcelos et al. provides a comprehensive analysis of a renewable battery-hydrogen system, and only Iverson et al. offers a detailed cost analysis of a hydrogen system.

To build on this foundation, it would be beneficial to model various technical configurations and evaluate them based on the Levelized Cost of Electricity (LCOE) to facilitate comparison. Additionally, assessing the carbon footprint of these configurations is essential, particularly since [19] highlights the carbon emissions associated with solar panels and batteries. Addressing these aspects makes it easier to understand the feasibility and environmental impact of battery-hydrogen solutions for data centers.

Therefore, the objective of this thesis is to identify a feasible and cost-effective configuration for a 100 MW data center that utilizes 100% renewable energy on an hourly basis and evaluate the associated environmental impacts in terms of CO_2 emissions from production and land use requirements of the selected configuration. The cost-effective configuration is defined as one that achieves the LCOE.

Main Question:

What is the most feasible and cost-effective configuration for an energy system that enables a data center to utilize 100% renewable energy on an hourly basis, and what are the associated environmental impacts in terms of CO_2 emissions from production and land use requirements?

This research question is answered through a case study in the Netherlands. In the Netherlands, the high costs associated with connecting to the energy grid present a considerable challenge [21][22][23], a detail not covered in the existing literature. This highlights an interesting gap in researching the economic feasibility of scaling data centers to 100 MW to achieve 100% renewable energy utilization on an hourly basis. Furthermore, existing literature often describes battery-hydrogen systems as a feasible solution for making data centers 100% renewable on an hourly basis.

To answer the main question, five sub-questions are comprised. The first sub-question concerns researching which assets are suitable for the data center. The second involves assessing the possible configurations between these assets. The third and fourth sub-questions determine the dimensions of the most feasible and cost-effective configurations and the LCOE. Lastly, based on the most cost-effective and feasible configuration, an environmental impact assessment focuses on CO_2 emissions and land usage. An overview of the five sub-questions is shown below.

Subquestions:

1. Which energy system assets are most suitable for a 100 MW data center in the Netherlands?
2. What are the possible configurations for the storage system of a data center?
3. What are the feasible and most cost-effective dimensions of the system assets, considering a 100 MW data center?
4. What is the Levelized Cost of Electricity when integrating these energy systems assets into the energy system of the 100 MW data center?
5. What is the environmental impact of the cost-effective configurations in terms of emission of CO_2 and the land use requirement?

2

Methodology

In this chapter, the methodology of this research is described to answer the research questions and subquestions. First, an overview of the methodology is provided in section 2.1. Then, the criteria for storage technologies are detailed in section 2.2. Next, the model of the energy system and the formulas used in the model are shown in section 2.3 and section 2.4. The optimization method, objective functions, calculations, variables, and constraints are then explained in section 2.5, followed by the methodology of the economic analysis in section 2.6. Lastly, the methodology of the environmental assessment for CO_2 emissions and land usage is described in section 2.7.

2.1. Overview of Methodology

This section provides an overview of the methodology, which is structured into seven steps to answer the described research questions. These steps show a systematic approach to identifying the storage components and optimizing the dimension of energy storage solutions for a data center's energy system, which consists of renewable energy sources combined with various energy storage technologies. This structured approach provides an overview of the method process, resulting in the selection of the most cost-effective and feasible configurations for a 100 MW data center that is 100% renewable on an hourly basis. In Figure 2.1 is an overview of the corresponding steps provided.

1. **Criteria for Technology Selection:** The first step is determining and describing the criteria for selecting suitable energy storage technologies. The six important criteria are scalability, response time, self-discharge, (dis)charge at rated capacity, technology maturity (Technology Readiness Level), and location independence. These criteria are important for selecting suitable technologies for the data center. In section 2.2, the different criteria are described.
2. **Overview of Energy Storage Technologies:** The second step provides an overview of the main energy storage technologies, including mechanical, electrochemical, electrical, and chemical storage methods. This gives insight into possible solutions for the energy system. After a short introduction to the classification of storage technologies, multiple technologies are described for each classification. The technologies are described based on the criteria mentioned in the previous step. The overview and the classification of different technologies are described in section 3.1 and section 3.2.
3. **Technology Selection and Configuration:** In the third step, when all the technologies are described, they are selected based on the criteria mentioned in the previous steps. During the selection, a combination of different storage types, including short-term and long-term storage, is taken into account. Based on this selection, configurations are then comprised of suitable technologies. In section 3.3, the selection of the technology is shown, and in section 3.4, an overview of the configuration is provided. The most suitable configuration for a data center can be determined from these different configurations.
4. **Data Collection:** The fourth step is data collection. For the energy model, data on solar and wind profiles need to be collected. These profiles are used as energy input in the model. Additionally,

load profiles of a data center need to be collected. Based on this profile, the output of the energy model can be determined. The collected data of the solar, wind, and load profiles are adjusted for the model. The solar and wind profiles are normalized to a 1 kW installed capacity profile, and the load is extrapolated to 100 MW. In section 3.5 are the energy profiles shown. For the technologies in the configuration, now referred to as the assets, technical and economic parameters need to be collected. The technical parameters are needed to model the performance, behaviors, and constraints of the assets. Economic parameters are needed to calculate the costs associated with the assets. Overviews of the collected technical and economic parameters are shown in section 3.6 and section 3.7. Additionally, data on the CO_2 emissions from cradle to grave of the technologies are collected and determined. The CO_2 emissions per installed capacity are determined for these technologies. Moreover, the land usage requirement is determined based on the dimensions of existing projects. The land usage requirement is specified per installed capacity, similar to the CO_2 emissions. The CO_2 emissions and land usage requirements provide insights into the impact of building a large storage system on the environment and land usage. The collected data is shown in section 3.8 and in section 3.9 CO_2

5. **Development of the Energy Model:** In step five, the model is created. This model is developed using Python. First, all the assets are modeled and developed separately. Each asset has different operational modes, and all modes need to be varied. Once the assets and their functions are varied, the assets are combined to form an energy system. A decision tree determines when assets need to be in specific operational modes. After modeling the system, a 10-year simulation of the data center is executed. By executing a 10-year simulation, the degradation of the assets can be analyzed, and replacements are included when their performance falls below a certain threshold. After the complete system is modeled, a cost model is created to calculate the system's costs, considering the dimensions of the assets, the replacements during the 10-year simulation, and the remaining lifetime to calculate the residual costs. The costs are determined using parameters such as CAPEX, OPEX, replacement costs, and asset lifetime. The methodology for modeling the assets is detailed in section 2.4.
6. **Optimization:** In step six, if all the data is collected and the model of the energy flow is completed, the system is optimized. The system's dimensions are optimized based on LCOE. First, the cost needs to be modeled. This is done in section 2.5. This section shows how the cost of the system is calculated based on CAPEX, OPEX, and the replacement cost of the assets. Also, the residual costs of the assets are considered after the 10-year simulation. During the optimization, the dimensions of the assets are variable. This optimization determines the most cost-effective and feasible dimensions of the assets required to achieve 100% renewable energy on an hourly basis throughout the 10-year simulation.
7. **Results and Analysis:** In the last step, the optimization outcomes are analyzed in chapter 4. Then, the performance and behavior of the assets in the configuration are analyzed. The two configurations with the lowest LCOE are further evaluated for their environmental impact, including CO_2 emissions and land usage. A sensitivity analysis is executed to investigate the significance of uncertain parameters used in the model. First, the constraint of 100% renewable energy is reduced to see its impact. Then, the energy profile used as input is assessed. Lastly, the impact of the technical and cost parameters is evaluated. Based on these findings, the most suitable techno-economic configuration is selected. This is the configuration with the lowest LCOE and is 100% renewable.

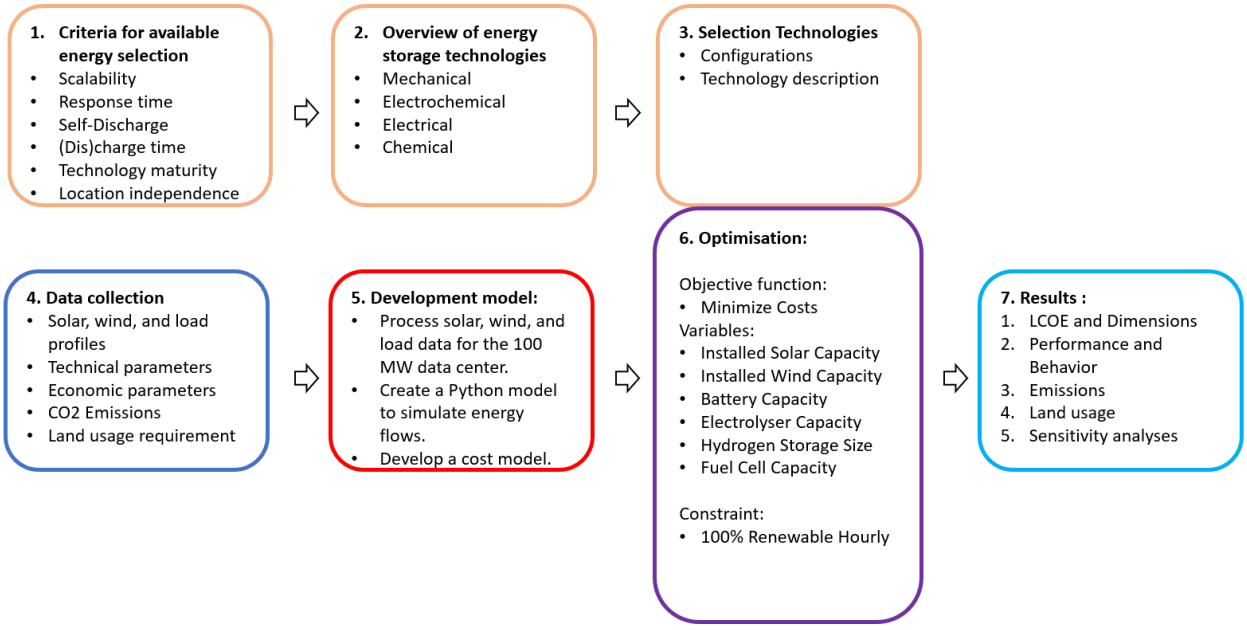

Figure 2.1: Overview of the Methodology

2.2. Criteria for Storage Technology Selection

This section evaluates and outlines the criteria used to select storage technologies for analysis in this research. Multiple criteria have been defined to ensure the technologies.

Scalability

The first criterion is scalability. Scalability is a key factor for storage technology in those configurations. A scalable technology can adjust its size and capacity to meet different needs. This means the system can increase or decrease its size based on the amount of energy it needs to store. This flexibility is important because it allows the technology to adapt to the results from the optimization without being fixed at one size. Additionally, a technology is considered scalable if it can be used at a large scale to meet global demand. Scalability is evaluated on a scale from 1 to 5, where a rating of 5 indicates highly scalable technology, and a rating of 1 indicates that the size is fixed, with no scalability.

Response Time

The second criterion is the response time of the storage systems. The system needs to be 100% renewable on an hourly basis. A quick response time is important to balance the fluctuations of wind and solar energy, enabling the energy system to store excess energy or release it when the data centers need it. In this model, the timestep is one hour, so a maximum response time of 15 minutes is chosen.

Self-Discharge

The third criterion is self-discharge, which refers to the rate at which storage assets lose energy when unused. Some technologies can only store energy for a short term because the energy ”leaks” away. In the energy system, solar and wind energy are the inputs, and any surplus needs to be stored for hours to days to overcome periods with less energy due to unpredictable weather circumstances. When energy is needed during a shortage, the energy in the storage assets needs to still be available. Otherwise, the system’s efficiency will be very low, and much energy will be lost. This means that the dimensions of the assets will need to be much larger. Therefore, the selected technologies should be capable of storing energy for at least several days with minimal discharge.

(Dis)charge time at Rated Capacity

The fourth criterion is the ability to charge and discharge for a long period at the rated capacity. For the energy model to ensure a 100% renewable energy supply, it needs to overcome shortages ranging from

hours to days. Therefore, the selected storage technologies must support long charge and discharge durations to handle fluctuations in energy availability and demand effectively. The discharge time at rated capacity needs to be a minimum of an hour.

Technological Maturity

The fifth criterion assesses the technological maturity and reliability of the storage technologies. Maturity is often indicated by the Technology Readiness Level (TRL), which helps determine the current stage of development of the technology. This ensures that only well-developed and reliable technologies are considered. A high TRL is crucial because it means the parameters of the technology are well understood, and the system can be implemented in the short term [24].

The table below shows the Technology Readiness Level (TRL) scores ranging from 1 to 9, with corresponding descriptions for each level.

Table 2.1: Technology Readiness Level Descriptions for Selection Storage Technologies [25]

TRL	Description
1	Primary principles documented and observed
2	Development of the technology concept and its application.
3	Analytical and experimental validation of crucial functions and/or proof of concept.
4	Validation of components and/or systems in a laboratory environment.
5	Validation of a laboratory-scale, similar system in a relevant environment.
6	Engineering/pilot scale validation of a similar (prototypical) system in a relevant environment.
7	Full-scale demonstration of a similar (prototypical) system in a relevant environment.
8	Actual system completed and qualified through testing and demonstration.
9	Actual system operated across the full range of expected mission conditions.

Location Independence

The last criterion is location independence. Although the case study is based on a data center in the Netherlands, the research should consider whether the optimal configuration could be applied globally, regardless of geographical conditions. Moreover, the Netherlands does not have geographical conditions that are advantageous for different types of storage.

2.3. Model Description of the Energy System

This section first provides an overview of the energy flows between the assets. Then, it describes the decision tree of the assets during a shortage and a surplus of energy.

The data center's energy system consists of energy input from solar and wind sources distributed through the grid. The data center is connected to the grid via a connection with a maximum capacity. Behind this connection lies the energy storage system, which consists of a battery, electrolyzer, fuel cell, and hydrogen tank. If the input from the renewable energy sources is higher than the data center's load, the energy is stored via the battery or electrolyzer. If the data center's load is higher than the input from renewable energy sources, the energy is discharged from the battery or produced by the fuel cell. A simplified overview of this energy system is provided in Figure 2.2.

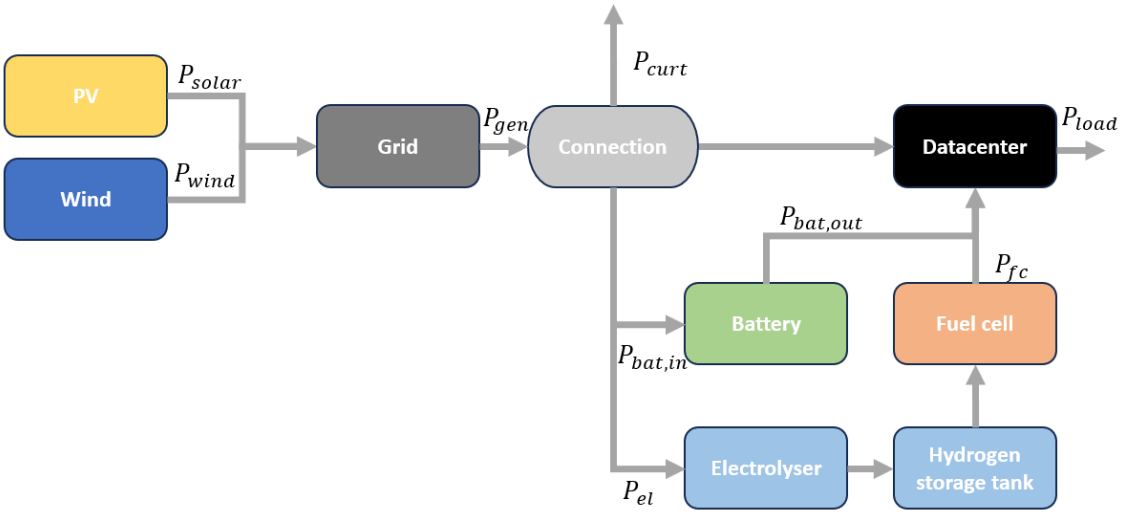

Figure 2.2: Overview of the Energy Flows Between the Assets

A decision tree manages the energy flow between the system's assets, determining when each asset needs to be active to deliver or store energy. First, the step to determine if there is a surplus or a shortage is described. Then, two decision trees are described to handle energy surpluses and shortages to ensure the data center is always powered. First, the decision tree for managing surpluses is described, followed by the decision tree for handling shortages.

Here are the steps shown to determine whether there is a surplus or a shortage, denoted as Δ_1:

1. **Determination of Δ_1**
   (a) **Generation Profile Combination:**
      - Combine the power profiles from solar and wind farms to form the generation profile (P_{gen}).
      - If P_{gen} exceeds the maximum connection capacity (P_{con}), a part of P_{gen} is curtailed:
      - If $P_{gen} > P_{con}$, then $P_{curt} = P_{gen} - P_{con}$ and $P_{gen} = P_{con}$.

   (b) **Power Distribution:**
      - The data center's load (P_{load}) is subtracted from P_{gen}, Δ_1 = P_{gen} -P_{load}
      - If the result is positive, Δ_1 is considered as a surplus and is directed to the energy storage system as outlined in step 2. If the result is negative, Δ_1 is considered as a shortage, and energy is discharged from the energy storage system described in step 3.

2. **Surpluss ($\Delta_1 > 0$)**
   (a) **Battery Charging**:
      - The maximum charging capacity of the battery ($P_{char,max}$) is calculated, as detailed in subsection 2.4.1.
      - If the surplus is less than $P_{char,max}$, all the energy is stored in the batteries.
      - If the surplus exceeds $P_{char,max}$:
        – Batteries are charged at a power input $P_{char,max}$.
        – Δ_2 = Δ_1 - $P_{char,max}$
        – The remaining surplus (Δ_2) is directed to the electrolyzer and storage tank.

(b) **Electrolyzer Operation and Storage Tank:**

- Before starting, the state of charge of the hydrogen tank (SoC) is checked against its maximum capacity (SoC_{max}).
- If SoC is not at its limit:
  - Check if Δ_2 is within the electrolyzer's operational range ($P_{el,min}$ to $P_{el,max}$).
  - If Δ_2 is within this range, hydrogen is produced as detailed in subsection 2.4.2.
  - If $\Delta_2 < P_{el,min}$, then Δ_2 is curtailed.
  - If $\Delta_2 > P_{el,max}$, then $P_{el} = P_{el,max}$ and the excess of Δ_2 is curtailed.
- When SoC reaches the limit SoC_{max}, then the remaining Δ_2 is curtailed.

This energy management process during shortages is shown in Figure 2.3b. The figure describes the step-by-step process of how shortages are managed.

3. **Shortage ($\Delta_1 < 0$)**

(a) **Battery Discharge:**

- First, the batteries are discharged.
- If $|\Delta_1| \leq P_{disc,max}$, the batteries fully balance the shortage.
- If $|\Delta_1| > P_{disc,max}$:
  - The batteries discharge at their maximum capacity ($P_{disc,max}$).
  - Δ_3 = Δ_3 - $P_{disc,max}$
  - The remaining shortage, denoted as Δ_3, is managed by the fuel cell system and storage tank.

(b) **Fuel Cell Operation and Storage Tank:**

- First, the State of Charge of the hydrogen tank (SoC) is checked against its minimum limit (SoC_{min}).
- If $SoC > SoC_{min}$:
  - The fuel cell operates to supply power within its operational range, from its minimum ($P_{fc,min}$) to maximum capacity ($P_{fc,max}$), as detailed in subsection 2.4.4.
  - If Δ_3 is within this range, the fuel cell produces energy to balance the shortage.
  - If $\Delta_3 < P_{fc,min}$:
    - The fuel cell operates at $P_{fc,min}$, generating a small surplus of energy.
    - This surplus energy is directed to charge the batteries.
  - If Δ_3 exceeds $P_{fc,max}$:
    - Additional energy is drawn from the grid to manage the remaining shortage.

This energy management process during shortages is illustrated in Figure 2.3b.

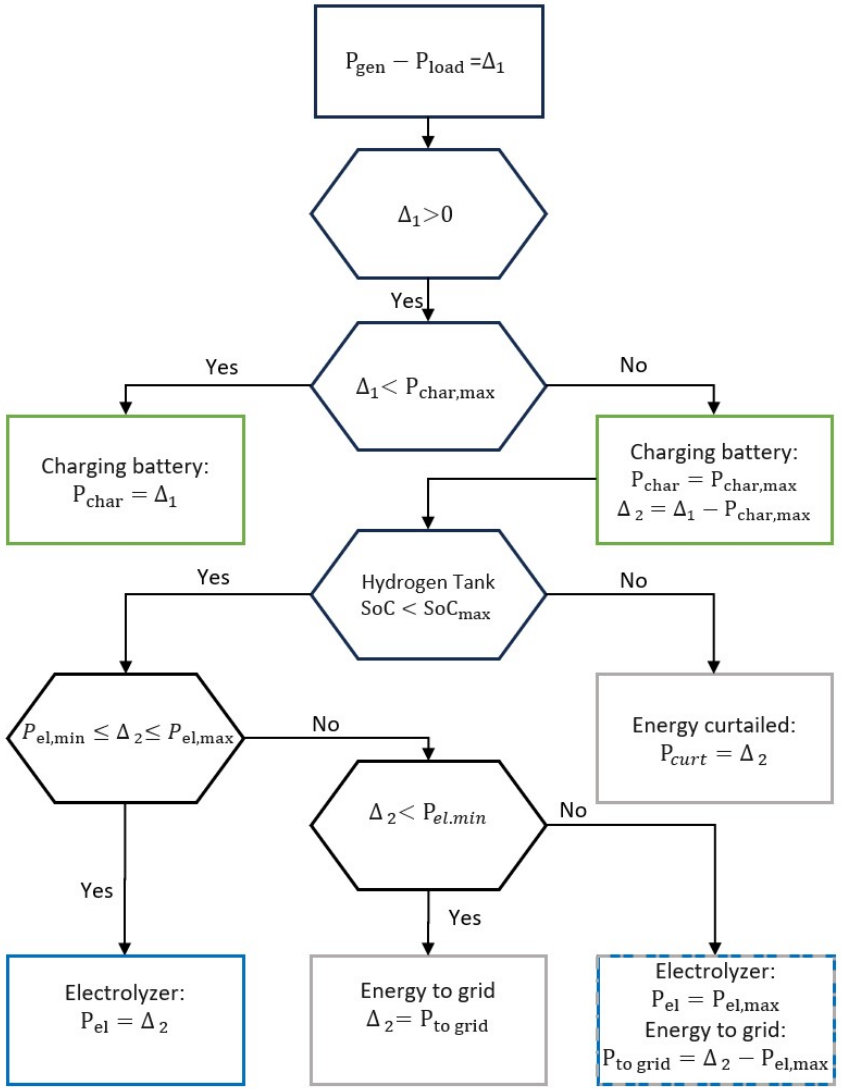

(a) Decisiontree: Surplus

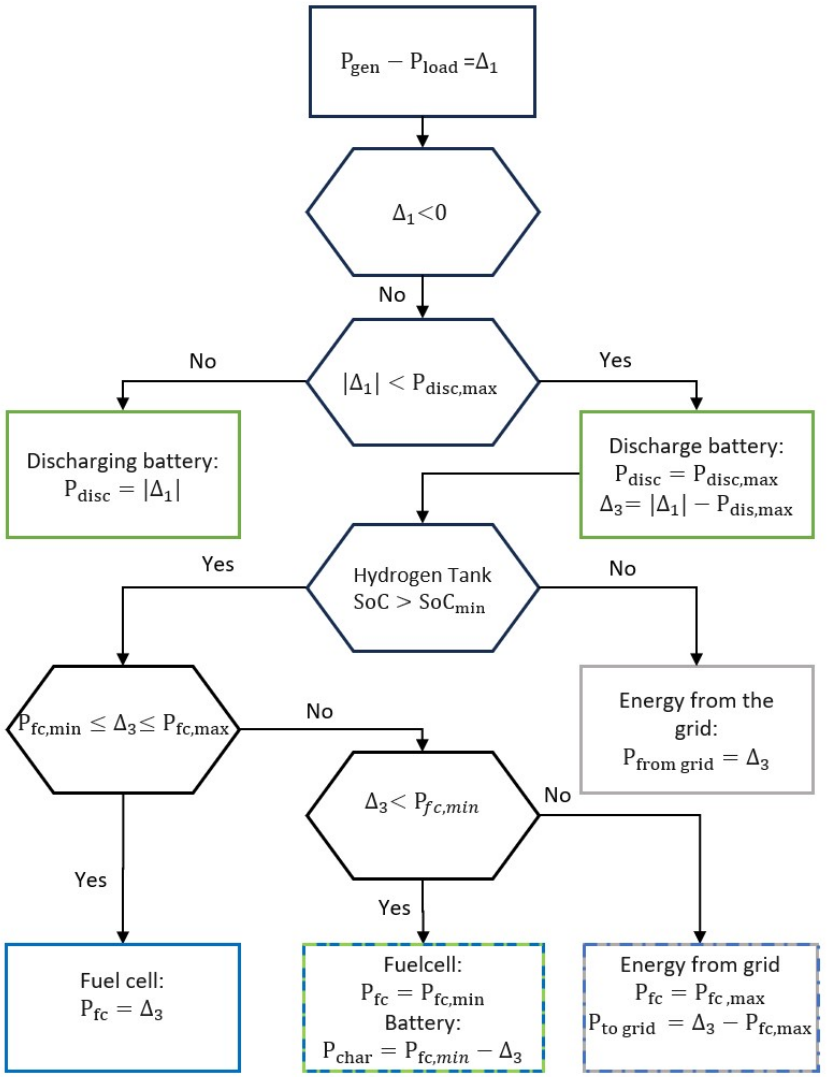

(b) Decisiontree: Shortage

Figure 2.3: Decision Tree of Energy Flow Between Assets During Surplus and Shortage Conditions

2.4. Model description of the Assets

In this section, the formulas and constraints of the assets used in the model are described. First, the model of the battery is detailed in subsection 2.4.1. Next, the operational modes and constraints of the electrolyzer are explained in subsection 2.4.2. This is followed by describing the storage tank in subsection 2.4.3. Lastly, the operational mode of the fuel cell is outlined in subsection 2.4.4.

2.4.1. Batteries

This section describes the battery model. The batteries receive a signal indicating either a surplus or shortage of energy, measured in kilowatts (kW), along with the duration of this signal. This signal determines how much energy needs to be either charged into or discharged from the battery. However, batteries operate within specific limits, including maximum charge and discharge power and minimum and maximum levels for storing and discharging energy. A battery's maximum energy charge and discharge rate depends on its C-rate, which is the ratio of the battery's maximum power to its capacity.

A C-rate of 1 means the battery can be fully charged or discharged in one hour. For the battery model used, lower C-rates are preferred. This is preferred because the battery needs to have enough capacity to supply power for several hours when renewable energy sources are insufficient. In the battery model, a C-rate of $\frac{1}{4}$ is assumed. This selection is made because the batteries must compensate for energy mismatches over several hours daily. Additionally, it is easier to compare different batteries if the ratio between capacity and power is the same.

Charging

The steps of the battery charging process at each timestep (Δt) are outlined as follows:

1. **Determine the Maximum Energy that can be Charged:**
   The maximum energy that can be charged, $E_{\text{char,max}}(t)$, is calculated using Equation 2.1. Here, $P_{\text{charge, max}}$ represents the initial capacity of the battery multiplied by the C-rate of the battery.

$$E_{\text{char,max}}(t) = P_{\text{charge, max}} \cdot \Delta t \tag{2.1}$$

2. **Calculate the Available Energy for Storage:**
   The available capacity for storage in the battery, denoted as $E_{\text{char,avail}}(t)$, is determined by Equation 2.2. The difference between the maximum State of Charge, SoC_{max}, and the current State of Charge, $SoC(t)$, multiplied by the battery's capacity, $C(t)$, determines the available capacity in the battery. Note that $C(t)$ is time-dependent due to battery degradation, which is further discussed in Equation 2.4.1.

$$E_{\text{char,avail}}(t) = (SoC_{\text{max}} - SoC(t)) \cdot C(t) \tag{2.2}$$

3. **Determine the Chargeable Energy:**
   The chargeable energy, $E_{\text{charge}}(t)$, is the surplus energy from renewable sources. By multiplying this surplus by the battery's charging efficiency, the amount of energy that can be stored is calculated, as defined by Equation 2.3. This efficiency (η_{charge}) indicates the proportion of energy that is successfully stored.

$$E_{\text{charge}}(t) = P_{\text{renewable}}(t) \cdot \Delta t \cdot \eta_{\text{charge}} \tag{2.3}$$

4. **Energy Input into the Battery:**
   The energy input into the battery, denoted as $E_{\text{in}}(t)$, is constrained by the minimum value among the calculated chargeable energy, the maximum energy chargeable, and the energy available for charge, represented by Equation 2.4. Here, $E_{\text{in}}(t)$ represents the energy that is charged into the battery.

$$E_{\text{in}}(t) = \min(E_{\text{charge}}(t), E_{\text{char,max}}(t), E_{\text{char,avail}}(t)) \tag{2.4}$$

5. **Update the State of Charge:**
   The updated state of charge for the next time period, $SoC(t+1)$, is calculated based on the energy input $E_{\text{in}}(t)$ and the battery capacity $C(t)$ at time t, as shown in Equation 2.5.

$$SoC(t+1) = SoC(t) + \frac{E_{\text{in}}(t)}{C(t)} \tag{2.5}$$

Discharging

The steps for the battery discharging process are outlined below. The steps are really similar to the charging process but the other way around.

1. **Determine the Maximum Energy that Can Be Discharged:**
   The maximum energy that can be discharged, $E_{\text{disc, max}}(t)$, is calculated using Equation 2.6. Here, $P_{\text{disc, max}}$ represents the initial capacity of the battery multiplied by the C-rate of the battery.

$$E_{\text{disc, max}}(t) = P_{\text{disc, max}} \cdot \Delta t \tag{2.6}$$

2. **Calculate the Available Energy for Discharge:**
   The available energy for discharge, denoted as $E_{\text{disc, avail}}(t)$, is determined by Equation 2.7. It is calculated as the difference between the current State of Charge, $SoC(t)$, and the minimum State of Charge,SoC_{min}, multiplied by the battery's capacity, $C(t)$. This value represents the capacity available for discharge.

$$E_{\text{disc, avail}}(t) = (SoC(t) - SoC_{\text{min}}) \cdot C(t) \tag{2.7}$$

3. **Determine the Dischargeable Energy:**
   The dischargeable energy, $E_{\text{disc}}(t)$, is the amount of energy that is needed from the battery to supply the demand. This amount of energy is divided by the battery's discharging efficiency, as described by Equation 2.8.

$$E_{\text{disc}}(t) = \frac{P_{\text{demand}}(t) \cdot \Delta t}{\eta_{\text{disc}}} \tag{2.8}$$

4. **Energy Output from the Battery:**
   The energy output from the battery, denoted as $E_{\text{out}}(t)$, is constrained by the minimum value among the calculated dischargeable energy, the battery's maximum discharging capacity, and the energy available for discharge, as shown in Equation 2.9. Here, $E_{\text{out}}(t)$ represents the energy that is discharged from the battery.

$$E_{\text{out}}(t) = \min(E_{\text{disc}}(t), E_{\text{disc, max}}(t), E_{\text{disc, avail}}(t)) \tag{2.9}$$

5. **Update the State of Charge:**
   The SoC is updated for the next timestep, $SoC(t+1)$, is calculated based on the energy output $E_{\text{out}}(t)$ and the battery capacity $C(t)$ at time t, as described by Equation 2.10.

$$SoC(t+1) = SoC(t) - \frac{E_{\text{out}}(t)}{C(t)} \tag{2.10}$$

Degradation of the batteries

In this section, the method of battery degradation is described. The battery consists of chemical components that degrade over time due to battery cycles. Therefore, this model takes into account the effect of cycling aging, which results from the battery's charge and discharge operations. This degradation leads to a reduction in capacity. Additionally, calendar aging, which occurs over time, is also considered. Although calendar aging does not affect performance significantly, it increases the chance of failure. The dominant aging effect depends on the type of battery. A model is developed

where is assumed that the capacity of the battery decreases linearly with each charge and discharge cycle. This linear decline in capacity is represented by the following equation (Equation 2.11), as detailed in the study by Gnibga, Blavette, and Orgerie [20].

Define $C(0)$ as the initial capacity of the battery and $C(t_{\text{EOL}})$ as the capacity at the end of life (EOL). The formula below calculates the remaining capacity of the battery ($C(t)$) at any given time t, taking into account the number of cycles completed up to time t (cycles(t)) and the total expected cycle life of the battery ($N_{\text{cycle life}}$). The capacity decrease is proportionally distributed across the battery's lifecycle, from its initial capacity to its defined end-of-life capacity.

$$C(t) = C(0) - \left[(1 - C(t_{\text{EOL}})) \cdot \left(\frac{\text{cycles}(t)}{N_{\text{cycle life}}}\right)\right] \tag{2.11}$$

2.4.2. Electrolyser

In this section, the operating modes of an electrolyzer are described. The operation mode depends on the input power P_{in}. The performance of an electrolyzer is based on the efficiency (η_{el}), which is also dependent on these conditions. The operating states are defined by whether the input power is below the minimum threshold P_{min}, within the optimal range, or above the electrolyzer's maximum capacity P_{max}. Each operation mode has different values for the volume of hydrogen generated, system efficiency, and the amount of energy that is used in operation.

In the first scenario, where the electrolyzer receives power less than the minimum capacity P_{min}, it does not operate. The electrolyzer is off. The conditions are as follows:

$$\text{for } P_{\text{in}} < P_{\text{min}} : \begin{cases} \text{Power Used} = 0 \\ \text{Hydrogen Produced} = 0 \\ \text{Efficiency} = 0 \\ \text{Runtime} = \text{Unchanged} \end{cases} \tag{2.12}$$

When P_{in} is within the operational range of the electrolyzer, the electrolyzer turns on and starts producing hydrogen. Before it starts producing hydrogen, the SoC of the hydrogen tank is checked to ensure there is available space. This process is described in subsection 2.4.3.

$$\text{for } P_{\text{min}} \leq P_{\text{in}} \leq P_{\text{max}} : \begin{cases} \text{Power Used} = P_{\text{in}} \\ \text{Hydrogen Produced} = H2_{produced} \\ \text{Efficiency} = \eta_{el} \\ \text{Runtime} = \text{Increased by operation duration} \end{cases} \tag{2.13}$$

If P_{in} exceeds the maximum capacity P_{max}, the electrolyzer operates at its maximum limit, and the surplus power is redirected. Again, before producing hydrogen is the SoC for the storage tank checked.

$$\text{for } P_{\text{in}} > P_{\text{max}} : \begin{cases} \text{Power Used} = P_{\text{max}} \\ \text{Hydrogen Produced} = H2_{produced,max} \\ \text{Efficiency} = \eta_{el} \\ \text{Runtime} = \text{Increased by operation duration} \end{cases} \tag{2.14}$$

The mass of hydrogen generated by the electrolyzer can be calculated using Equation Equation 2.15 [16]:

$$\dot{m}_{H_2} = \frac{P_{\text{in}} \cdot \Delta t \cdot \eta_{\text{el}}}{\text{HHV}_{H_2} + P_{\text{compressor}}} \tag{2.15}$$

In this equation, $\dot{m}_{H_2}$ represents the mass of hydrogen produced in kilograms (kg), P_{in} is the input power to the electrolyzer, Δt is the time interval over which the input power is applied, η_{el} is the efficiency of the

electrolyzer, HHV_{H_2} is the Higher Heating Value of hydrogen in kilowatt-hours per kilogram (kWh/kg), and $P_{\text{compressor}}$ is the energy required to compress the produced hydrogen from 30 bar, the operational pressure of the electrolyzer, to 300 bar, the pressure at which the hydrogen is stored in the tank. The HHV of hydrogen is 39.4 kWh/kg [26], and the energy needed for compression is 1.7 kWh/kg [27].

Degradation of the electrolyzer

The performance of electrolyzers degrades over time with usage. The efficiency of the electrolyzer is multiplied by the state of health ,$\text{SOH}_{\text{elec}}(t)$, of the electrolyzer. The state of health is the percentage of the initial performance of the electrolyzer [28]. This is shown in Equation 2.16 and Equation 2.17.

$$\text{SOH}_{\text{elec}}(t) = 100 - (\eta_{\text{degradation}} \times \text{Runtime}) \tag{2.16}$$

$$\eta_{\text{el}}(t) = (\text{SOH}_{\text{elec}}(t) \times \eta_{\text{initial\_el}}) \tag{2.17}$$

Where $\eta_{\text{el}}(t)$ denotes the efficiency of the electrolyzer, $\eta_{\text{degradation}}$ represents the fractional degradation of efficiency over a specified operational period, and $\eta_{\text{initial\_el}}$ is the initial efficiency of the electrolyzer.

In addition to the decrease in efficiency, electrolyzer manufacturers specify the operational lifetime in terms of operational hours to ensure system performance [29]. Therefore, the electrolyzer stacks are replaced when the SOH decreases to 90%. These parameters are detailed in Table 3.4.

2.4.3. Hydrogen Storage Tank

This section describes the equations and steps involved in managing the SoC of hydrogen in the storage tank, considering the electrolyzer and fuel cell operations.

To model the dynamics of hydrogen storage, Equation 2.18 is used to model the SoC when hydrogen is being produced, and Equation 2.19 is used to model the SoC when hydrogen is being consumed.

Before the electrolyzer starts producing hydrogen, it provides an input indicating how much hydrogen can be produced with the energy surplus. Based on the current $\text{SoC}_{H_2}(t)$, the next updated $\text{SoC}_{H_2}(t+1)$ is determined. If $\text{SoC}_{H_2}(t+1)$ does not exceed $\text{SoC}_{H_2\text{max}}$, the electrolyzer obtains a signal that it can start producing hydrogen. The hydrogen SoC is updated by adding the amount of hydrogen produced, $H_{2,\text{produced}}(t)$, during the time step t divided by $H_{2,\text{max}}$. This is shown in Equation 2.18:

$$\text{SoC}_{H_2}(t+1) = \text{SoC}_{H_2}(t) + \frac{H_{2\text{produced}}(t)}{H_{2,\text{max}}} \tag{2.18}$$

Contrariwise, when the fuel cell wants to produce energy, the SoC of the hydrogen tank is checked first. If $\text{SoC}_{H_2}(t+1)$ is not below $\text{SoC}_{H_2\text{min}}$, the fuel cell obtains a signal and starts producing. The hydrogen SoC is updated by subtracting the amount of hydrogen consumed, $H_{2,consumed}(t)$, during the time step t divided by $H_{2,\text{max}}$. This is shown in Equation 2.19:

$$\text{SoC}_{H_2}(t+1) = \text{SoC}_{H_2}(t) - \frac{H_{2,\text{consumed}}(t)}{H_{2\text{max}}} \tag{2.19}$$

2.4.4. Fuel cell

In this section, the operating modes of a fuel cell are described. These modes are quite similar to the operational modes of the electrolyzer. The operating conditions are defined by the power demand (P_{out}). The performance of a fuel cell depends on its efficiency (η_{fc}), which is described in subsection 3.6.4. The operational modes are characterized by whether the power demand is below the minimum operational threshold (P_{min}), within the optimal range, or above the fuel cell's maximum power output (P_{max}). Each mode presents different outcomes regarding electricity production, system efficiency, and hydrogen usage.

In scenarios where the power demand falls below the fuel cell's minimum capacity (P_{min}), the system operates at P_{min}. Since P_{min} exceeds the demand, this operation generates a minor surplus of power, which is directed toward charging the battery. At P_{min}, the fuel cell's efficiency is very low, making the

process of charging the battery relatively inefficient. However, this step is essential to ensure that the energy system relies only on renewable energy. Before the fuel cell starts generating, it is checked if there is enough capacity left in the storage tank. This is described in subsection 3.8.3.

$$\text{For } P_{\text{out}} < P_{\min}: \begin{cases} \text{Electricity Generated} = P_{\min} \\ \text{Fuel Consumption} = H_2 \text{ consumed}, \min \\ \text{Efficiency} = \eta\text{fc} \\ \text{Runtime} = \text{Increased by operation duration} \end{cases} \tag{2.20}$$

When P_{out} is within the fuel cell's operational range, it starts generating electricity to balance the shortage.

$$\text{for } P_{\min} \leq P_{\text{out}} \leq P_{\max}: \begin{cases} \text{Electricity Generated} = P_{\text{out}} \\ \text{Fuel Consumption} = H2_{consumed} \\ \text{Efficiency} = \eta_{fc} \\ \text{Runtime} = \text{Increased by operation duration} \end{cases} \tag{2.21}$$

If P_{out} exceeds the fuel cell's maximum output capacity ($P_{\max}$), the fuel cell operates at its maximum limit, and any additional demand must be met through alternative sources.

$$\text{for } P_{\text{out}} > P_{\max}: \begin{cases} \text{Electricity Generated} = P_{\max}, \\ \text{Fuel Consumption} = H2_{consumed,max} \\ \text{Efficiency} = \eta_{fc} \\ \text{Runtime} = \text{Increased by operation duration} \end{cases} \tag{2.22}$$

To determine the mass of hydrogen consumed by the fuel cell, Equation 2.15 is used [16].

$$H2_{consumed} = \frac{P_{\text{out}} \cdot \Delta t}{\text{LHV}_{H_2} \cdot \eta_{\text{fc}}} \tag{2.23}$$

Here, $H2_{consumed}$ represents the amount of hydrogen used in kg, P_{in} the input power to the fuel cell, Δt is the timestep over which the input power, η_{ez} is the efficiency of the, and LHV_{H_2} is the Lower Heating Value of hydrogen in kWh/kg

The operation of the fuel cell is limited by its power range, defined as $P_{\text{min}} \leq P_{\text{in}} \leq P_{\text{max}}$, where P_{min} and P_{max} are the minimum and maximum allowable power inputs for the fuel cell. The efficiency of the fuel cell, η_{fc}, is thoroughly discussed in subsection 3.6.4. The lower heating value (LHV) of hydrogen is 33.3 kWh/kg [26].

Degradation of the fuel cell

The performance of fuel cells degrades over time with usage. This degradation is proportional to the initial efficiency of the fuel cell. This is similar to the electrolyzer degradation. Equation 2.24 calculates the current efficiency of the fuel cell:

$$\eta_{\text{fc}(t)} = (100 - \eta_{\text{degradation}} \times \text{Runtime}) \times \eta_{\text{initial\_fc}} \tag{2.24}$$

where $\eta_{\text{fc}}(t)$ denotes the current efficiency of the fuel cell, $\eta_{\text{degradation}}$ represents the fractional degradation of efficiency over a specified operational period, and $\eta_{\text{initial\_fc}}$ is the initial efficiency of the fuel cell.

In addition to efficiency degradation, fuel cell manufacturers specify the operational lifetime of operational hours to ensure the device's performance [29]. The fuel cell stacks are replaced when they reach operational hours. This is when the state of health is decreased to 90%. These critical parameters are detailed in Table 3.6.

2.5. Optimization

This section first describes which optimization methods are suitable for this problem. Then, the steps of the optimization method used in this research are explained in subsection 2.5.1. After the optimization method is explained, subsection 2.5.2 describes how the objective function is determined based on the cost calculations, which are described in subsection 2.5.3. Finally, subsection 2.5.4 describes the variables and the constraints of the optimization problem.

Optimizing complex systems with many variables is challenging because these problems often have multiple local minima due to the many degrees of freedom in the problem. There are two main types of search algorithms for optimizations that are easy to implement in Python. The first type is Genetic Algorithms (GA), where a group of solutions goes through random changes to create new solutions one by one. Only the best solutions are kept for the next round [30]. The second type is Particle Swarm Optimization (PSO). In the PSO group of particles, moves around the search area following the best solution. In the report of Perrigot et al. was, the performance of the PSO algorithm and the GA analyzed. From this report, it is concluded that PSO converges slower than GA, but it eventually comes close to the optimum minia. PSO's performance is assigned to find the global optimum in non-linear problems, which often have many local minima [31] However, using PSO doesn't always lead to the mathematically best solution, it always converges close to the optimal minimum, which is beneficial for complex problems because it saves computational time.

2.5.1. PSO

This section shows the steps involved in the PSO process [32][33][34]. From the PySwarms package, the PSO class in Python is used [35]. The formulas used in the class are shown and described below. The class is modified by adding a constraint and stepsize to save computational time.

1. **Initialization of Particle Positions**:

   A swarm of particles (S) is randomly distributed within the problem space. Each particle is a set of values of the variables of the objective function that is optimized. The default setting uses 100 particles. The initial position of each particle is determined based on the lower and upper boundary variables. The position of each dimension of the optimization problem is initialized using the following equation:

   $$x_{i,d}^{(0)} = x_{\text{min},d} + \text{rand}() \cdot (x_{\text{max},d} - x_{\text{min},d}) \tag{2.25}$$

   Here, $x_{i,d}^{(0)}$ represents the starting position of particle i in dimension d, with $x_{\text{min},d}$ and $x_{\text{max},d}$ being the minimum and maximum boundaries, respectively. The dimension represents the variable in the optimization, and the minimum and maximum boundaries of this variable are input at the beginning of the optimization. These boundaries are set to limit the problem space.

2. **Initialization of Particle Velocities**:

   The velocities of the particles are initialized similarly to their positions. This determines their subsequent movements. The equation that initializes the particle velocity is shown below:

   $$v_{i,d}^{(0)} = v_{\text{min},d} + \text{rand}() \cdot (v_{\text{max},d} - v_{\text{min},d}) \tag{2.26}$$

   Here, $v_{i,d}^{(0)}$ represents the initial velocity of particle i in dimension d, with $v_{\text{min},d}$ and $v_{\text{max},d}$ being the minimum and maximum velocity boundaries, respectively. The initial minimum and maximum velocity boundaries are equal to the minimum and maximum boundaries of the positions

3. **Velocity Update**:

   From now on, the iteration process begins. For each iteration, the velocity of each particle is updated based on its individual best position and the global best position. The individual best position is the best position found by the particle, and the global best position is the best position found by any particle in the swarm. The distance between the current position and the individual and global best positions, scaled by the cognitive and social scaling factors (ϕ_p and ϕ_g), also known as the acceleration factors, along with the inertia weight (ω), determines the new velocity. These factors (ϕ_p, ϕ_g, and ω) determine how particles move from their individual best positions

towards the global best position. For this optimization, the default setting for ϕ_p, ϕ_g, and ω is used, which is 0.5:

$$v_{i,d}^{(t+1)} = \omega v_{i,d}^{(t)} + \phi_p \text{rand}()(p_{i,d} - x_{i,d}^{(t)}) + \phi_g \text{rand}()(g_d - x_{i,d}^{(t)}) \tag{2.27}$$

In this equation, $p_{i,d}$ represents the best position found by particle i in dimension d, g_d represents the best position found by any particle in the swarm in dimension d. Each particle is a set of values of the variables.

4. **Position Update**:

   Based on the new velocity, the new position of each particle is determined:

$$x_{i,d}^{(t+1)} = x_{i,d}^{(t)} + v_{i,d}^{(t)} \tag{2.28}$$

5. **Position Update, Step Size, and Constraint Check**: In this step, the updated position is modified according to the step size used in the optimization to reduce computational time. The new positions based on the step size are checked against the constraints. This is done by the following steps:

$$x_{i,d}^{(t+1)} = \text{NewPositions}(x_{i,d}^{(t+1)}, \text{stepsize}) \tag{2.29}$$

   The new position, modified by the step size function, can be defined as:

$$\text{NewPositions}(x_{i,d}^{(t+1)}, \text{stepsize}) = \text{round}(x_{i,d}^{(t+1)}/\text{stepsize}) \cdot \text{stepsize} \tag{2.30}$$

   The positions are updated based on the step size. The position, consisting of values for each variable, is then evaluated using the objective function. The objective function checks if a constraint is met. If the constraint is unmet, a penalty value of 1000 is assigned to the objective value at $x_{i,d}^{(t+1)}$. In subsection 2.5.2 and subsection 2.5.4, the objective function and the constraint are described.

6. **Update of Individual Optimum**:

   Each particle updates its record of the best position (optimum) it has discovered based on its performance:

$$p_{i,d}^{(k)} = [x_{1,\text{best},i}^{(k)}, x_{2,\text{best},i}^{(k)}, \ldots, x_{D,\text{best},i}^{(k)}] \tag{2.31}$$

   Here, $p_{i,d}^{(k)}$ represents the best-known position of particle i up to iteration k. This is the position where the objective function has the lowest value for that particle, considering all the dimensions.

7. **Global Optimum Refresh**:

   The swarm updates its knowledge of the overall best position found by any particle. This collective intelligence guides the swarm's movement:

$$g_d = [x_{1,d}^{(k)}, x_{2,d}^{(k)}, \ldots, x_{D,d}^{(k)}] \tag{2.32}$$

   Here, $g_d^{(k)}$ represents the best-known position of the entire swarm up to iteration k. This is the lowest objective function of the whole swarm.

8. **Termination Criterion**:

   The optimization process stops if the change in the global best position (g_d) between subsequent iterations is less than 0.0001. This threshold is set due to the step size. The objective values change by approximately 1E-4 to 1E-5 when one variable changes with the stepsize, depending on the influence of the variables on the objective value. This approach sometimes results in the optimization converging to a local minimum close to the global minimum or stopping too soon. However, these termination criteria is important to ensure this iteration process will not go on infinity due to unmet criteria. However, this introduces a significance of 0.001 on the outcome of the objective function.

$$g_d^{(k+1)} - g_d^{(k)} < 0.0001 \tag{2.33}$$

2.5.2. Objective Function

The objective of the function is to minimize the LCOE, as shown in Equation 2.34. The LCOE calculates the electricity price on average over the project's lifetime in €/kWh. This equation is based on the reports by Hansen and Marocco et al.[36][29].

$$\text{LCOE} = \frac{C_{\text{invest, total}} + C_{\text{O\&M, total}} + C_{\text{replacement, total}} - C_{\text{residual}}}{\sum_{i=1}^{n} \frac{E_{t,i}}{(1+r)^i}} \tag{2.34}$$

In this formula, $C_{\text{invest, total}}$ represents the initial investment costs, also known as Capital Expenditure (CAPEX). This is calculated by Equation 2.35. This cost is the sum of the investment cost of all assets, j=[PV; Wind; Batteries; Electrolyzers; Storage Tanks; Fuel Cells] in scenarios 1 to 8.

$$C_{\text{invest, total}} = \sum_{j} C_{\text{invest},0,j} \tag{2.35}$$

Here, $C_{\text{invest},0,j}$ is the sum of the investment cost for all assets j in year i = 0.

The total operation and maintenance costs ($C_{\text{O\&M, total}}$) represent the costs of maintaining the asset. These costs of each asset (j) ($C_{\text{O\&M,j}}$) are calculated annually and discounted at the rate for that year and then summed. Additionally, the grid connection costs are included in this calculation because a yearly fee needs to be paid. The details of the cost of connection are also explained in subsection 3.7.5. This is shown in Equation 2.36.

$$C_{\text{O\&M, total}} = \sum_{i=1}^{n} \frac{C_{\text{O\&M},i,j}}{(1+r)^i} \tag{2.36}$$

Assets may degrade due to frequent use and aging. When the performance of an asset decreases significantly or the risk of failure becomes high, the Asset is (partially) replaced. The total Replacement Costs ($C_{\text{replacement, total}}$) of the assets during the project's lifetime are calculated by summing the costs of each replacement, discounted by the rate of the year of replacement, as shown in Equation 2.37:

$$C_{\text{replacement, total}} = \sum_{i=1}^{n} \frac{C_{\text{replacement},i,j}}{(1+r)^i} \tag{2.37}$$

In this equation, $C_{\text{replacement},i,j}$ represents the cost in year i of replacing asset j, adjusted to its Net Present Value (NPV) using the discount rate r.

The residual value, represented as C_{residual}, quantifies the economic value of a component after the analysis period. The residual value of assets is associated with two lifetimes: the overall Assets lifetime and the assets storage block's lifetime. Components of the asset, such as the balance of the system, power equations, control, and system integration, are assigned to the asset's lifetime. The entire asset will be replaced once this lifetime is exceeded. The storage block's lifetime is especially relevant for assets that degrade over time or are frequently used within the system, contributing to degradation [37].

The Capital Recovery Factor (CRF) is used to determine the annual equivalent cost of each asset over its lifetime and is defined as in Equation 2.38:

$$CRF = \frac{r}{1-(1+r)^{-L}} \tag{2.38}$$

Here, r represents the discount rate, and L signifies the lifespan of the Asset. The investment cost of the asset is then the initial cost times the CRF and is discounted every year till the end of its lifetime. This spreads the investment cost across each year of the asset's life based on the NPV.

The total investment cost is equivalent to the sum of the NPV of the annual spread investment cost. This is calculated as the initial investment cost in year 0 minus the residual value of the asset. To compute the residual value of the asset at the end of a project, the years remaining from the end of the project (L_{project}) to the end of the asset's lifetime (L_{asset}) are considered. The replacement costs, which are the value of the asset's storage block components, are subtracted from the investment costs, as the storage block components have different lifespans and costs. This calculation is presented in Equation 2.39:

$$C_{\text{residual, system}} = \sum_{i=L_{\text{project}}}^{L_{\text{system}}} \frac{CRF \times (C_{\text{invest},j} - C_{\text{replacement},j})}{(1+r)^i} \tag{2.39}$$

The calculation for the residual value of the replaced components of the asset is similar. The residual value is adjusted by multiplying by the CRF and discounting for the years remaining after the project to calculate the NPV. The remaining lifetime of the replacement components ($L_{\text{replacement}}$) is determined by the time when each component is first replaced. The first replacement calculates the average lifetime, and the last replacement year plus the first replacement year determines when ($L_{\text{replacement}}$) the next replacement will be. This calculation for the residual cost of replaced components is outlined in Equation 2.40:

$$C_{\text{residual, replacement}} = \sum_{i=L_{\text{project}}}^{L_{\text{replacement}}} \frac{CRF \times C_{\text{replacement},j}}{(1+r)^i} \tag{2.40}$$

2.5.3. Cost calculation

This section describes the general formulas used to calculate each asset's investment cost, O&M cost, and replacement cost.

The investment cost for each asset j is calculated using the Equation 2.41.

$$C_{\text{invest, total},j} = P_{\text{installed},j} \times C_{\text{invest},j} \tag{2.41}$$

In Equation 2.41, $C_{\text{invest\_total},j}$ is the total investment cost for asset j, $P_{\text{installed},j}$ represents the installed capacity of asset j (in kWh, kW, or kg), and $C_{\text{invest},j}$ is the cost per unit of capacity for the asset.

The annual O&M costs for asset j can be calculated by using Equation 2.42

$$C_{\text{O\&M, total},j} = P_{\text{installed},j} \times C_{\text{O\&M},j} \tag{2.42}$$

In Equation 2.42, $C_{\text{O\&M\_total},j}$ represents the total O&M cost for asset j . $P_{\text{installed},j}$ refers to the installed capacity, and $C_{\text{O\&M},j}$ denotes the cost that is annually required for operation and maintenance.

In Equation 2.43 is the O&M costs associated with the connection calculated. This is based on the contracted power C_{Contract} and the maximum power C_{Max} of the connection. The coefficients C_{Contract} and C_{Max} are specified in subsection 3.7.5.

These costs are multiplied by 12 to calculate the annual O&M costs. It is assumed that the contracted power and the maximum power are equal, which is a suitable approximation given that the load profile of data centers is relatively constant and often operates close to or at the maximum capacity.

$$O\&M_{\text{connection}} = P_{\text{connection}} \times (C_{\text{Contract}} + C_{\text{Max}}) \times 12 \tag{2.43}$$

The monthly maximum power ($P_{\text{connection}}$) is limited by the maximum capacity of the data center plus the maximum capacity of the electrolyzer or battery, which directly influences these costs. This is calculated by Equation 2.44.

$$P_{\text{connection}} = (P_{\text{data center, max}} + \max(P_{\text{battery}}, P_{\text{electrolyzer}})) \tag{2.44}$$

The investment cost of the connection in year 0 is considered negligible and is excluded from the cost analyses.

$$C_{\text{replacement\_total},j} = P_{\text{installed},j} \times R_{\text{replacement},j} \tag{2.45}$$

In Equation 2.45, the cost associated with replacing an asset is determined. $C_{\text{replacement\_total},j}$ represents the total replacement cost for asset j. Here, $R_{\text{replacement},j}$ denotes the replacement cost. The total cost is calculated by multiplying this replacement cost by the installed capacity.

2.5.4. Variables and constraints

This section describes the variables and constraints used in the optimization method.

The dimensions described in the optimization steps in subsection 2.5.1 are the variables of the objective function. The objective function includes 6 variables that influence the LCOE of energy over a 10-year simulation. For the wind and solar assets, the installed capacities ($P_{\text{installed},j}$) are the variables measured in kilowatts (kW). The battery capacity is measured in kilowatt-hours (kWh). The capacities of the electrolyzer and fuel cell, both measured in kilowatts (kW), represent the input of the electrolyzer and the output of the fuel cell, respectively. The capacity of the hydrogen storage tank is quantified in kilograms (kg). The table below provides an overview of the variables optimized for each configuration.

Table 2.2: Variables of the Optimization

Variable	Unit
Wind	kW
Solar	kW
Battery	kWh
Electrolyzer	kW
H_2 Storage	kg
Fuel Cell	kW

The main constraint of this model is that the data center operates on 100% renewable energy on an hourly basis. This implies that no energy is sourced from the grid. The constraint ensures that all the energy demand of the data center is met exclusively through renewable sources. This requirement is mathematically expressed by Equation 2.46.

$$\frac{\sum_i (E_{\text{demand},i} - E_{\text{grid},i})}{\sum_i E_{\text{demand},i}} \times 100\% = 100\% \tag{2.46}$$

To conclude, this research uses the PSO method to optimize the dimensions of the energy system. The dimensions of the energy system are the variables of the optimization. Initially, random values are chosen for the variables within the set boundaries. Based on these values, the model simulates the system for 10 years, and subsequently, the LCOE is determined using the economic model of the energy system.

The best solution for each particle is saved, along with the best solution among all particles. New values are then determined based on the steps described in subsection 2.5.1, and the new LCOE is calculated. If the constraint is met and the LCOE is lower than the previously lowest LCOE, the values of the variables are saved. If the constraint is not met, a value of 1000 is assigned to the LCOE. These iterations continue until the difference between the new and current objective functions is less than 0.0001. The values of the optimized dimensions are then presented.

2.6. Economic Analysis

For the economic analysis, different prices are collected from existing literature. All the numbers that are used in this paper are indexed to the end of 2023. To index the numbers, Table 2.3 shows the factor required to convert values from different years and currencies to the equivalent value in euros

at the end of 2023. For conversions from euro prices of different years to the 2023 euro value, the data of Eurostat is utilized [38]. This data has been adjusted by the annual exchange rate from dollars to euros to establish the dollar-to-euro index for 2023. The exchange rates used are based on the average prices reported by the Board of Governors of the Federal Reserve System [39].

Table 2.3: Annual Indices and Exchange Rates for Converting Values from Different Years and Currencies to $€_{2023}$ [38][39]

Year (i)	**2014**	**2015**	**2016**	**2017**	**2018**	**2019**	**2020**	**2021**	**2022**	**2023**
$€_i$ to $€_{2023}$ Index	1.270	1.269	1.266	1.245	1.222	1.204	1.195	1.161	1.064	1.000
$\$_i$ to $€_{2023}$ Index	0.955	1.144	1.143	1.101	1.034	1.075	1.047	0.982	1.010	0.924
€ to $	0.752	0.875	0.901	0.885	0.846	0.893	0.876	0.849	0.948	0.924

It is important to consider different values to provide a cost analysis of the different configurations. One important factor is the project duration, which is often determined based on the lifespan of the components [40]. For this study, a fixed project duration of 10 years is selected to compare the different configurations. This approach aims to maintain consistency and reliability in the evaluation process. The economic parameters used for this analysis are shown in Table 2.4.

Table 2.4: General Economic Parameters

Parameter	**Abbreviation**	**Value**
Project Duration	L_{project}	10 years
Discount Rate	r	8%

2.7. Environmental Impact and Land Lsage Described

This section describes the methods used for assessing environmental impact and land usage. After presenting the results, the two configurations with the best outcomes are compared based on their CO_2 emissions during manufacturing and their land usage.

For the environmental impact, the emissions during manufacturing are assessed using the global warming contribution index, which measures the impact of a substance released into the atmosphere on global warming. This index is primarily influenced by greenhouse gas emissions, such as methane and carbon dioxide. It is expressed over a time horizon of 100 years in terms of kilograms of CO_2 equivalent per kilogram of emission (kg CO_2e) [41]. Since burning different fuels for material production contributes to global warming, this impact category is essential for any relevant study. The functional unit for emissions indicates the amount of CO_2 equivalent produced by the materials used in the system's production, from the cradle to the grave. First, the range of CO_2 emissions per installed capacity of the components is determined.

These values are multiplied by the installed capacity of the assets. However, not all assets are at the end of their lifetime. Additionally, some assets are replaced, and the CO_2 emissions from these replacements are also considered. Based on the replacements during the 10-year simulation, the replacements for the total lifetime of the assets are determined. Thus, the total emissions for the assets are the sum of the total emissions from replacements during their lifetimes and the initial emissions. These values are then added up and multiplied by the fraction of the lifetime that the assets are used after the 10-year simulations. By applying these multipliers, the total CO_2 emissions for each component can be estimated, accounting for the components' lifetimes and replacements over the 10-year period.

The same methodology is applied to determine the system size. The capacity density of the assets is determined. For all assets, the size per square meter is considered. When the capacities are determined, the installed capacity of the assets is divided by the capacity density to estimate the potential size of the energy storage technology.

Table 2.5: Units for CO_2 Emissions and Capacity Densities of the Assets

Component	**Emissions**	**Capacity Density**
Solar PV	kg CO_2e/kWp	kWp/m^2
Wind Turbine	kg CO_2e/kW	kW/m^2
Li-ion Battery	kg CO_2e/kWh	kWh/m^2
Vanadium Redox Flow Battery	kg CO_2e/kWh	kWh/m^2
Alkaline Electrolyzer	kg CO_2e/kW	kW/m^2
Hydrogen Storage Tank (300 bar)	kg CO_2e/kg	kg/m^2
Fuel Cell	kg CO_2e/kW	kW/m^2

3

Data Collection

This chapter outlines all the data that is collected as input for the model. First, an overview of the possible energy storage technologies is provided in section 3.1. Second, a detailed description of the main technologies for each category is discussed in section 3.2. Then, based on the dissection criteria, the technologies selected are presented in section 3.3. Consequently, the different configurations are comprised of the selected technologies, as detailed in section 3.4. Then, the data collection of the renewable energy sources and the data center's load, which are inputs for the model, are described in section 3.5. In the following sections, the technical and economic parameters, which serve as input for the model, are described in section 3.6 and section 3.7. Lastly, the parameters for the environmental assessment, based on CO_2e emissions from production and land usage, are outlined.

3.1. Overview of Available Energy Storage Technologies

In this section, an overview of various energy storage technologies is provided. The energy storage technologies that are described are Mechanical, Electrochemical, Electrical, and Chemical storage [42].

Mechanical energy storage systems store gravitational potential energy, kinetic energy, or compression potential energy. This category contains technologies like pumped hydro energy storage (PHES), gravitational energy storage (GES), compressed air energy storage (CAES), and flywheel energy storage (FES) technologies [43]

Electrochemical storage, commonly known as batteries, involves storing energy in chemical compounds and releasing it through electrochemical reactions. A battery consists of two or more cells connected in series or parallel to achieve the desired voltage and capacity for a specific application. The recharging frequency of a battery depends on its usage pattern and discharge depth. Charge times can range from one to twelve hours, influenced by the battery's condition and external factors [44]. The most commonly used electrochemical batteries for utility-scale applications include lead-acid, lithium-ion (Li-ion), sodium-sulfur (NaS), nickel-cadmium (Ni-Cd), and flow batteries [45].

The primary technologies for electrical energy storage are Superconducting Magnetic Energy Storage (SMES) systems and Supercapacitors (SC). These systems store electricity efficiently in electric and electromagnetic fields, respectively, with minimal energy loss [43].

Chemical storage involves storing energy in chemical bonds, which can be released through chemical reactions. Among various methods, hydrogen storage stands out due to its high energy density and potential for clean energy applications. Hydrogen energy storage uses an electrolyzer to produce hydrogen by converting electricity into chemical energy. This stored energy can be released by burning the hydrogen in a fuel cell when needed. Hydrogen storage offers benefits such as the ability to transport and store energy and produce water as a non-toxic combustion product [46].

3.2. Classification of the Technologies

In this section, the main technologies of each classification are explained and described based on the criteria outlined in section 2.2. First, mechanical energy storage is discussed in subsection 3.2.1, followed by electrochemical storage in subsection 3.2.2. Subsequent, electrical energy storage in subsection 3.2.3. Finally, chemical storage is described in subsection 3.2.4.

3.2.1. Mechanical energy storage

Pumped Hydro Energy Storage (PHES)

PHES systems convert electrical energy into potential energy by pumping water from lower to higher reservoirs. This conversion typically takes place when electricity prices are low and surplus energy is available, using pumps to transfer water to the upper reservoir. During periods of high energy demand, the stored water is released down through a hydraulic turbine to generate electricity [46]. PHES systems are highly scalable, allowing the size to be adjusted according to needs. They have a medium response time ranging from seconds to minutes [47][45]. This means it responds quickly to changes in the energy demand. The self-discharge rate of these systems is very low, ensuring minimal energy loss over time [48]. The charge and discharge cycle ranges from several hours to days, depending on the specific system and size [47][45]. Despite the relatively high initial investment, PHES is considered an economical solution for long-term energy storage. The technology for PHES is mature and has been commercialized, demonstrating a high level of reliability and efficiency [46][47]. The technology maturity level is rated at 9 [47][25][49]. However, PHES systems need specific geographical conditions to operate well. It depends on having suitable water reservoirs. These reservoirs, ideally at different heights, are essential for the system's energy storage. Without these geographical features, the efficiency of PHES technology is reduced. Additionally, the costs increase because the height difference would need to be artificially created.

Gravity Energy Storage (GES)

GES systems store and release energy using a heavy mass instead of water. The use of solid materials results in higher energy density compared to PHES. GES systems are scalable, but they encounter significant challenges in management and construction as their size increases beyond a certain point [43]. Therefore, the scaling score is lower than the PHES score. GES also have a medium response time ranging from seconds to minutes and a very low self-discharge rate, ensuring minimal energy loss [48][47][45]. The charge and discharge cycles can last from hours to days [47][45]. Despite high initial costs, they are cost-effective for long-term storage. The technology maturity of GES is rated at 8, indicating advanced but less mature and commercialized technology compared to PHES [47][25][49]. GES systems also depend on specific geographical conditions, similar to PHES.

Compressed Air Energy Storage (CAES)

CAES systems capture surplus electricity by powering a compressor to store air in confined spaces, such as underground caverns. When there is a demand for electricity, the stored air is released to drive a turbine and produce power. CAES systems are highly scalable, allowing for size adjustments. They have a medium response time of a few minutes and a low self-discharge rate, ensuring minimal energy loss [48][47][45]. The charge and discharge cycles range from hours to days [47][45], making them flexible for various applications. Despite high initial costs, CAES is cost-effective for long-term storage. The technology maturity is rated at 7.5, and implementation depends on specific geographical conditions[25][49][47].

Flywheel Energy Storage (FES)

FES operates by accelerating a rotor to store energy and decelerating it to release energy. The performance of FES technology depends significantly on the rotor's characteristics, such as its maximum rotational speed and mass. Flywheels are suited for short-term energy storage, typically ranging from a few seconds to several minutes [46]. FES systems are scalable but technically limited beyond a specific size. Therefore, FES and GES have the score on scalability. FES offers an immediate response time [47][45]. However, FES has a high self-discharge rate, with energy typically dissipating within an hour, sometimes within minutes [48]. The charge and discharge cycles occur in seconds to minutes [47][45]. While the initial cost is high, the technology is mature, rated at 9, and it is location independent[25][49][47].

3.2.2. Electrochemical

Lead-Acid Batteries

Lead-acid batteries are one of the oldest energy storage technologies used since the nineteenth century. There are two main types: flooded and sealed. Flooded lead-acid batteries are cheaper, have a longer lifetime, and are available in various configurations, making them more commonly used in stationary applications due to their cost-effectiveness and longevity. Conversely, sealed lead-acid batteries are designed to be safer and require less maintenance. In sealed batteries, the liquid electrolyte is transformed into a gel, allowing the battery casing to be sealed, which is preferable for applications where safety and low maintenance are essential [50].

Lead-acid batteries are characterized by their low cost, easy manufacturing process, and high recyclability, with more than 97% of the lead being recyclable. However, they have a limited lifetime of approximately 500 cycles and low energy density due to the high density of lead [51]. Lead-acid batteries are highly scalable, as they can easily be connected in containers. They have a rapid response time ranging from milliseconds to seconds and exhibit a self-discharge rate of 0.1-0.3% per day.y [48][47][45]. The charge and discharge cycles range from minutes to hours [47][45]. Despite their limitations, lead-acid batteries are a feasible option for various applications due to their maturity, rated at a technology maturity level of 9 [25][49][47].

Lithium-Ion Batteries

Li-ion batteries dominate the energy storage market, with a market share capacity of 1.66 GW. Their success is attributed to high efficiency, long lifecycle, and high power and energy density, driving their rapid growth [42]. Most commercial Li-ion batteries are made of a graphite anode, a cathode made of a lithium-containing transition metal oxide or phosphate, and a nonaqueous liquid electrolyte that conducts Li-ions. The main types used in stationary energy storage are lithium iron phosphate (LFP) and lithium nickel manganese cobalt oxide (NMC), with LFP being approximately 10% less expensive [50]. Li-ion batteries are highly scalable, easily bundled into containers and connected, similar to lead-acid batteries. Li-ion offers a fast response time of milliseconds to second and has a low self-discharge rate of 0.1-0.3% per day [48][47]. The charge and discharge cycles range from minutes to hours [47][45]. Despite high initial costs, the technology is mature, rated at a TRL of 9 [25][49][47]. However, challenges include the need for an advanced Battery Management System (BMS), thermal runaway risks, material scarcity, and recycling difficulties [52].

Sodium-Sulfur Batteries

Conventional secondary batteries, like lead-acid and Li-ion batteries, use a solid electrode and a liquid electrolyte. In contrast, the NaS battery employs a molten liquid electrode and a solid electrolyte. NaS batteries offer advantages such as a high specific energy, which is comparable to lead-acid batteries, and a very high discharge current density. However, NaS batteries also have significant disadvantages. NaS batteries operate at high temperatures between 300-350°C, where sodium and sulfur are liquid. A short circuit due to damaged ceramic electrolytes can cause sodium and sulfur to react violently, producing temperatures up to 2000°C and leading to severe safety issues. Additionally, these batteries have a low working rate, making them unsuitable for high power and fast charging and discharging [48]. NaS batteries are highly scalable and have a fast to medium response time [47]. NaS batteries have a high self-discharge rate of around 20% per day, which is really high and therefore not suitable for medium to long-term storage [48][47]. The charge and discharge cycles range from minutes to hours [45]. Although NaS has medium costs, their technology maturity is rated at 8 [25][49][47].

Nickel-Cadmium Batteries

The Ni-Cd battery comprises a positive electrode made of nickel oxyhydroxide and a negative electrode made of metallic cadmium, separated by a nylon divider. The electrolyte is aqueous potassium hydroxide, which remains stable during operation. During discharging, the nickel oxyhydroxide reacts with water to form nickel hydroxide and a hydroxide ion, while cadmium hydroxide forms at the negative electrode [45]. Ni-Cd batteries are relatively affordable and robust, offering the lowest cost per cycle. However, Ni-Cd has several drawbacks, including the memory effect, the harmful environmental impact of cadmium, and a high initial cost. Consequently, Ni-Cd technology is not highly recommended for renewable energy systems [53]. Ni-Cd batteries are highly scalable, like all the other electrochemical batteries. Ni-Cd has a fast response time ranging from milliseconds to seconds and a self-discharge

rate of 0.2-0.6% per day [47]. The charge and discharge cycles range from minutes to hours [45]. Despite their high initial costs, Ni-Cd batteries are a mature technology, rated at a technology maturity level of 9 [25][49][47].

Redox Flow Batteries

A Redox Flow Battery (RFB) functions as an electrochemical energy storage system with a unique design that separates the energy storage and conversion components. Unlike traditional batteries that use solid metals for the cathode and anode, RFBs utilize electrolyte solutions (catholytes and anolytes) to store energy. Electrical energy is stored in large-volume liquid electrolytes contained in separate tanks and converted to electricity in a stack of multiple cells, similar to fuel cells. The electrolytes are pumped through porous electrodes, with an ion-exchange membrane or porous separator preventing mixing. Electron-exchange chemical reactions occur on the electrode surfaces [54][55].

The separation between the components that manage power and those that store energy is a distinctive feature of RFBs, offering a significant advantage and making them an excellent option for energy storage across different scenarios [56]. RFBs can release energy over durations ranging from a few minutes to several hours and are designed to withstand both overload conditions and complete discharges without sustaining damage [57]. Due to their advantages, such as separate energy and power capacities, high safety, good efficiency, and extended cycle life, RFBs are highly suitable for incorporating renewable energy into the electrical grid. They are particularly effective for energy storage systems of up to 100 megawatts, capable of storing energy for 4 hours or more, making them ideal for data centers [58].

The two main types of flow batteries are the vanadium redox flow battery (VRFB) and the zinc-bromine hybrid flow battery (ZBFB) [43][42]. The main difference between them is that in VRFBs, energy is linked to the electrolyte volume and power to the electrode area, whereas in hybrid flow batteries, energy is limited by the size of the battery electrode [45].

Vanadium Redox Flow Batteries

VRFBs are a leading technology for large-scale energy storage among metal-based flow batteries and have been in commercial use in recent years [58]. VRFBs offer multiple advantages: they can last up to 20 years, their electrolytes can be reused, and their capacity can be increased, making them ideal for building energy storage stations ranging from a few kilowatts to 100 megawatts. VRFBs are also safe, less likely to catch fire, and can withstand complete discharge without harm. They are particularly efficient for storing energy in renewable sectors like solar and wind power. However, their high cost remains a significant barrier to widespread commercial use [59].

VRFBs are highly scalable, with adjustable sizes of the tank with electrolyte. Also, VRFBs have a fast response time of seconds and a very low self-discharge rate [48][47]. The charge and discharge cycles are multiple hours [47][45]. Despite moderate costs, VRFBs are considered mature technology with a technology maturity level of 8 [25][49].

Zinc-bromide Flow Batteries (ZBFB)

A key advantage of ZBFB is the abundance and low cost of the materials used, making them suitable for sustainable and economical energy storage solutions [60]. Multiple companies around the world, are developing and commercializing ZBFB, indicating growing interest and investment in this technology [60].

ZBFB is highly scalable, like the VRFB. ZBFB has a fast response time of seconds and a small self-discharge rate [48][47]. The charge and discharge cycles are also multiple hours [47][45]. The cost of a ZBFB is moderate costs, and their technology maturity is rated at 7 [25][49][47].

3.2.3. Electrical Energy Storage

Supercapacitors and Superconducting Magnetic Energy Storage

SC and SMES systems efficiently store electricity in electric and electromagnetic fields, respectively, with minimal energy loss. These technologies are particularly advantageous for the storage and rapid release of high energy levels in short bursts [43].

Both SC and SMES are scalable but are technologically and economically limited due to their low energy density. Therefore, the scalability score is set for both on 3. Their charge and discharge cycles range from seconds to minutes [47][45]. SC has a fast response time, with a self-discharge rate of 5-40% [48][47]. Although they are moderately costly, supercapacitors are a mature technology, rated at 8 in terms of maturity [25][49][47]. SMES have a self-discharge rate of 10-15% [47][48][45]. Despite their higher costs, SMES systems are considered a moderately mature technology, with a maturity level of 7. A limited number of small-scale SMES systems are now commercially available, primarily employed for power quality control in manufacturing settings, including microchip fabrication facilities [25][49][47].

3.2.4. Chemical storage

The main chemical storage technology is hydrogen energy storage. This is a process where energy is stored in the chemical bonds of molecules. An electrolyzer produces hydrogen by converting electricity into chemical energy. This produced hydrogen is stored under pressure in a hydrogen tank. This stored energy can be released by burning the hydrogen in a fuel cell when needed. Despite its benefits, such as the ability to transport and store energy and its non-toxic combustion product, hydrogen gas storage remains costly due to its expensive infrastructure [46]. However, hydrogen has no self-discharge and leakage from hydrogen tanks is minimal, so it is negligible. Moreover, the scalability of hydrogen is high. The size of the electrolyzer, storage, and fuel cell is easily adjustable to the requirements of the energy system. This makes it suitable for long-term storage. In the section below are the different types of electrolyzers described

Electroylzer

This section describes the different types of electrolyzers. The discharge time and self-discharge are not relevant parameters for electrolyzers, as they are conversion components instead of a storage components.

Alkaline Electrolyzer

Alkaline water electrolysis (AWE) dates back to 1789, credited to Troostwijk and Diemann, marking it as the pioneering technology in water electrolysis. Its longevity, non-reliance on expensive materials, and modular design have established alkaline electrolysis as the most mature and widely implemented technology for water electrolysis worldwide [61]. It currently represents nearly two-thirds of the global electrolyzer capacity [62]. This technology operates at low temperatures, typically between 60 to 80°C, using a 20%–30% KOH or NaOH solution as the electrolyte. Alkaline electrolyzers are noted for their durability, cost-effectiveness, and the absence of precious metal requirements in their components, making them a preferred choice in industrial applications. They can operate under near-atmospheric or increased pressures, up to 1.5 MPa [63]. The response time of the alkaline electrolyzer is medium. This electrolyzer technology is, compared to the other technologies, the cheapest technology. However, it is still expensive. Due to its maturity, the TRL is set to 9.

Proton exchange membrane Electrolyzer

Even though Proton exchange membrane water electrolyzers (PEMWE) are a relatively new technology, they account for 20% of the global capacity [62].PEM electrolyzers operate within a temperature range of 50–80 degrees Celsius and can reach current densities of up to 1 A/cm² [61]. In PEM electrolysis, water decomposes at the anode to produce protons, electrons, and oxygen. These protons and electrons traverse through the proton exchange membrane to the cathode, where hydrogen is produced. The core components of PEM electrolyzers include electrodes separated by a solid polymer electrolyte. This technology is known for its high efficiency, compact design, and fast response time to changing power inputs, making it suitable for dynamic applications such as energy storage in renewable power systems. The technology is more expensive than the alkaline electrolyzer [63]. Due to its wide usage and implementation, the TRL is set at 9.

Anion Exchange Membrane

Anion Exchange Membrane (AEMWE) water electrolysis offers several advantages, such as the use of cost-effective transition metal catalysts instead of noble metal catalysts, making it a high-performance yet low-cost alternative to conventional electrolysis technologies. Also, it has a high response time but not as fast as the PEM electrolyzer. Despite these advantages, AEMWE requires further investigation

and improvements in membrane stability and cell efficiency [63]. Moreover, the technology is still in developmental status, which makes it expensive to implement. Therefore, the TRL is set to 7 [64].

Solid Oxide Electrolyzer

Solid Oxide Ectrolyzer cells (SOEC) are unique because they use heat to generate hydrogen from steam. This makes them perfect for places with a heat source, like nuclear plants or industrial sites. They work at high temperatures, typically between 500 and 850 degrees Celsius, because they operate at higher temperatures, and the response time is slow [62]. This technology does not require noble metal electrocatalysts and provides high conversion efficiency. Despite these advantages, insufficient long-term stability has hindered the commercialization of solid oxide water electrolysis [63]. Consequently, the technology is still in the research and development phase, which makes it expensive. Therefore, the TRL is set to 7.

Fuel Cell

A fuel cell is essential for converting hydrogen produced by the electrolyzer and stored in the storage tank into usable power. There are different types of fuel cells, including Alkaline Fuel Cells, Polymer Electrolyte Membrane Fuel Cells (PEMFC), Phosphoric Acid Fuel Cells, Molten Carbonate Fuel Cells, and Solid Oxide Fuel Cells [65]. However, if hydrogen technology is to be applied in data centers, the PEM fuel cell should be considered. This is because data centers are already planning to use PEM fuel cells integrated for backup power [66]. Thus, analyzing other types of fuel cells is out of the scope of this research.

PEM Fuel Cell

PEM fuel cells are primarily used in transportation and stationary applications, such as backup power [67][65]. PEM fuel cells are highly popular because they use hydrogen as fuel and oxygen as the oxidant. These cells provide high power density and are lightweight and compact compared to other types of fuel cells. They utilize a solid polymer electrolyte and porous carbon electrodes that contain a platinum or platinum alloy catalyst. The advantages of the PEM fuel cell include quick response time. However, the catalyst of the fuel cell is expensive, which makes the overall cost high[68]. Due to the widely used application, the TRL of the PEM Fuel Cell is set to 9.

3.3. Selection of Technologies

This section is based on all the technologies described in section 3.2 technologies selected to comprise different configurations for data to be 100% renewable on an hourly basis. An overview of all the described technologies is shown in Table 3.1.

Mechanical storage components are highly scalable, except for FES. Technologies such as PHES, GES, and CAES are easy to scale up by increasing the reservoir, mass, or cavern size. While flywheel systems are modular, managing them on a large scale becomes technologically complex. Additionally, flywheels are not completely scalable and have a discharge time that is too short for energy systems. PHES, GES, and CAES depend on the geographical characteristics of the location, making them less adaptable. This results in the mechanical storage components being unsuitable for the data center's energy storage system.

Electrochemical technologies are all scalable and have a discharge time at the rated capacity ranging from minutes to hours, meeting the necessary requirements [47]. Both lead-acid and Li-ion batteries have a fast response time and a minimal self-discharge rate, and they are well-developed with a TRL of 9. Moreover, Poullikkas describes in their report that lead-acid batteries are currently used to stabilize wind farm power generation [45]. Therefore, it is interesting to research how lead-acid batteries would function in this energy system. The same applies to Li-ion batteries, which are already used in multiple energy storage systems.

Ni-Cd batteries, when assessed against the criteria, have approximately the same score as the Li-ion battery and Lead-acid Batteries. Recently, Ni-CD batteries have become popular for solar generation storage due to their ability to withstand high temperatures. However, they perform poorly during peak shaving applications, making them generally unsuitable for energy management systems. Moreover, cadmium is really harmful to the environment [47][45].

On the other hand, the NaS batteries have a very high self-discharge rate of around 20% per day, which is too high since the battery needs to store energy for days to weeks [47].

To strengthen this research, the number of technologies that are focused on is limited. Therefore, lead-acid and Li-ion batteries are chosen over Ni-Cd batteries. Besides, NaS batteries are unsuitable for this system due to their high discharge rate.

The VRFB and the ZBFB offer advantages such as flexible layout, long cycle life, quick response times, and no harmful emissions. They also offer low maintenance and tolerance to overcharge and/or over-discharge [45]. Therefore, they score high in scalability and response time. Moreover, the self-discharge is neglectable, and the discharge time at rated capacity can go up to hours. The most mature flow battery is the VRFB, which can operate efficiently on a large grid scale. VRFB also has a long cycle life. Zinc bromide batteries, which are hybrid flow batteries, are also commercially available. Although the cycle life of zinc bromide hybrid flow batteries is much shorter than that of vanadium, the materials cost is considerably lower [50]. Therefore, researching the VRFB and ZBFB is interesting.

Electrical components store energy with high power but for a short duration, with a high daily discharge rate. While this is beneficial for balancing an energy system, it is unsuitable for addressing daily or seasonal shortages.

Hydrogen storage is ideal for long-term storage with no energy losses over time due to neglectable leakage in the hydrogen tank. Moreover, the technology is highly scalable. The size of the electrolyzer storage tank and fuel cell is easily adjustable. Based on the TRL, the two most promising electrolyzer technologies are Alkaline and PEM. As a fuel cell, the PEM fuel cell has been selected for this system because it has already been implemented by data centers and, therefore, is not a choice in this research.

It can be concluded that the Li-ion, Lead-acid, VRFB, ZBFB, and hydrogen systems of an Alkaline and PEM electrolyzer with storage tank and PEM fuel cell are suitable technologies for the energy storage system of a data center, which can be renewable on an hourly basis.

Table 3.1: Energy Storage Technologies and Their Characteristics

Technology	Classification	Scalability	Response time	Self-discharge %/day	Discharge time at rated capacity	TRL	Location independence
PHS	Mechanical	5	Medium	Very small	hours to days	9	No
GES	Mechanical	3	Medium	Very small	hours to days	8	No
CAES	Mechanical	5	Medium	Small	hours to days	8	No
FES	Mechanical	3	immediately	100	Seconds to minutes	9	Yes
Lead-Acid	Electrochemical	5	Fast	0.1-0.3	Minutes to hours	9	Yes
Li-ion	Electrochemical	5	Fast	0.1-0.3	Minutes to hours	9	Yes
NaS	Electrochemical	5	Fast-Medium	20	Minutes to hours	8	Yes
Ni–Cd	Electrochemical	5	Fast	0.2-0.6	Minutes to hours	9	Yes
VRFB	Electrochemical	5	Fast	Very small	Hours	8	Yes
ZBFB	Electrochemical	5	Fast	Small	Hours	7	Yes
SC	Electrical	3	Fast	5-40	Seconds to minutes	8	Yes
SMES	Electrical	3	Fast	10-15	Seconds to minutes	7	Yes
AWE*	Chemical	5	Medium	-	-	9	-
PEMWE*	Chemical	5	Fast	-	-	9	-
SOEC*	Chemical	5	Slow	-	-	7	-
AEM *	Chemical	5	Medium-Fast	-	-	7	-
PEMFC *	Chemical	5	Fast	-	-	9	-

*indicates technologies that are used for energy conversion.

3.4. Configurations

The technologies described and selected in section 3.3 include Li-ion, lead-acid, VRFB, ZBFB, alkaline electrolyzers, PEM electrolyzers, storage tanks, and PEM fuel cells. With these technologies, 8 different configurations are made. These technologies are classified into two distinguished groups: batteries and hydrogen. The batteries are suitable for short-term storage and supply, while the hydrogen is used for long-term storage because of the lack of energy losses over time and the easily scalable size of the system's required storage system. Therefore, different configurations could be comprised. Each configuration integrates different types of batteries and electrolyzers. For every configuration, energy supply is consistently derived from wind and PV. A large tank is required to store the hydrogen produced by the electrolyzer efficiently. This tank serves as a reservoir for hydrogen. The PEM fuel cell is used to generate power during times of shortage, such as when batteries are empty during a long-term shortage. Table 3.2 shows these configurations.

Table 3.2: 8 Configurations of the Selected Technologies

Configuration	Energy Supply	Battery	Electrolyzer	Storage	Fuelcell
1	Wind + PV	Li-ion	Alkaline	Tank	PEM
2	Wind + PV	Lead-acid	Alkaline	Tank	PEM
3	Wind + PV	Li-ion	PEM	Tank	PEM
4	Wind + PV	Lead-acid	PEM	Tank	PEM
5	Wind + PV	VRFB	Alkaline	Tank	PEM
6	Wind + PV	ZBFB	Alkaline	Tank	PEM
7	Wind + PV	VRFB	PEM	Tank	PEM
8	Wind + PV	ZBFB	PEM	Tank	PEM

3.5. Data Collection

In this section, the energy profiles of solar, wind, and the data center are described based on their characteristics. The solar and wind profiles are used as inputs for the energy system, while the load profile represents the demand.

In Figure 3.1a and Figure 3.1b are the energy profiles of wind and solar energy shown. These profiles are derived from the actual output of wind and solar farms for the year 2019. The same weather year is chosen to take the correlation between solar irradiation and wind into account. the wind and solar profile data may not be shared and are therefore anonymized; only the weekly output of the energy profiles is presented. Additionally, the energy profiles are normalized by their installed capacity. So, the energy profiles in the figures represent the output of 1 kW(p) installed capacity.

The capacity factors for solar and wind profiles used in this research are 0.12 and 0.48, respectively. Figure 3.1b clearly shows the characteristics of a solar profile in the Netherlands, with a significant difference in energy output between summer and winter due to the country's high latitude. The wind profiles in Figure 3.1b show that the Netherlands has a more constant output throughout the year, although they show more weak fluctuations compared to the solar profile. Wind output is slightly lower in the summer than in the winter months. Therefore, a combination of wind and solar as inputs for the energy system is considered suitable.

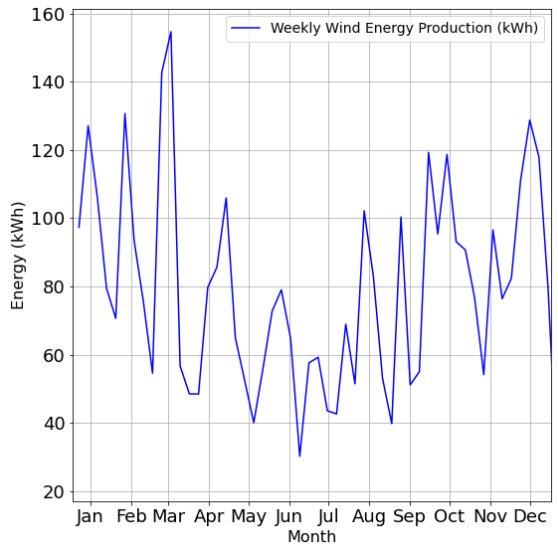

(a) Wind Energy Generation profile in the Netherlands for 1 kW installed capacity

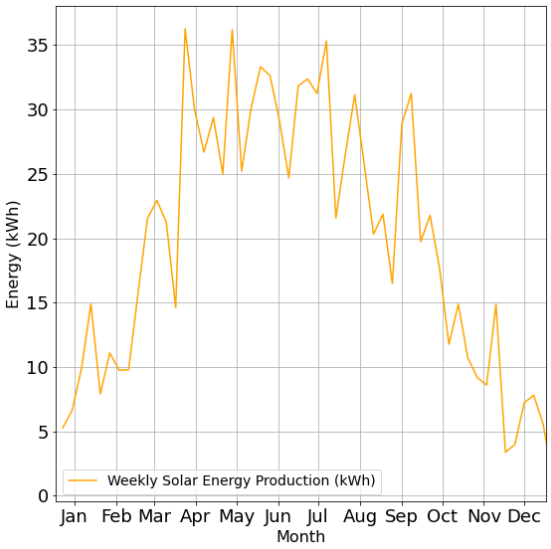

(b) Solar Energy Generation profile in the Netherlands for 1 kWp installed capacity

Figure 3.1: Energy Generation Profiles for Wind and Solar in the Netherlands

The data of the energy profile of the data center has been provided by Repowered [40]. The energy profile of the data center is shown in Figure 3.2. Also, the data of the energy profile may not be shared, and therefore, the weekly average is presented. Moreover, the profile used is normalized by the average output and scaled to represent a 100 MW data center. The energy profile of the data centers shows that it consume more energy in the summer than in the winter due to the increased cooling needs during warmer months. However, the average weekly load remains relatively constant throughout the year.

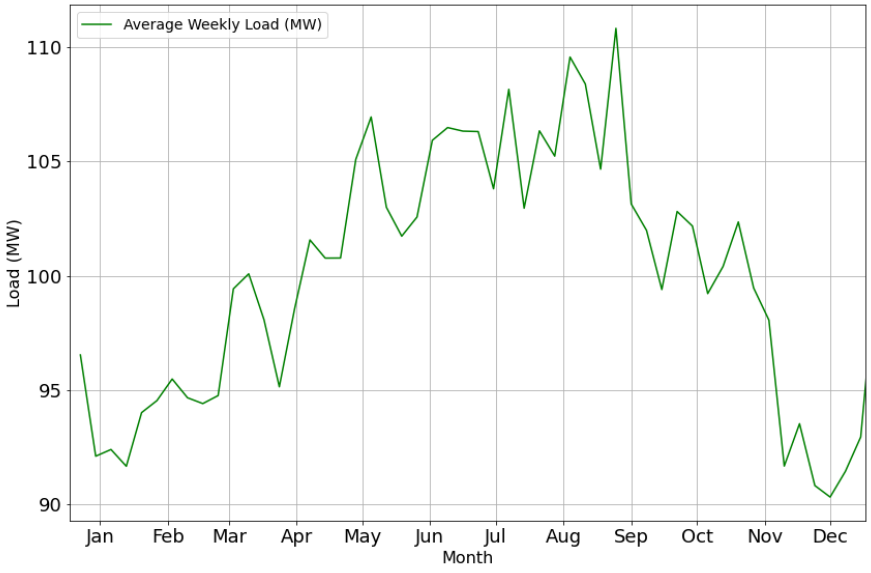

Figure 3.2: Energy Profile of a 100 MW Data Center in the Netherlands

3.6. Technical Parameters of the Assets

In this section, the technical parameters and limitations of each asset in the energy system are described. These parameters and limitations are used as input in the model. First, in subsection 3.6.1, the parameters of the Li-ion, Lead-acid, VRFB, and ZBFB batteries are detailed. Next, in subsection 3.6.2, the parameters of the Alkaline and PEM electrolyzers are provided, followed by the parameters of the storage tank in subsection 3.6.3. Lastly, in subsection 3.6.4, the parameters of the PEM fuel cell are described.

3.6.1. Batteries

This section describes the parameters of the batteries used in the model. The parameters considered for the batteries are efficiency, minimum and maximum SoC, cycle life, and end-of-life (EOL) capacity, which determines the degradation during the battery's lifetime.

Lithium-ion and Lead-Acid Battery

This section discusses the technical characteristics of Li-ion and lead-acid batteries. Li-ion batteries have a higher efficiency than lead-acid batteries. The round-trip efficiency for Li-ion batteries is 85%, while it is 72% for lead-acid batteries [69][29]. The depth of discharge (DoD) of the battery impacts degradation over time. Therefore, it is important to consider DoD as a parameter. The DoD is the range between the max and min SOC of the battery. Li-ion battery parameters are set at DoD of 0.7, resulting in a minimum and maximum SoC at 0.2 and 0.9 [40]. Considering these limits, the battery's capacity will decrease to 0.8 of the initial capacity of approximately 2000 cycles [20]. Based on the analysis of various datasheets for lead-acid batteries, it has been determined that at a DoD of 0.5, the battery's capacity reduces to 60% after 500 cycles [70][71][72]. This sets the minimum and maximum state of charge at 0.4 and 0.9.

For the Li-ion battery, it is chosen to replace the battery when the capacity decreases to 80% of its initial value. In contrast, for the lead-acid battery, replacement occurs when the capacity decreases to 60%. The higher EOL capacity for the Li-ion battery is selected due to its lower degradation rate of 0.01% per cycle compared to 0.08% per cycle for the lead-acid battery. Furthermore, the usable capacity of the lead-acid battery is limited by its lower DoD. Consequently, with the same installed capacity, the lead-acid battery will cycle more frequently. Therefore, an EOL capacity of 60% is considered for the lead-acid battery to reduce the frequency of replacements. In Table 3.3 are the discussed parameters summarized.

Vanadium Redox Flow Battery and Zinc Bromide Flow Battery

In this section, the technical parameters of VRFB and ZBFB are discussed. The round-trip efficiency of VRFB is approximately 75%, while ZBFB achieves a similar efficiency of 74% [37]. The VRFB has a long lifetime and cycle life compared to most other battery technologies, such as Li-ion and lead-acid batteries [54]. According to Doetsch and Pohlig, these batteries have negligible electrolyte degradation, allowing them to last for decades without replacement. ZBFB has a shorter cycle life, around 4,500-5,000 cycles. Both battery types have good circulation performance, and a 100% DoD does not damage them. The state of charge for both VRFB and ZBFB is set between 0% and 100% [48]. For both batteries, it is assumed that there is no degradation, and the EOL is set to 100%. This means that the performance of the battery remains constant. However, the battery is replaced when the cycle life is exceeded. The parameters discussed are summarized in Table 3.3.

Table 3.3: Battery Model Parameters

Li-ion and Lead-acid Battery Model Parameters					
Parameter	**Abbreviation**	**Unit**	**Li-ion**	**Lead-acid**	**Source**
Capacity	C	kWh	Variable	Variable	
Efficiency	η	%	85	72	[69]
Minimum SoC	SoC_{min}	%	20	40	[69][37]
Maximum SoC	SoC_{max}	%	90	90	[69][37]
Cycle Life	$N_{\text{cycle life}}$	-	2000	500	[20][37]
Capacity End Of Life	C_{EOL}	%	80	60	[20][37]
Vanadium and Zinc-Bromide Flow Battery Model Parameters					
Parameter	**Abbreviation**	**Unit**	**Vanadium Flow**	**Zinc-Bromide Flow**	**Source**
Capacity	C	kWh	Variable	Variable	
Efficiency*	η	%	74	75	[73][37]
Minimum SoC	SoC_{min}	%	0	0	[74][37]
Maximum SoC	SoC_{max}	%	100	100	[74][37]
Cycle Life	N_{cycles}	-	10000	4750	[74][37]
Capacity End Of Life	C_{EOL}	%	-	-	[74][37]

* In the models, $\eta_{\text{discharge}}$ and η_{charge} are used.This is equal to $\eta^{0.5}$.

3.6.2. Electrolyzer

This section describes the parameters of Alkaline and PEM electrolyzers. First, the efficiency curves are detailed. Then, the other key parameters, such as peak efficiency, efficiency degradation, and operation hours, are discussed.

Efficiency of electrolysers

The Faraday efficiency, or current efficiency, measures the actual hydrogen output of an electrolyzer against its theoretical potential, accounting for losses due to parasitic currents [75][76]. Voltage efficiency, distinct from DC efficiency, evaluates energy utilization by comparing the thermoneutral voltage (typically 1.48 V) to the actual cell voltage [76]. Besides the intrinsic losses within the electrolyzer cell, there are additional losses in the electrolyzer system and auxiliary components. The efficiency curves for alkaline and PEM electrolyzers, as detailed in the report by Marocco et al., are used for in this model [29]. These curves are fitted and adjusted based on the High Heating Values (HHV). In this model, the efficiency of the HHV is used, while in the report of Marocco et al. is, the Lower Heating Value (LHV) used. The efficiency of the electrolyzer is displayed in a Figure 3.3, where efficiency is plotted on the y-axis against the normalized load on the x-axis. The normalized load extends from the minimal operational load to 1, representing the maximum capacity of the electrolyzer. Below the minimal operational is no efficiency because the electrolyzers are turned off.

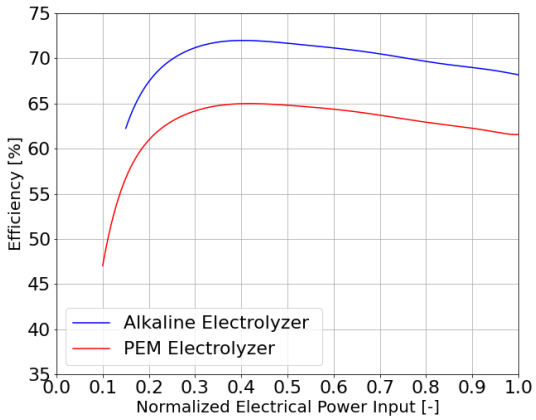

Figure 3.3: Efficiencies of the Alkaline and PEM Electrolyzers Versus Normalized Load (HHV)

Parameters of the Electrolyzer

This section describes the parameters of Alkaline and PEM electrolyzers, outlined by Marocco et al. PEM electrolyzers can operate at a lower minimum capacity of 10%, compared to 15% for Alkaline, offering operational flexibility. Alkaline electrolyzers have a higher peak efficiency of 72%, whereas PEM electrolyzers have a lower peak efficiency of 65%. Additionally, PEM electrolyzers have a higher efficiency degradation rate of 0.25% compared to 0.13% for Alkaline per 1,000 hours. Alkaline systems also have a higher operational lifetime than the PEM electrolyzer, approximately 80.000 hours against 40,000 hours [29]. This means that when the peak efficiency decreases to 90% of the initial peak efficiency, the stacks of the electrolyzer are replaced to maintain high performance. In Table 3.4 are the key parameters of the electrolyzer summarized

Table 3.4: Technical Parameters of Alkaline and PEM Electrolyzers

Parameter	Abbreviation	Alkaline	PEM	Reference
Maximum Capacity	$C_{\max}$	variable	variable	-
Minimum Capacity (% of Max)	$C_{\min}$	15%	10%	[29]
Efficiency at Peak	η_{peak}	72%	65%	[29]
Efficiency Degradation (%/1,000h)	$\Delta\eta_{1,000h}$	0.13%	0.25%	[29]
Total Operating Hours	$N_{\text{h,tot,EL}}$	80,000 h	30,000 h	[29]

3.6.3. Storage Tank

This section describes the technical parameters of the hydrogen storage tank. These parameters include the tank's maximum capacity, maximum pressure, and minimum and maximum SoC. The SoC ranges from 0 to 1, indicating the tank's full usable capacity. Hydrogen is stored at a maximum pressure of 300 bar to minimize the required storage volume.

Storing hydrogen is challenging due to its low density. At room temperature and atmospheric pressure, hydrogen gas occupies over 11 m³ per kilogram. To make storage economically viable, hydrogen must be compressed to increase its density [77]. The parameters used in the model are summarized in Table 3.5.

Table 3.5: Technical Parameters of the Hydrogen Storage Tank

Parameter	Symbol	Value	Unit
Maximum Capacity	C_{max}	Variable	tonne
Maximum Pressure	P_{max}	300	bar
Minimum State of Charge (SoC)	SoC_{min}	0	-
Maximum State of Charge (SoC)	SoC_{max}	1	-

3.6.4. Fuel Cell

This section describes the parameters of the PEM Fuel Cell. First, the efficiency curves is shown. Then, other key parameters, such as peak efficiency, efficiency degradation, and operation hours, are discussed.

Efficiency of the Fuel Cell

The model describes the efficiency curve for the PEM fuel cell as outlined in the report by Marocco et al. These curves are fitted similarly to the electrolyzer's, described in subsection 3.6.2. The model uses efficiency considering the Lower Heating Value (LHV), similar to the methodology used by Marocco et al. The fuel cell's efficiency is shown in Figure 3.4, plotting efficiency on the y-axis against normalized load on the x-axis.

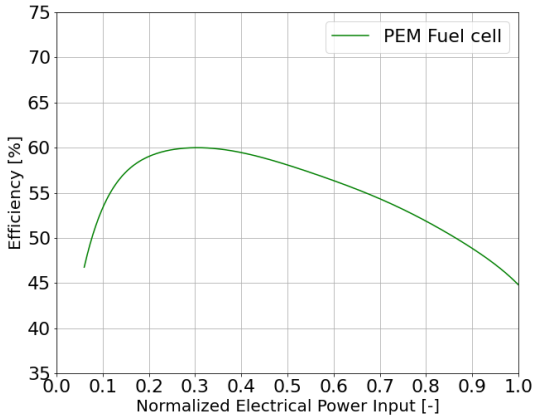

Figure 3.4: Efficiencies of the PEM Fuel Versus Normalized Load (LHV)

Parameters of the Fuel Cell

The range of normalized load begins at a minimal operational load of 6%, extending to 1, denoting the fuel cell's full capacity [29]. This shows that the fuel cell has a wider operation range compared to the electrolyzer. The report by Stropnik et al. investigates the degradation of the PEM fuel cell. The report concludes that the dynamic operation of the PEM fuel cell results in an average degradation rate of energy efficiency of 0.88% per 1000 hours of operation. In contrast, for steady-state operation, the degradation rate of PEM fuel cell efficiency is 0.28% per 1000 hours. This finding establishes that dynamic operations cause a higher degradation rate [78]. The stacks of the fuel cell are replaced when the initial peak efficiency decreases to 90% of its initial efficiency. An overview of the parameters is shown in Table 3.6.

Table 3.6: Technical Parameters of the PEM Fuel Cell

Parameter	Abbreviation	Value	Reference
Minimum Capacity (% of Maximum)	$C_{\text{min}}\%$	6%	[29]
Efficiency at Peak	η_{peak}	60%	[29]
Efficiency Degradation (%/1000 h)	$\Delta\eta_{1000h}$	0.88	[78]
Operating Hours	$N_{h,tot,FC}$	11300	

3.7. Economic Parameters of the Assets

In this section, the costs associated with all assets within the system are described, which impact the overall cost of the data center. The costs consist of investment and operating and maintenance (O&M) costs. The O&M cost is cost per year (yr). For assets with degradation, replacement costs are determined. The lifetime of the assets is also determined, which is important for calculating the residual cost of the assets after the 10-year simulation. Initially, subsection 3.7.1 describes the parameters of solar and wind energy. The parameters of different types of batteries are detailed in subsection 3.7.2, while subsection 3.7.3 focuses on the parameters of electrolyzers. Then, subsection 3.7.4 outlines the cost of the fuel cell and storage tanks. Lastly, subsection 3.7.5 looks into the cost of connection and transport, which are considerable at this scale of connection.

3.7.1. PV and Wind powerplants

For onshore wind energy, the investment costs and O&M costs have decreased due to the scale of economics, increased competitiveness, and the sector's maturing nature [79]. PV technology has also experienced a significant downward trend in module costs. This one has demonstrated the highest learning rates among all renewable energy technologies. In Europe, the prices for crystalline silicon modules dropped by 88% to 94% between December 2009 and December 2022 [79].

The costs associated with renewable energy sources are detailed in a report by IRENA, which provides estimates for the installation costs of wind energy. According to this report, the average installation cost for onshore wind energy in Europe is approximately 1640 €/kW. In contrast, for PV technology, the average price in the Netherlands is significantly lower, at about 730 €/kWp at the utility-scale, as currently reported by Repowered [40].

Furthermore, a techno-economic analysis by Fabianek and Madlener suggests that the O&M costs for wind energy are approximately 5% of the total investment cost, resulting in an 82 €/kW/yr. For PV systems, it is estimated the total O&M costs are at about 2% of the investment cost. This results in an O&M cost of 15 €/kWp/yr [40].

The lifetime of solar panels is typically 30 years [81], representing the average operational duration. Wind turbines have a minimum lifetime of 20 years, extending up to 25 years. Due to improvements in technology, the lifetime of newly installed turbines is considered to be 25 years [82].

3.7.2. Batteries

Lithium-ion and lead-acid batteries

In this section, the cost of the Li-ion and Lead-acid are determined. Li-ion battery systems costs have been reduced over recent years, caused by declines in component costs, system integration improvement, and distribution advancements. However, commodity prices for battery materials surged in 2021 due to escalating demand for Li-ion battery systems in both the stationary and larger vehicle markets [37]. Although the technology of stationary lead-acid batteries is well-established, manufacturers continue to innovate and increase competition with other battery technologies. Efforts are being made to enhance performance and further reduce costs [83].

Due to price reduction in Li-ion batteries, producers capable of delivering large-scale systems with capacities exceeding 10 MWh can now offer prices of around 245 €/kWh [40]. This price is for a battery with a C-rate of 1/4. In comparison, the cost of lead-acid batteries remains slightly higher, at approximately 290 €/kWh [29]. The annual O&M costs for both Li-ion and lead-acid batteries are estimated to be comparable, at 10 €/kWh/yr [24][29].

The cost breakdown for both Li-ion and lead-acid battery systems includes capital costs of the energy storage system, power conversion, balance of plant, and construction. This is detailed in the report by Mongird et al. Due to the frequent use and cycling of these batteries, they degrade over time and must eventually be replaced. The replacement costs for these batteries account for approximately 50% of the initial investment for both Li-ion and lead-acid batteries [29].

The system's lifetime, so all the other components of the assets are assumed to have a lifetime of 20 years. Critical components like inverters and power conversion systems play significant roles in the overall durability and performance of the battery systems, influencing operational efficiencies and lifecycle costs.

Vanadium and Zinc-Bromide Redox Flow batteries

In this section, the costs of the VRFB and ZBFB are determined. The investment costs of redox flow batteries vary significantly with increasing discharge time. This is because the components that manage power and those that store energy are distinct[56]. Therefore, an initial analysis for the VRFB is executed for different prices and discharge durations. Based on these analyses, the most cost-effective and feasible C-rate for the battery configuration is determined.

The different prices for the different C-rates are shown in Table 3.7. During the test run, the installed capacity of the battery increased up to a C-rate of 1/6. However, the price reduction and increased installed capacity did not result in a LCOE. This is because the capacity of the electrolyzer and the storage tank did not decrease sufficiently, and the fuel cell remained the same to compensate for long-term shortages when the batteries were empty. As a result, the C-rate of the redox flow batteries is also set at 1/4. Therefore, the price of the VRFB is set at 465 €/kWh [37].

Table 3.7: Overview of the Investment Cost of VRFB for Different C-Rates

C-rate	Vanadium (€/kWh) [37]
1/4	465
1/6	420
1/8	395
1/10	380

The ZBFB is a promising technology due to the lower prices of the materials from which the battery is made. Despite the lower cost of materials, the costs of these ZBFBs remain higher than those of the VRFB [84]. This is because the VRFB is more developed and thus has experienced lower manufacturing costs than the ZBFB. The price of the ZBFB with a C-rate of 1/4 is set at 560 €/kWh [84].

Additionally, the O&M cost of VRFB and ZBFB is 10.5 €/kWh/yr, with a lifetime of 20 years. Notably, there are no replacement costs associated with VRFB and ZBFB, as they degrade minimally over time [37].

3.7.3. Alkaline and PEM Electrolyzer

In this section, the costs associated with the Alkaline and PEM electrolyzer are described. The alkaline electrolyzer is a mature and well-established technology that is scalable up to a MW capacity. It is widely used for industrial applications, offering lower costs compared to newer commercialized technologies such as the PEM electrolyzer, which has higher component costs [85]. The cost drivers in these systems include the stacks, power electronics, and gas conditioning [86].

The capital costs for alkaline and PEM electrolyzers are set at 765 €/kW and 1300 €/kW [86][40]. The O&M costs for both types of electrolyzers are estimated at 2% of the initial investment annually, resulting in O&M costs of 15 €/kW/yr for alkaline and 26 €/kW/yr for PEM electrolyzers [40]. The higher costs associated with PEM electrolyzers are largely attributed to the use of expensive platinum-group metals [86].

A cost breakdown for alkaline and PEM electrolyzers categorizes expenses into four main components: the electrolyzer stacks, power electronics, gas conditioning, and balance of plant [86]. The power electronics, which include rectifiers and transformers, convert AC to DC and manage voltage levels. Gas conditioning involves compressing the gas to suitable storage pressures and purifying the produced hydrogen by drying. The balance of the plant contains support components that do not directly contribute to hydrogen production, such as heat management, control systems, safety measures, and power distribution infrastructure. The stack is the primary cost driver in both alkaline and PEM systems. In an electrolyzer with a scale of around 1 MW, the stack accounts for 40 to 60 percent of the total costs for both alkaline and PEM electrolyzer systems. Additionally, a cost breakdown for a 100 MW electrolyzer shows that as the scale increases, the proportion of costs attributed to the stack also rises, accounting for 72% in alkaline and 82% in PEM systems [86]. This is because scaling the electrolyzer necessitates scaling the stacks linearly, but this is not the case with their surrounding components.

As discussed in Equation 2.4.2, the degradation of electrolyzer performance is caused by operating hours. This necessitates stack replacement when performance falls below a critical threshold to restore efficiency to original levels. The replacement cost for stacks is 551 €/kW for alkaline and 1066 €/kW for PEM electrolyzer. If the stacks are not replaced within 10 years. It is assumed that there is no economic value left. The lifetimes of other system components are estimated at 20 years [86].

3.7.4. Fuel cell and hydrogen storage tank

This section describes the cost of the fuel cell and the hydrogen storage tank. Over the past decade, significant advancements have been made in reducing the costs of PEM Fuel Cells [87].

The initial cost of the PEM fuel cell is slightly higher than that of the PEM electrolyzer, approximately 2000 €/kW [40]. The O&M costs are equal to those of the electrolyzer, at 2%. This results in an O&M cost of 40 €/kW/yr.

The costs associated with a PEM fuel cell are categorized into four parts: the stack, balance of plant, system balancing, and water management. The stack, the core component where electrochemical reactions generate electricity, is crucial. The balance of the plant includes air, fuel, and thermal management systems, along with necessary assembly components that ensure optimal airflow, fuel delivery, and temperature control for efficient operation. System balancing involves regulating the equilibrium between different subsystems for stable operation. Lastly, water management is essential for controlling water production and utilization. According to [87], the stack accounts for 50% of the cost breakdown, similar to a 1 MW electrolyzer as described in subsection 3.7.3. It is assumed that when the fuel cell is scaled to a 100 MW scale, the share of the stacks in the fuel cell increases to 80%, based on the report by [79]. Consequently, the replacement cost of the stacks when they degrade is 80% of the investment cost of the fuel cell, set at 1600 €/kW. The lifetime of the other components of the fuel cell is set at 20 years.

For the hydrogen tank capable of storing hydrogen at a pressure of 300 bar, it is assumed that the investment cost is 700 €/kg, and the O&M costs are 3% of the investment cost [40]. This sets the O&M cost at 21 €/kg/yr [40]. The lifetime of such a tank is approximately 30 years [20].

3.7.5. Connection and transport cost

The costs related to the electrical grid represent an important share of the total operational costs for data centers. An annual fixed price is charged to maintain the connection. These fixed prices, known as the periodic connection price, cover management, maintenance, and potential replacement of the connection [21][22][23]. Although this annual fixed price costs several thousand euros per year and looks high, it is relatively small in the context of total costs. Therefore, this cost is neglected. Besides, data centers must pay a monthly fee for their connection to the electricity grid. This consists of two fees. One fee is based on the amount of power that is contracted, and the other is the peak in power consumption within a month. In Table 3.8 is an overview of the rates for the three largest network operators in the Netherlands:

Table 3.8: Monthly Prices of Contracted Power and Maximum Power for the Three Largest Network Operators in the Netherlands

Network Operator	Contracted Power (€/kW/month)	Max Power (€/kW/month)	Source
Enexis	3.10	3.81	[21]
Liander	3.65	5.06	[22]
Stedin	3.54	4.72	[23]
Average	3.43	4.53	

3.7.6. Overview of the Economic Parameters

This section provides an overview of the economic parameters of all the assets. In Table 3.9 are the parameters such as investment cost, O&M costs, replacement cost, and the lifetime of systems summarized.

Table 3.9: Overview of the Economic Parameters of Assets

Asset	C_{invest}	$C_{\text{O\&M}}$	$R_{\text{replacement}}$	L_{system}	**Reference**
PV	730 €/kWp	15 €/kWp/yr	-	30 years	[40][79][80][81]
Wind	1640 €/kW	82 €/kW/yr	-	25 years	[40][79][80][82]
Li-ion Battery	245 €/kWh	10 €/kWh/yr	122.5 €/kWh	20 years	[29][40][24][25]
Lead-acid Battery	290 €/kWh	10 €/kWh/yr	145 €/kWh	20 years	[29][40][24][25]
VRFB	465 €/kWh	10.5 €/kWh/yr	-	20 years	[37][84][40]
ZBFB	560 €/kWh	10.5 €/kWh/yr	-	20 years	[37][84][40]
Alkaline Electrolyzer	765 €/kW	15.3 €/kW/yr	551 €/kW	20 years	[86][40][88]
PEM Electrolyzer	1300 €/kW	26 €/kW/yr	1066 €/kW	20 years	[86][40][88]
Hydrogen Tank	700 €/kg	21 €/kg/yr	-	30 years	[40]
PEM Fuel Cell	2000 €/kW	40 €/kW/yr	1600 €/kW	20 years	[40][20]
Connection Cost	-	95.5 €/kW/yr	-	-	[21][22][23]

3.8. Emission Parameters of the Assets

In this section, the parameters for the environmental assessment focusing on CO_2 emissions (CO_2e) are described. This analysis evaluates the environmental impacts of these systems from cradle to grave. The results for wind turbines and PV panels are detailed in subsection 3.8.1. In subsection 3.8.2, the emissions of Li-ion batteries and VRFB are described. The hydrogen installation, consisting of alkaline electrolyzers, storage tanks, and PEM fuel cells, is described in subsection 3.8.3. Lastly, an overview of all the CO_2e of the assets is provided in subsection 3.8.4.

3.8.1. Wind and PV

This section compares the emissions of wind turbines and solar panels based on different studies, focusing on the different types and capacities of these renewable energy sources.

In the report by Besseau et al., the emissions of a wind turbine are compared with those in the study by Burger, Bauer, and Scherrer [89][90]. The studies provide emission values for different types and capacities of wind turbines as follows:

- For a 1-3 MW onshore wind turbine, the emissions are 609 and 730 kg CO_2e/kW.
- For an onshore turbine of 3 MW or greater, the emissions are 833 and 962 kg CO_2e/kW.
- For an offshore turbine of 1-3 MW, the emissions are 817 and 981 kg CO_2e/kW.

Based on these values, a reasonable approximation for the emissions of an onshore wind turbine that is used in the model can be estimated. A 3 MW onshore turbine has higher emissions than a 1-3 MW onshore turbine, and offshore turbines generally have higher emissions. An onshore wind turbine that is now built has a higher capacity than 3 MW. Therefore, emissions would likely fall between the higher capacity onshore 3 MW or greater. Therefore, it is estimated to be approximately 830 to 1000 kg CO_2e/kW.

In the report by Müller et al., the emissions of solar panels are described based on the type of solar panel and the country of production. The study highlights that production in China has higher emissions due to an energy mix with higher CO_2 rates. The report describes two types of panels: the glass-backsheet models and the glass-glass modules [91]. The glass-glass modules have a lower CO_2e/kWp. However, in this research, data from the glass-backsheet models are used because they are cheaper and more commonly used. The emission values for different types of glass-backsheet solar panels produced in various locations are as follows:

- For glass-backsheet modules [91]:
  - Produced in China: 810 kg CO_2e/kWp.
  - Produced in Germany: 580 kg CO_2e/kWp.
  - Produced in the EU: 480 kg CO_2e/kWp.

Based on these values, a good approximation for the emissions of solar panels in my analysis should consider the range between the minimum and maximum values observed. Therefore, an emissions range of 480 to 810 kg CO_2e/kWp is used for solar panel production.

3.8.2. Lithium-ion and Vanadium Redox Flow battery

The following section discusses the CO_2e associated with Li-ion and VRFB battery production, highlighting the impact of production location, battery type, and specific manufacturing processes on the overall environmental footprint.

The CO_2 emissions during the battery production stage mainly come from mining and transporting raw materials [92]. Most Li-ion batteries are manufactured in China, where the grid mix is highly carbon intensive. In 2020, China's electricity mix consisted of 76.6% conventional sources, primarily coal, and 23.4% green power generation [93]. This carbon-intensive grid mix directly impacts the CO_2e of battery production [94]. In contrast, in countries with a low-carbon electricity mix, like Sweden, the CO_2e impact is mostly from materials production [92]. Therefore, the carbon footprint of Li-ion batteries can differ a lot between countries because of different production methods and manufacturing processes.

The report by Zhao et al. analyzes the CO_2e of Li-ion batteries based on various factors, including battery type and production location. The studies provide emission values for different types of Li-ion batteries, ranging from 5.40 to 1,730 kg CO_2e/kWh, with an average value of 187 kg CO_2e/kWh [94].

Li-ion batteries based on lithium iron phosphate (LFP) cells are currently used for stationary applications [95].LFP batteries are considered in the report by Komesse et al. In this report, a range of 6.16 to 340.0 kg CO_2e/kWh is given for cradle-to-grave emissions [94].

Another report estimates cradle-to-grave emissions for Li-ion batteries to be 200–225 kg CO_2e/kWh. This report also describes the emissions per component, indicating the replacement emissions when it degrades. It is concluded that 40-50% of the total CO_2e are assigned to the battery, with the other half due to the inverter module, assembly of the container, and Battery Mangement System [96].

In the report by Komesse et al., the cradle-to-grave CO_2e/kWh emissions are also described. This report assumes a 20-year lifetime with one replacement, resulting in total emissions of around 380 kg CO_2e/kWh with the replacement taken into account. The report states that around 140 kg CO_2e is attributed to the replacement. This results in CO_2e without replacement of 240 kg CO_2e/kWh is.which means that a replacement results in approximately 50-60% additional CO_2e,[95].

Overview of the numbers that are discussed:

- 187 kg CO_2e/kWh on average, and for an LFP battery, 6.16–340.0 kg CO_2e/kWh [94].
- 200–225 kg CO_2e/kWh (replacement 40-50%)[96].
- 240 kg CO_2e/kWh for the battery system and 140 kg CO_2e/kWh for one replacement (replacement 50-60%) [95].

The values range from 6.16 to 340 kg CO_2/kWh. An additional 40% to 60% of CO_2e is added for a replacement. Based on these studies, a reasonable range for the CO_2e of Li-ion batteries from cradle-to-grave can be estimated. A range of 190-240 kg CO_2/kWh is taken with a 50% additional emission for a replacement in a range of 95-120 kg CO_2/kWh.

VRFBs contribute to CO_2e through various processes, with the production of vanadium electrolytes being a significant factor. The primary production of vanadium pentoxide (V_2O_5), a key electrolyte component, is associated with the steelmaking process in South Africa. The extraction of V_2O_5 from ore is inefficient and energy-intensive, leading to higher emissions. South Africa's electricity mix is 71% more kg CO_2e/kWh intensive compared to Europe, primarily due to the coal-based ore preparation and energy demand for the furnace in the pre-kiln stage [97].

The report by Weber et al. describes the cradle-to-gate analysis of a VRFB in terms of CO_2e per used capacity[98]. The emissions are 38.2 kg CO_2e/MWh. The report assumes a battery cycle rate of 1.12 cycles per day over a 20-year lifetime with an efficiency of 75%. Using these parameters, the total CO_2e per installed capacity (kWh) is approximately 235 kg CO_2/kWh.

In the report by Blume et al., a similar analysis is done. The cradle-to-gate CO_2e per MWh discharge energy is approximately 37 kg CO_2e, similar to the previous study. However, this report assumes a total of 20,000 cycles instead of 8,176 cycles. Additionally, the CO_2 emissions for the electrolyte are assumed to be twice as high compared to Weber et al. This report also includes an analysis of energy losses due to efficiency and end-of-life emissions. The losses due to efficiency are excluded because PV and wind are analyzed separately. The end-of-life emissions are included, which account for an additional 3 kg CO_2e/MWh. This represents approximately 7.5% of the total emissions of 40 kg CO_2e/MWh . With an efficiency of 75% and 20,000 cycles, the total emissions per installed capacity of the battery during the entire life is estimated to be 600 kg CO_2/kWh.

Two other reports, which are less detailed in their calculations, provide values of 173 kg CO_2e/kWh for cradle-to-cradle and 184 kg CO_2e/kWh for cradle-to-gate emissions [99] [100].

Overview of the numbers that are discussed:

- 235 kg CO_2e/kWh (cradle-to-gate) [98].
- 600 kg CO_2e/kWh, including end-of-life (7.5%) (cradle-to-grave) [97].
- 173 kg CO_2e/kWh (cradle-to-grave) [99].

- 184 kg CO_2e/kWh (cradle-to-gate) [100].

The values range from 173 to 600 kg CO_2e/kWh. Based on these studies, a reasonable range for the CO_2e of VRFBs from cradle-to-grave can be estimated. The value of 600 kg CO_2e/kWh appears to be an outlier. However, it is important to consider end-of-life emissions. Excluding the outlier value of 600 kg CO_2/kWh, the remaining values suggest a range from 173 to 235 kg CO_2/kWh. Including end-of-life emissions, a range of 220 to 280 is estimated.

3.8.3. Hydrogen

This section evaluates the carbon emissions of alkaline electrolyzers, storage tanks, and PEM fuel cells, focusing on the environmental impacts of manufacturing of the assets and replacement of the stacks.

Electrolyzer

The report by Khan et al. describes the CO_2e of an alkaline electrolyzer. The emissions are estimated to be between 0.1 and 0.2 kg CO_2e per kg of hydrogen produced. It is assumed in the paper that over the lifetime of the alkaline electrolyzer, 1,000 tonnes of hydrogen are produced with a 1 MW electrolyzer. This results in 100-200 kg CO_2e per kW installed capacity of the electrolyzer [101].

The report by Tripathi and Subramanian calculates the CO_2e for a 100 MW alkaline electrolyzer. The CO_2e are discussed regarding the balance of the plant and the stacks. From these numbers, it can be determined that the stacks contribute approximately 80% of the total emissions. The total emission is estimated to be between 200 and 240 kg CO_2e per kW installed capacity [102].

Overview of the numbers that are discussed:

- 100-200 kg CO_2e per kW installed capacity [101]
- 200-240 kg CO_2e per kW installed capacity (80% from stacks) [102]

Based on these numbers, a range of 100-240 kg CO_2 per kW installed capacity can be estimated. The replacement of stacks contributing approximately 80% of the emissions sets the replacement emissions between 80-190 kg CO_2 per kW.

Storage Tank

Multiple large tanks are required to store the hydrogen at a high pressure of 300 bar. Limited literature exists on the environmental analyses of hydrogen storage at this pressure. In the report by Bionaz et al., a small tank with a capacity of 100 kg hydrogen at 45 bar is described, with emissions calculated at 680 kg CO_2e/kg H_2 storage [103]. In the report by Mori et al., around 20% of the emissions are attributed to the storage tank, amounting to 75 tonnes of CO_2e. The storage tank has a capacity of 20 m³ at 25 bar, storing approximately 40 kg of hydrogen. This results in 1,875 kg CO_2e/kg H_2 storage [104].

Different types of hydrogen tanks are considered for the safety of vehicles. In the report by Cheng et al., emissions are considered in terms of CO_2 equivalent per kg of stored hydrogen. Type II hydrogen tanks, which are all-metal cylinders with carbon fiber or glass fiber filament wrapped around their straight body part, are used for stationary applications with a working pressure of around 300 bar [105]. In the report by Kubilay Karayel, Javani, and Dincer, Type-III hydrogen tanks, which are similar to Type II tanks but at a higher pressure of 350 bar, have been analyzed. The report concluded that the storage tank emits 14.2 kg CO_2e per kg of H_2 storage [106]. In the report by Agostini et al., three small tanks for cars are analyzed, also Type III. Considering the largest tank with a capacity of 35 L at 350 bar, the emissions are calculated to be 536 kg CO_2e for 0.83 kg of hydrogen storage, resulting in approximately 645.7 kg CO_2e/kg H_2 storage [107].

Overview of the numbers that are discussed:

- Small Tank (100 kg, 45 bar): 680 kg CO_2e/kg H_2 storage [103].
- Storage Tank (20 m³, 25 bar): 1,875 kg CO_2e/kg H_2 storage [104].
- Type-III Hydrogen Tanks (350 bar): 14.2 kg CO_2e/kg H_2 storage [106].
- Type-III Tanks for Cars (35 L, 350 bar): 645.7 kg CO_2e/kg H_2 storage [107].

For this analysis, it can be concluded that the various tanks with different pressures and corresponding CO_2e/kg values are not directly comparable. The storage tank at 25 bar is an outlier due to its low pressure, resulting in a high CO_2e/kg value. In this report, the storage size is much larger than in these studies, suggesting that CO_2e/kg values will decrease due to the scale effect. However, due to the uncertainty, a broad range of 200-600 kg CO_2e/kg H_2 storage is considered.

Fuelcell
In the report by Mori et al., a lifecycle assessment was conducted for a stack with a capacity of 48 kW. The total emissions for the stacks alone are 1,160 kg CO_2e. The Life Cycle Assessment results of a PEM Fuel Cell system by Stropnik et al. show that during the manufacturing phase, the stack contributes 60-90% of the total environmental impacts, while the Balance of Plant components contribute 10-20%. Based on these numbers, the total emissions per kW and the emissions per kW for only the stacks are determined [108][109]. In the environmental assessment, platinum was found to account for 63.5% of the total emissions.

Based on the report of Tripathi and Subramanian, the average CO_2 emissions per kg/kW are between 40-50 [102].

Overview of the numbers that are discussed:

- 1,160 kg CO_2e for a 48 kW stack [108].
- Stack contributes 60-90% of total environmental impacts [109].
- 40-50 kg CO_2e per kW [102].

Based on these values, the emission range of 40-50 kg CO_2e/kW is considered. When stacks are replaced, they contribute 60-90% of the total emissions, which is approximately between 24-45 kg CO_2e/kW. This is slightly above the stack emissions of 24.17 kg CO_2e/kW, which are added to the total emissions. Therefore, the replacement emissions are set to 25-35 kg CO_2e/kW.

3.8.4. Overview of Emissions per Technology

Table 3.10 presents a summarized analysis of CO_2 emissions associated with various energy technologies. The table details the emission ranges per installed capacity or replacement for each component.

Table 3.10: Overview of CO_2 Emission Ranges for Configuration 1 and Configuration 5 Assets or Replacement per Unit

Component	**CO_2 Emission Range**
Wind Turbine	880 - 1000 kg CO_2e/kW
Solar PV	480 - 810 kg CO_2e/kWp
Li-ion Battery (replacement)	190 - 240 (95-120) kg CO_2e/kWh
VRFB	220 - 280 kg CO_2e/kWh
Alkaline Electrolyzer (replacement)	100 - 200 (80-190) kg CO_2e/kW
Hydrogen Storage Tank	200 - 600 CO_2e/kg H_2
PEM Fuel Cell (replacement)	24 - 45 (25 - 35) kg CO_2e/kW

3.9. Land Usage Requirements

The section on land usage describes the land use requirements for the assets, expressed in installed capacity per square meter (m²). In subsection 3.9.1, the land usage of wind and solar is described. Then, in subsection 3.9.2, the land usage of Li-ion batteries and VRFB is described. This is followed by the land usage of the hydrogen installation, including the alkaline electrolyzer, storage tank, and PEM fuel cell, in subsection 3.9.3. Lastly, an overview of the land usage of all the assets is provided in subsection 3.9.4.

3.9.1. PV and Wind

This section analyzes the capacity density for large-scale onshore wind and utility-scale solar installations, highlighting recent trends and providing estimates for planning and optimizing renewable

energy projects.

In the report by Enevoldsen and Jacobson, an analysis of 19 wind farms in Europe, consisting of 7 to 178 turbines each, is presented. The study concludes that the average capacity density onshore is 20 MW/km², with a standard error of 3.8 MW/km². Therefore, a range of 16 to 24 MW/km² is a reasonable approximation. Additionally, the land required for onshore wind farms can be utilized for dual purposes. In the Netherlands, wind turbines are often placed at the agricultural site

Overview of the numbers that are discussed:

- Average installed capacity of recent onshore wind turbines in Europe is 20 MW/km², with an error of 3.8 MW/km² [110].

Based on these numbers, the average capacity per square meter is determined to be between 16 and 24 W/m².

For solar installations, although the capacity density of a single solar panel is very high at around 200 Wp/m², utility-scale installations require more space between panels for safety and maintenance. An analysis of multiple solar parks in the Netherlands provides a more realistic estimate of capacity density for utility-scale solar installations.

A solar park in the Netherlands, the 33 MWp solar park over 45 hectares, has a lower capacity due surrounding of water, hedges, and roads [111]. Therefore, two other solar parks in the Netherlands are also considered. A solar park in Emmen of 30 MWp over 38 hectares and a solar park in Budel of 44 MWp over 60 hectares [112].

Overview of the numbers that are discussed:

- 33 MWp solar park over 45 hectares [111].
- solar park in Emmen of 30 MWp over 38 hectares [112].
- Solar park in Budel of 44 MWp over 60 hectares [112].

These three solar parks have power densities of 73, 73, and 79 Wp/m², respectively. Based on this analysis, an average capacity density of 70-80 Wp/m² is taken for utility-scale solar installations. Based on these studies, the capacity density for utility-scale solar installations ranges from 70 to 80 Wp/m².

3.9.2. Lithium ion and Vanadium redox flow battery

This section provides an analysis of the energy densities and land usage requirements of Li-ion batteries and VRFB. The energy density of Li-ion batteries ranges from 150 to 500 kWh/m³, while VRFBs have an energy density between 10 and 70 kWh/m³. This indicates that Li-ion batteries' energy density is higher than VRFBs. Additionally, the specific energy of Li-ion batteries is around 200 Wh/kg, whereas, for VRFBs, it is between 10 and 35 Wh/kg [47].

Both battery types have construction limitations due to the weight of Li-ion batteries and the size of VRFBs. According to Reber, Jarvis, and Marshak [113], the required space for these battery systems varies. The report analyzes 21 systems with capacities on the MWh scale. Li-ion battery installations, such as Tesla Megapacks arranged in blocks, achieve an energy densities up to 62 kWh/m², with an average value across the studied systems being 32 kWh/m² [113].

In Eemshaven, Netherlands, a large-scale Li-ion battery installation with a capacity of 41 MWh is under construction [114]. The size required for the batteries is around 3,000 m².

Key Points for Li-ion Batteries:

- Tesla Megapacks arranged in blocks achieve energy densities up to 62 kWh/m² [113].
- Average value across the studied systems is 32 kWh/m² [113].
- Eemshaven installation: 41 MWh, 3,000 m² required, so average around 14 kWh/m² [114].

The capacity in kWh/m² in the installation in Eemshaven is much lower than that of the Tesla Megapack block, because when multiple blocks are installed next to each other, space between them is required for safety. Therefore, it is better to use the capacity density value of the Li-ion battery installation in Eemshaven than the of the Tesla block. Hence, the range is 8 kWh/m² to 20 kWh/m².

For VRFBs, the report by Reber, Jarvis, and Marshak indicates an average areal capacity density of 14 kWh/m² [113]. However, some VRFB systems demonstrate higher energy densities. For example, the 2 MW/20 MWh battery at the Fraunhofer Institute für Chemische Technologie in Germany achieves 33 kWh/m², and the 100 MW/400 MWh Rongke Power battery in Dalian, China, achieves 46 kWh/m², which is currently the largest installed VRFB installation [113].

Key Points for VRFBs[113]:

- Average areal capacity density: 14 kWh/m² .
- Fraunhofer Institute, Germany: 2 MW/20 MWh, achieving 33 kWh/m².
- Rongke Power, China: 100 MW/400 MWh, achieving 46 kWh/m².

Based on these figures, the range for Vanadium Redox Flow Battery systems is determined to be 33 kWh/m² to 46 kWh/m². This analysis includes considerations for large-scale VRFB installations.

3.9.3. Hydrogen installation

This section determines the area requirements for large-scale hydrogen installations, including electrolyzers, fuel cells, and storage components, based on various reference cases and reports.

The 100 MW Green Hydrogen Plant by SinoHyEnergy, the 100 MW HELA2000, covers an area of 3,600 m²[115]. In the report by Gasunie and Port of Rotterdam, possible large-scale hydrogen plants for the hydrogen backbone in the Netherlands are analyzed [116][117]. The hydrogen backbone is a network of electrolyzers and pipelines. For a potential 200 to 250 MW plant at the Maasvlakte, an area of 11 hectares is available. The report by Arthur D. Little details the size requirements for an alkaline electrolyzer. It specifies 4.5 hectares without safety and storage and 15.5 hectares with safety considerations for a 1 GW electrolyzer. In the report by ISPT, it is noted that a 1 GW electrolyzer requires 17 hectares.

Hydrogen is stored at 300 bar to increase its storage density. At this pressure, the density of hydrogen is approximately 20 kg/m³ [120]. According to Arthur D. Little, hydrogen storage at 200 bar requires 0.3 hectares for 500 tons of hydrogen [118]. However, specific information on large-scale hydrogen storage on land is limited. Often, large-scale storage considers salt caverns, which is outside the scope of this project [77]. Therefore, a simple estimation is made to determine the size of the hydrogen storage and compare it to other reports.

A tube trailer transports hydrogen at a pressure of 350 bar and carries 880 kg of hydrogen, roughly the size of a standard container [40]. This container size is used as a reference for a potential storage tank. The container dimensions are 12.2 m long, 2.5 m wide, and 2.5 m high [121]. For this analysis, the tank (container) is assumed to be positioned vertically, giving it a height of 12.2 m. For safety reasons, the container's width is always maintained between containers in both directions. Consequently, it can be concluded that 880 kg of hydrogen is stored in 25 m², resulting in an approximate storage density of 35 kg/m². This setup is schematically illustrated in Figure 3.5.

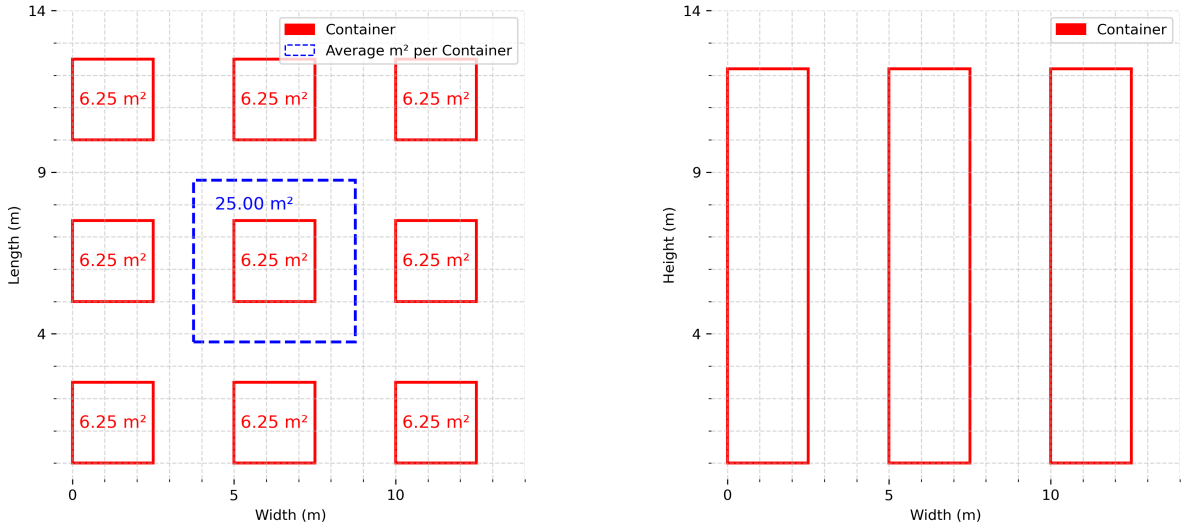

(a) Top view of the storage tank layout

(b) Side view of the storage tank layout

Figure 3.5: Schematic Overview of the Storage Tank, Showing Both Top and Side Views of the Container Dimensions and Placement

The same area requirements are applied to the PEM fuel cell installation as those for the electrolyzer setup. This is because not many reports are written on large-scale fuel cell installations, which involve the largest part: the hydrogen storage components.

Below are the key points for electrolyzers/fuel cellss:

- 100 MW HELA2000 system with a size of 3,600 m². This results in an average of 28 kW/m² [115].
- 1 GW electrolyzer with safety and storage with a size of 11 hectares (110,000 m²). This is around 9 kW/m² [118].
- 1 GW electrolyzer with a size of 17 hectares (170,000 m²). This is around 6 kW/m² [119].

Key Points for Storage:

- At 200 bar, 0.5 kton requires 0.3 hectares (3,000 m²), which is approximately 167 kg/m² [118].
- 880 kg is stored in 25 m², which is approximately 35 kg/m².

So, the average capacity density for hydrogen storage ranges from 35 kg/m² to 167 kg/m².

Based on these studies, the capacity density for electrolyzers and fuel cells ranges from 6 kW/m² to 28 kW/m². For hydrogen storage, the capacity density ranges from 35 kg/m² to 167 kg/m². These values provide a basis for estimating the area required for large-scale hydrogen installations.

3.9.4. Overview of the capacity density

In Table 3.11 provides a summary of the energy densities for various energy assets, offering a comparative understanding of their efficiency per unit area.

Table 3.11: Overview of capacity density Ranges for Configuration 1 and Configuration 5 Assets per m^2

Component	capacity density	Unit
Solar PV	70 - 80	Wp/m^2
Wind Turbine	14 - 24	W/m^2
Li-ion Battery	8 - 20	kWh/m^2
VRFB	33 - 46	kWh/m^2
Alkaline Electrolyzer	6 - 28	kW/m^2
Hydrogen Storage Tank (300 bar)	35 - 167	kg/m^2
Fuel Cell	6 - 28	kW/m^2

4

Results

This chapter presents the study's results. In section 4.1, the LCOE and the corresponding dimensions for each configuration are discussed. The most cost-effective and feasible results for each configuration are shown, with a detailed analysis of their performance, behavior, and costs. In section 2.7, the environmental impact based on CO_2 emissions and the land usage of the two configurations with the lowest LCOE are described. Finally, in section 4.3, the sensitivity of the two configurations with the lowest LCOE is tested, focusing on the constraint of renewable energy percentage and the most critical financial and technical parameters.

4.1. LCOE and Dimensions.

This section presents the LCOE for different configurations of energy storage and electrolyzer technologies, highlighting their cost differences.

Configurations 5 and 1, consisting of a VRFB and alkaline electrolyzer and Li-ion batteries and alkaline electrolyzer, respectively, show the lowest LCOEs at 0.241 and 0.243 €/kWh. Following closely behind were configuration 6, using a ZBFB with an alkaline electrolyzer, and configuration 2, using a lead-acid battery with an alkaline electrolyzer, with LCOEs of 0.252 and 0.261 €/kWh, respectively.

Configuration 7, which combines a VRFB with a PEM electrolyzer, has an LCOE of 0.255 €/kWh. Configurations 8, using a ZBFB with a PEM electrolyzer, and 3, using a Li-ion battery with a PEM electrolyzer, show LCOEs of 0.258 and 0.254 €/kWh, respectively. The highest LCOE is seen in configuration 4, which uses a lead-acid battery with a PEM electrolyzer at 0.273 €/kWh. The configuration with the PEM electrolyzer shows the highest LCOE.

It is notable that configurations 2 and 4, which include lead-acid batteries, exclude the battery completely. Furthermore, in configurations 3, 4, and 8, the PEM electrolyzer has a lower installed capacity compared to configurations using the alkaline electrolyzer combined with the same battery type.

The performance, behavior, and cost are analyzed in more detail in subsection 4.1.1 and subsection 4.1.3 to explain these outcomes. The LCOE values across all configurations are relatively close, indicating a competitive range of costs for different energy storage and electrolyzer setups. An overview of the LCOE for each configuration and the associated dimensions is provided in Table 4.1.

Table 4.1: Overview of Dimensions and Results for Optimized Asset Configurations 1 to 8

Config.	LCOE (€/kWh)	Solar (MWp)	Wind (MWp)	Battery (MWh)	Electrolyzer (MW)	Storage (tons)	Fuel Cell (MW)	Connection (MW)
1	0.243	333	294	402	114	266	113	239
2	0.261	356	362	0	119	283	112	244
3	0.254	387	306	438	97	251	113	234
4	0.273	404	395	0	111	240	112	236
5	0.241	362	302	348	80	260	111	212
6	0.252	436	310	159	94	251	115	219
7	0.255	434	297	401	75	239	115	225
8	0.258	379	328	309	79	244	115	203

4.1.1. Model Performance and Component Behaviour

This section discusses the performance and behavior of different assets across different configurations. First, the capacity factors (CF) for solar and wind energy, curtailment levels, and the percentage of assets to load are discussed. Then, the performance of batteries, electrolyzers, storage tanks, and fuel cells, as well as the state of these assets at the end of the simulation, are discussed. Analyzing these factors clarifies why each configuration's dimensions are the most cost-effective and feasible, allowing conclusions to be drawn from the results.

The CF for solar and wind energy remain consistent across all configurations at 0.12 and 0.48, respectively. This consistency is due to the same weather input data being used for all configurations. Curtailment occurs when the generated renewable energy is not used because it exceeds the grid connection or because storage systems are full. The percentage of the energy that is curtailed is shown in Table 4.2. The amount of curtailment can vary based on the capacities of the assets. The lowest curtailment percentages are observed in configuration 1 with 33%, which uses a Li-ion battery. In this configuration, the sum of the installed capacities of the renewable energy sources is the least. This indicates less over-dimensioning of renewable energy capacity, contributing to lower curtailment.

The Renewable Energy Source (RES) to load is the percentage of the load that comes directly from the RES. The battery to load and the fuel cell to load are the percentages of the total load when it is powered by the battery or fuel cell. The percentages are shown in Table 4.2. The RES to load percentage varies between 82% and 86%. The highest percentages, 85%, and 86%, are seen in configurations 2 and 4, respectively. This is due to the overdimensions of the RES, because of the absence of batteries. In these configurations, the fuel cell supplies all the power during a RES shortage. These numbers indicate that only 14% to 18% of the data center's energy load is supplied by the storage system.

Table 4.2: Overview of Capacity Factor, Curtailment, Direct Use, Battery Use, and Fuel Cell Use for Configurations 1 to 8

Configuration	1	2	3	4	5	6	7	8
Renewable Energy Source:								
Solar CF	0.12	0.12	0.12	0.12	0.12	0.12	0.12	0.12
Wind CF	0.48	0.48	0.48	0.48	0.48	0.48	0.48	0.48
Curtailment	33%	41%	36%	45%	40%	38%	37%	39%
Energy Use to Load:								
RES to Load	82%	85%	83%	86%	83%	84%	83%	84%
Battery to Load	7%	-	7%	-	8%	4%	8%	7%
Fuel Cell to Load	11%	15%	10%	14%	10%	12%	8%	9%

4.1.2. Battery, Electrolyzer, Storage Tank, and Fuel Cell Performance

This section discusses the performance of batteries, electrolyzers, fuel cells, and storage tanks during the 10-year simulation, as well as their state of health (SOH) at the end of the simulation.

In configurations 1 and 3, battery replacements are needed during the 10-year simulation period due to low curtailment percentages, which increase battery usage. Li-ion battery replacements are required in

year 8 for configuration 1 and year 10 for configuration 3. The results further indicate that the lead-acid battery was entirely excluded from configurations 3 and 4, primarily due to its high degradation rate and associated costs. Therefore, a lead-acid battery is not suitable for these configurations. The state of health (SOH) for the flow batteries in configurations 5 to 8 remains at 100% because no degradation is assumed.

Electrolyzer replacements are only necessary in configuration 4 due to the absence of battery capacity, which leads to degradation exceeding the 90% replacement threshold. In configuration 2, where also no battery capacity is installed, the alkaline electrolyzer degrades less rapidly and, therefore, does not require replacement. Other configurations maintain degradation below this threshold, with electrolyzer SOH at the end of the 10-year simulation ranging from 92.7% to 97.9%. The electrolyzers in all configurations, except for 2 and 4, experienced around 4000-5000 on/off events during the 10-year simulation, averaging about 1.2 on/off per day. In configurations 2 and 4, the electrolyzer has approximately 2 on/off events times per day.

Configurations 3, 4, 7, and 8 with PEM electrolyzers have slightly higher runtimes than those with the same battery type and alkaline electrolyzers. This is due to the wider operation window of the PEM electrolyzer, leading to more runtime and increased degradation. The storage tank cycles are higher for configurations 2 and 4, due to the lack of installed battery capacity. For other configurations, there are around 150 cycles during the simulation, averaging about 15 cycles per year. Figure 4.1 shows the SOC of the storage tank for configuration 1. A cycle is when the complete capacity of the hydrogen tank is used. The figure shows that the lowest peak occurs in March, and the system is dimensioned based on this peak. However, there are multiple low peaks around the same level throughout the year. This indicates that the capacity of the tank is efficiently used year-round. Moreover, no seasonal pattern is shown in the figure. This is due to a slightly higher load of the data center during the summer. The higher energy output from the solar profile is used for this increase in load. In winter, when there is no wind, this results in a direct energy shortage because the solar profile has a low output. However, the dimensions of the solar and wind systems result in around 30-40% curtailment. This overdimensioning leads to a relatively constant load because the peaks are cut off, leveling the seasonal pattern.

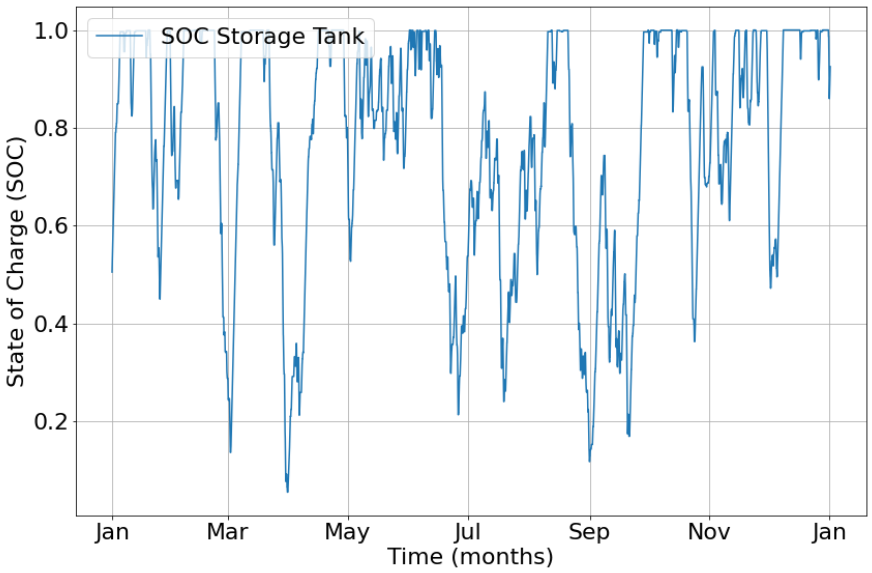

Figure 4.1: SOC of the Storage Tank for Configuration 1 During the First Year of the 10-Year Simulations

An overview of the performances of the battery, electrolyzer, fuel cell, and storage tank is shown in Table 4.3.

Table 4.3: Overview of Asset Behavior and Performance for Optimized Configurations 1 to 8 of a 10-Year Simulation

Configuration	**1**	**2**	**3**	**4**	**5**	**6**	**7**	**8**
Battery:								
Total Cycles	2,561	-	2,437	-	2,217	2,787	2,125	2,268
Total Replacement	1	-	1	-	0	0	0	0
SOH (%)	94%	-	96%	-	100%	100%	100%	100%
Electrolyzer:								
Replacements	0	0	0	1	0	0	0	0
SOH (%)	96%	95%	94%	99%	95%	96%	91%	91%
FLH	23,628	31,988	27,672	35,674	29,984	31,583	31,558	32,924
Run time	28,374	39,147	32,042	42,866	33,608	36,258	32,150	37,353
on/off cycles	4,354	7,515	4,380	7,359	4,658	5,987	4,421	5,097
Fuel Cell:								
Replacements	1	2	1	1	1	1	1	1
SOH (%)	96%	99%	98%	90%	96%	92%	98%	96%
FLH	8,427	12,020	7,535	11,125	7,580	9,233	6,468	7,132
Runtime	16,205	24,358	14,036	22,569	16,159	20,939	17,831	16,209
on/off cycles	2,756	7,170	2,436	6,870	3,370	5,560	3,020	3,830
Storage Tank:								
Cycles	164	217	156	237	149	190	142	153

4.1.3. Cost Analysis

The cost analysis shows the costs of the 8 different configurations, focusing on different Assets, including solar, wind, battery, electrolyzer, storage, fuel cell, and connection costs. All the described costs are presented as NPV of a 10-year simulation. The total costs for each configuration range from €1.43 billion (bln) for configuration 5 to €1.60 bln for configuration 4. This section highlights and analyzes differences in these costs. A complete breakdown of the costs for each configuration is provided in Appendix A

Renewable energy sources, wind and solar, form a notable share of the total costs across all configurations. In configuration 1, this share is the lowest, with renewable sources accounting for 45.1% or €643 million (mln) of the total cost. This share increases to 52.5% or €841 mln in configuration 4 due to higher wind energy costs because more direct use of renewable energy is needed since no battery is installed. This indicates the investment required for these sources.

Battery costs show differences among the configurations. Despite the energy sources being less expensive in configuration 1, configuration 5 has the lowest LCOE. The total share of the battery cost in configuration 1 is 8.3%, or €118 mln, whereas in configuration 5, battery costs rise to 9.5%, or €135 mln. Despite the lower installed capacity of the VRFB in configuration 5 compared to the Li-ion battery, the operational capacity is higher because the VRFB has an operational range of 100% versus 70% for the Li-ion battery. Additionally, the Li-ion battery requires replacement in year 8, adding further costs. This results in a larger usable storage capacity, necessitating a smaller electrolyzer.

This is shown by the share of the electrolyzer in configurations 1 and 5. The cost of the alkaline electrolyzer is €91 mln in configuration 1, while in configuration 5, it is lower at €64 mln due to the reduced installed capacity needed. Moreover, in configurations 3, 4, 7, and 8, the share of the total cost of the electrolyzer is higher. This is due to the higher CAPEX cost of the PEM electrolyzer and the need for replacement in configuration 4, where the stacks of the PEM electrolyzer are replaced.

The storage tank costs vary from €136 mln in configuration 8 to €158 mln in configuration 2. Configuration 2 has no battery, so all surpluses must be stored as hydrogen to overcome shortages. Additionally, in all configurations with the PEM electrolyzer, the storage tank is smaller due to the electrolyzer's reduced installed capacity.

The cost of the fuel cell remains relatively consistent across configurations, with a CAPEX price varying from €222 mln to €226 mln. However, due to degradation, the replacement cost can be notable. In configuration 2, the stacks are replaced twice, resulting in a total cost of €362 mln. Similarly, in

configuration 4, where the fuel cell is replaced once, the total cost is €321 mln. This is because the SOH of the stack is 90.5%, indicating a need for replacement and, thus, a minimal residual stack cost.

Connection costs remain relatively stable across all configurations, accounting for 8.6% in configuration 8, which is €131 mln, to 10.7% in configuration 1, which is €153 mln. These costs are a constant factor in the total cost of energy. Figure 4.2 provides an overview of each asset's total cost and share.

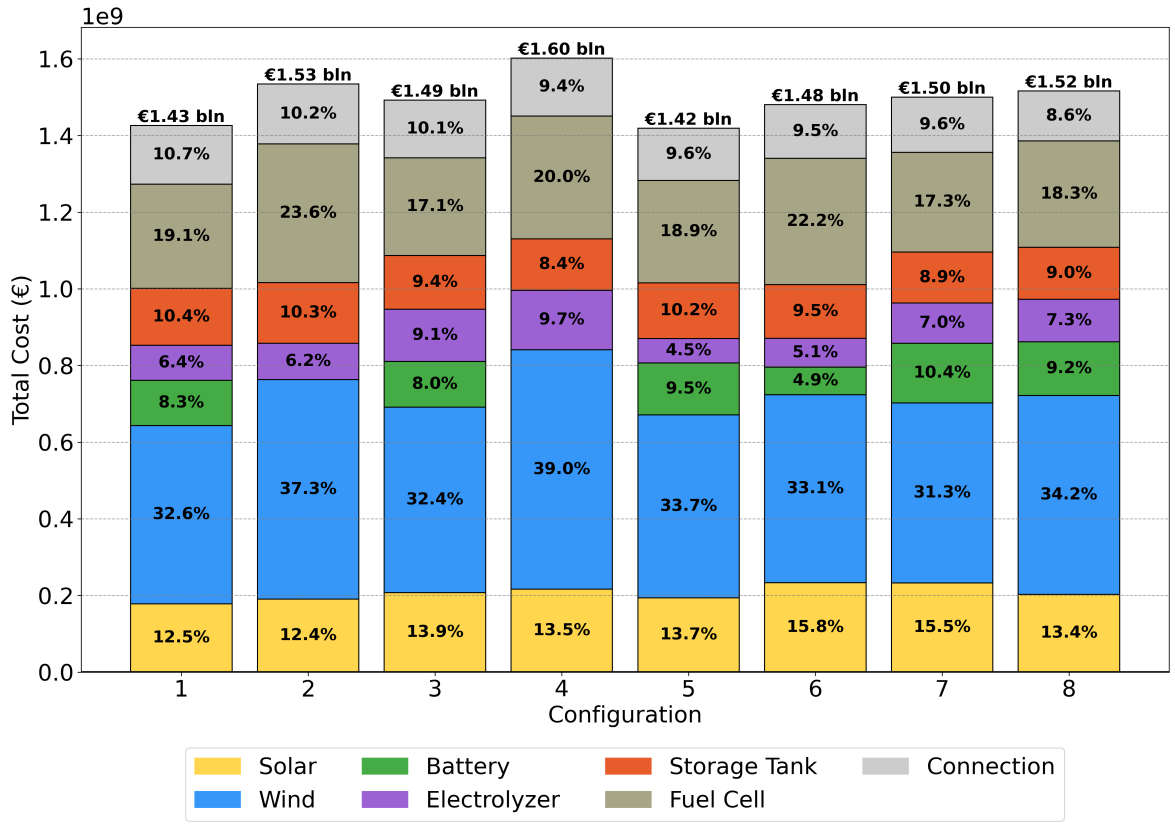

Figure 4.2: Overview of the Total Cost and Asset Share in the Total Cost for Configurations 1 to 8

4.2. Environmental Impact and Land Usage

This section evaluates the environmental impact and land usage associated with configurations 1 and 5. It examines CO_2e and land use requirements, providing an analysis of the emissions and land use of different assets based on the dimension, including wind turbines, solar PV, batteries, electrolyzers, hydrogen storage tanks, and fuel cells.

4.2.1. Environmental Impact

This section describes and discusses the results of the environmental impact. This analysis considers the CO_2e over the 10-year simulation period, including replacements due to degradation.

In Figure 4.3, it is shown that the wind turbines have slightly higher CO_2e in configuration 5 compared to configuration 1. Wind contributes the largest share of CO_2e in both configurations, with 108 and 111 ktonnes of CO_2e, respectively. PV is lower for both configurations, approximately 75 ktonnes CO_2e. In configuration 1, the battery share is higher than the PV emissions. Also, the emissions of the Li-ion battery are twice as high as the VRFB, due to its shorter lifetime and higher installed capacity. The Li-ion battery, with a shorter lifespan, needs replacement more frequently, leading to increased CO_2e, with respective values of 86.5 ktonnes and 43.5 ktonnes CO_2e. In configuration 1, the battery is replaced twice during the 20-year lifetime of the asset.

For the CO_2e of the electrolyzer and fuel cell, one replacement during the 20-year lifetime is considered for both configurations. Similarly, the PEM fuel cell is replaced twice during the lifetime in both configurations. However, in both configurations, the contribution to the total emissions from the electrolyzer and fuel cell is low. The electrolyzer and fuel cell contribute to 20 ktonnes CO_2e.

The storage of hydrogen has more impact than the fuel cell and the electrolyzer due to the large amount of hydrogen that needs to be stored. From the analysis, in both configurations, hydrogen storage contributes 35 ktonnes of CO_2e.

Due to the difference in batteries, configuration 1 has higher overall CO_2e than configuration 5. The frequent replacement of the Li-ion battery in configuration 1 contributes to the total CO_2e. For configuration 1, the total emission is equivalent to 322.5 ktonnes of CO_2e, and for configuration 5, the total CO_2e is 283 ktonnes.

This results in an average CO_2e per kWh:

- Configuration 1: 0.037 kg CO_2e / kWh
- Configuration 5: 0.032 kg CO_2e / kWh

Configuration 1 has a higher average CO_2e per kWh primarily due to the larger contribution from the Li-ion battery, which has a shorter lifespan and thus higher emissions over the simulation period. Configuration 5 benefits from the longer lifespan of its components, particularly the VRFB, resulting in lower average CO_2e per kWh.

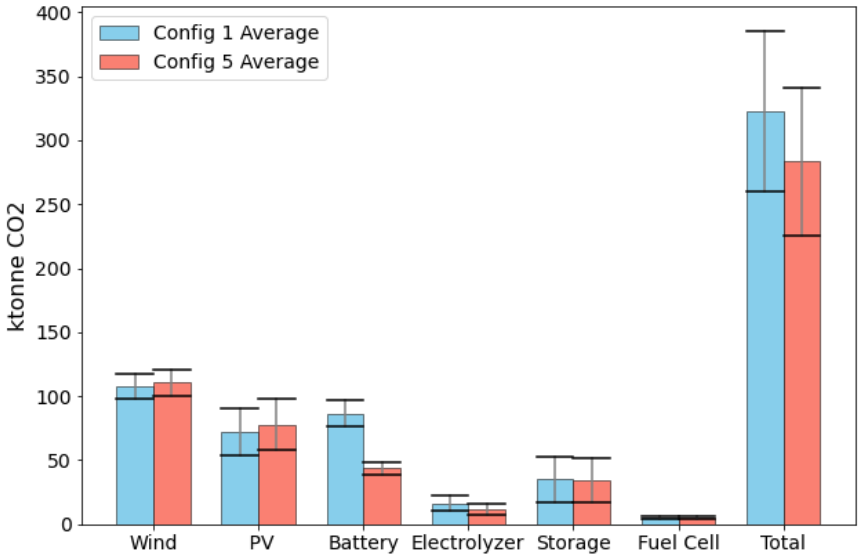

Figure 4.3: CO_2e by Each Asset with Min-Max Range for Configurations 1 and 5, and Total Emissions for the Configurations

4.2.2. Land usage

To determine the land usage of the energy system, the dimensions are derived from the numbers described in section 3.9 and detailed in Table 3.11.

The wind turbine and the solar PV uses the most land, with configuration 1 requiring 15 km² and 4.6 km², respectively, and configuration 5 requiring even more at 16 km² and 5.0 km². This reflects the large land usage, especially for wind energy.

The land usage for Li-ion and VRF batteries is relatively small compared to the renewable energy sources, at 0.035 km² for configuration 1 and 0.009 km² for configuration 5. Batteries are essential for energy storage, but their land usage requirements are minimal compared to generation components

like wind turbines and solar panels. The electrolyzer requires 0.012 km² for configuration 1 and 0.008 km² for configuration 5. Fuel cells are around the same order of size, 0.011 km² in both configurations.

The hydrogen storage tank requires 0.005 km² for configuration 1 and 0.004 km² for configuration 5, indicating minimal land usage for hydrogen storage compared to other components.

If you exclude the generation assets from the analysis, the required space for Configuration 1 is 63,000 m², and for Configuration 5, it is approximately 33,000 m².

In conclusion, the combined land usage for these assets is approximately 20 and 21 km² of configurations 1 and 5, respectively. The generation components require a substantial amount of space due to onshore wind installations, which could create conflicts when finding suitable locations for onshore wind turbines. Therefore, in chapter 5, the offshore wind option is discussed. Despite having a capacity density of 6-7 W/m², which is lower than onshore wind, onshore turbines are often placed in long lines with the land used for multiple purposes. In contrast, offshore turbines are arranged in a grid pattern with large distances between them to reduce wake effects. However, offshore wind offers several advantages, including a higher capacity factor, more continuous output, and designated areas for future projects are being proposed.[122][123].

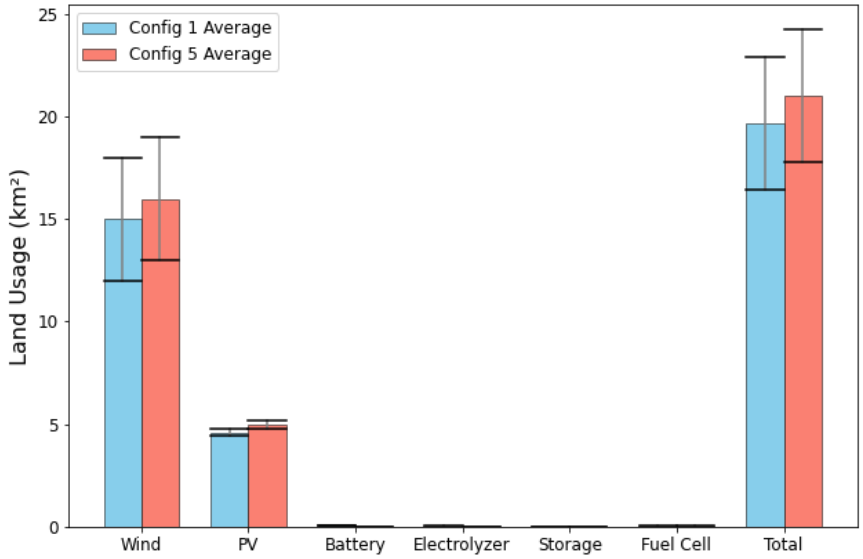

Figure 4.4: Land Usage by Each Asset for Configurations 1 and 5, and Total Land Usage for the Configurations

4.3. Sensitivity Analyse

This section discusses the sensitivity of parameters used in the model of configurations 1 and 5, as these are the most cost-effective options. First, the constraint of 100% renewable energy is analyzed. Then, the capacity factor of the wind is analyzed using a different profile. Following this, the sensitivity of the technical and economic parameters used in the model is evaluated.

4.3.1. Constraint

The model's main constraint is that the energy system must be 100% renewable on an hourly basis. The model dimensions are based on a combination of the residual peak energy demand and periods of insufficient renewable generation. Therefore, it is important to analyze the impact of this constraint on the LCOE. Additionally, the impact on CO_2e and land usage is analyzed when the constraint is reduced to 80%.

The average EPEX price is currently around 0.09 €/kWh [124]. These prices are expected to decrease in the coming year[40]. During periods of shortage, renewable energy production is insufficient, and

energy is taken from the grid. These hours can be very expensive if they coincide with peak hours. However, this often occurs at night when there is no solar production, making these hours much cheaper. Therefore, in this sensitivity analysis, it is assumed that the energy taken from the grid is priced at 0.10 €/kWh, which is approximately the average price. In Figure 4.5, it is shown how the LCOE decreases. The solid bullet points are the data points from the optimization.

An exponential trendline is drawn through the points to make the trend more evident for configurations 1 and 5 as the renewable energy constraint is decreased from 100% to 80%. Both configurations follow a similar exponential trendline.

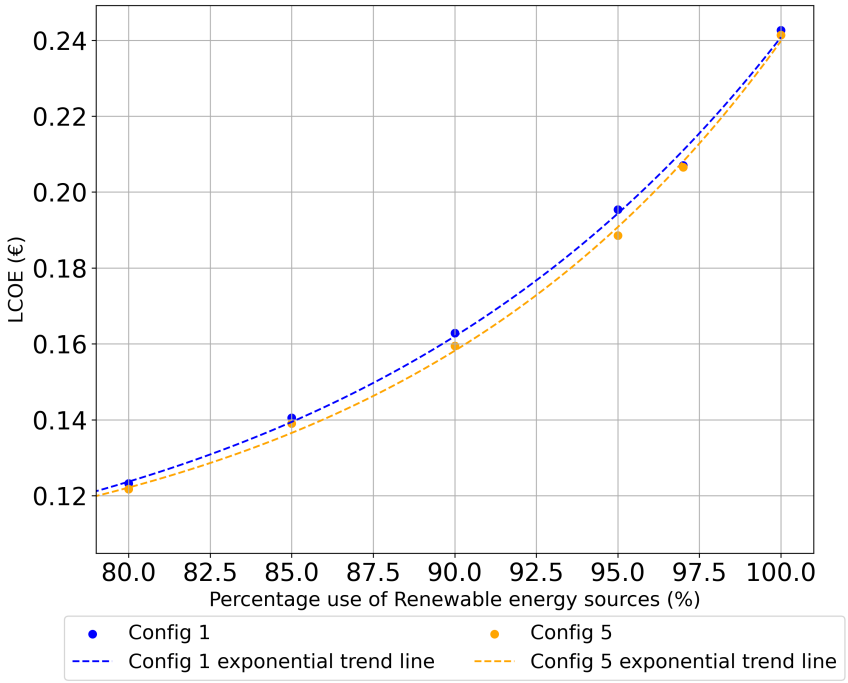

Figure 4.5: Sensitivity Analysis of Constraints on Percentage Renewable Energy

In Table 4.4, the dimensions of the assets are shown for configurations 1 and 5. At 80% renewable energy, both configurations exclude the hydrogen systems, consisting of the electrolyzer, hydrogen tank, and fuel cell, and rely only on battery storage to balance the intermittency of renewable sources. Configuration 1 has an installed capacity of 144 MWh for Li-ion batteries and 105 MWh for VRFB. In Table 4.4, it is shown that the curtailment percentages are 38%, and the renewable energy source (RES) directly to the load is high, above 76%. However, the energy supplied by the batteries decreases to 3% and 4%. In this configuration, the energy from the grid is used 20% of the time.

Table 4.4: LCOE, Dimensions, and Energy Use of Configurations 1 and 5, Constrained by 80% and 100% Renewable Energy Use

Configuration	1 (80%)	5 (80%)	1 (100%)	5 (100%)
LCOE (€/kWh)	0.123	0.121	0.243	0.241
Solar (MWp)	166	196	333	362
Wind (MWp)	233	225	294	302
Battery (MWh)	144	105	402	348
Electrolyzer (MW)	-	-	114	80
Storage (tons)	-	-	266	260
Fuel Cell (MW)	-	-	113	111
Curtailment	38%	38%	33%	38%
RES to Load	76	77%	82%	83%
Grid to Load	20%	20%	-	-
Battery to Load	4%	3%	7%	8%
Fuel cell to load	-	-	11%	9%

When the renewable energy constraint is reduced from 100% to 80%, both configurations show reductions in CO_2e across all components.

In Configuration 1, CO_2e from PV is reduced by 50%, from Wind by 21%, and from Li-ion batteries by 55%. The emissions from the alkaline electrolyzer, hydrogen storage tank, and PEM fuel cell are completely eliminated, leading to a total reduction of 57 ktonnes of CO_2.

Similarly, Configuration 5 shows a 46% reduction in CO_2e from PV, a 26% reduction from Wind, and a 70% reduction from the vanadium redox flow battery. The emissions from the alkaline electrolyzer, hydrogen storage tank, and PEM fuel cell are also completely eliminated, resulting in a total reduction of 51 ktonnes of CO_2.

These results highlight the substantial impact that reducing the renewable energy constraint from 100% to 80% can have on lowering CO_2e in both configurations. In both configurations, the CO_2e of the assets are reduced by 50% and 51%, respectively. However, in the configuration with 80% renewable energy, energy is also taken from the grid, which contributes to CO_2e. When energy from the grid is used, it is assumed that the electricity is generated from gas power plants in the Netherlands, as this typically occurs during periods when renewables are not available due to weather circumstances. The average emissions of a kWh produced by a gas power plant are 0.30 to 0.32 kg CO_2e [125][126].

This emission is added to the total tonnes of CO_2e. This is shown in Figure 4.6. From this analysis, it can be concluded that Configuration 1 results in 703 ktonnes of CO_2e, and Configuration 5 results in 683 ktonnes of CO_2e, which is more than twice as high as the 100% renewable configuration.

This results in an average CO_2e per kWh of the 10-year simulation:

- Configuration 1: 0.080 kg CO_2e / kWh
- Configuration 5: 0.078 kg CO_2e / kWh

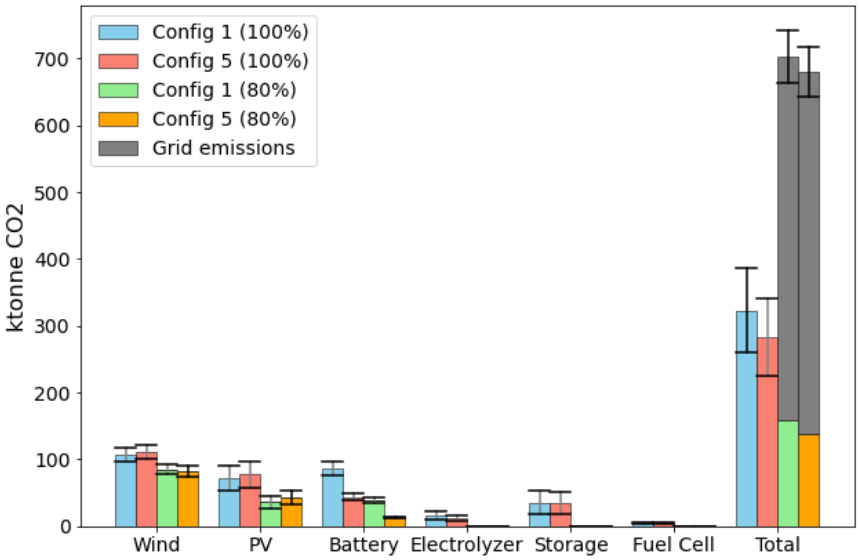

Figure 4.6: CO_2 Emissions Comparison with 100% and 80% RES by Each Asset and the Total for Configurations 1 and 5

The impact of reducing the constraint to 80% of the land usage is now described. In Configuration 1, land usage for solar PV is reduced by 50%, from 4.6 km² to 2.3 km². The land usage of the wind turbine decreases by 20%, from 15 km² to 12 km², and the land required for battery capacity decreases by 64%, from 0.035 km² to 0.013 km². The land usage for the alkaline electrolyzer, hydrogen storage tank, and PEM fuel cell is completely eliminated, leading to a total reduction of 0.028 km².

Similarly, Configuration 5 shows a 42% reduction in land usage for solar PV, from 5.0 km² to 2.9 km², and a 25% reduction for wind turbines, from 16 km² to 12 km². The land required for VRFB decreases by 67%, from 0.009 km² to 0.003 km². As in Configuration 1, the land usage for the alkaline electrolyzer, hydrogen storage tank, and PEM fuel cell is completely eliminated, resulting in a total reduction of 0.024 km².

These results are shown in Figure 4.7 and show the impact that reducing the renewable energy constraint from 100% to 80% can have on lowering land usage in both configurations. In Configuration 1, the total land usage decreases from approximately 20 km² to 14 km², and in Configuration 5, the land usage decreases from 21 km² to approximately 14 km². Moreover, if only the onsite assets, battery, electrolyzer, storage, and fuel cell, are considered, the required land usage is reduced by 80% and 91%, respectively.

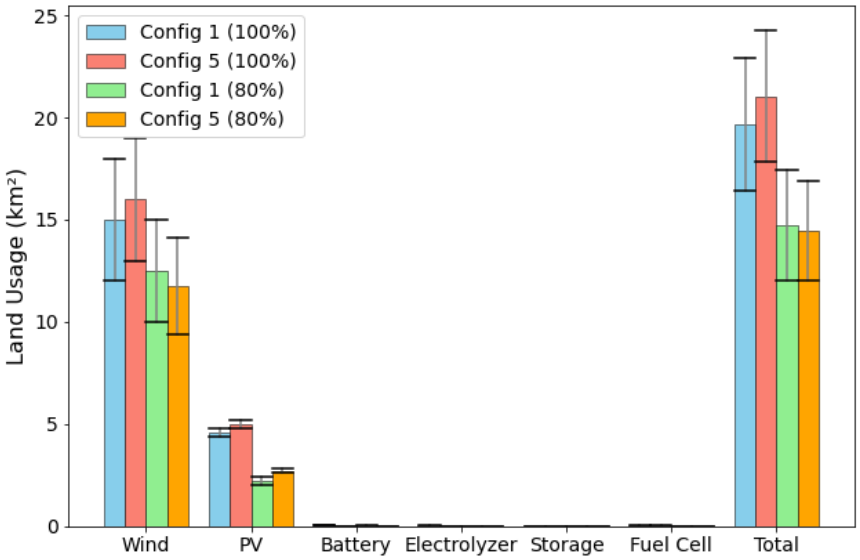

Figure 4.7: Land Usage by Each Component for Configurations 1 and 5

4.3.2. Energy profile

This section analyzes the impact of different wind profiles on the LCOE. It examines the wake effect on wind turbine performance by varying CF. Additionally, it compares two energy profiles, the current and new wind profiles, to understand their influence on the LCOE.

The wind profile used in this study has a CF of 0.48, which is high for onshore wind. The CF of new onshore wind farms now ranges from 30-48%, while new offshore wind farms mostly have a CF of 50% [127]. This indicates that the wind profile is at the upper boundary for onshore wind. Additionally, when multiple turbines are placed close to each other, the wake effect can cause a 10-20% loss in energy production per year [128]. The wake effect is the influence a wind turbine has on others because it changes the wind conditions. Furthermore, different types of wind turbines operate at rated capacity at different wind speeds. Therefore, in this section, two parameters are tested: the wake effect, by changing the capacity factor due to decreased wind farm output, and a different energy profile of the same year from different turbines is analyzed.

Table 4.5: Characteristics of Current and New Wind Profiles

Wind Profile	CF	% Hours with Zero Output	% Hours at Rated Output (%)
New	0.28	21	5
Current	0.48	13	20

In Table 4.5, it is shown that the new wind profile has a lower CF and operates less frequently at its maximum capacity compared to the current wind profile used in the analysis. Additionally, the hours with zero output, when the wind is below the cut-off profile, are higher. Both wind profiles have their CF adjusted by multiplying them by a factor. The LCOE of the current wind profile and the new wind profile are shown in Figure 4.8.

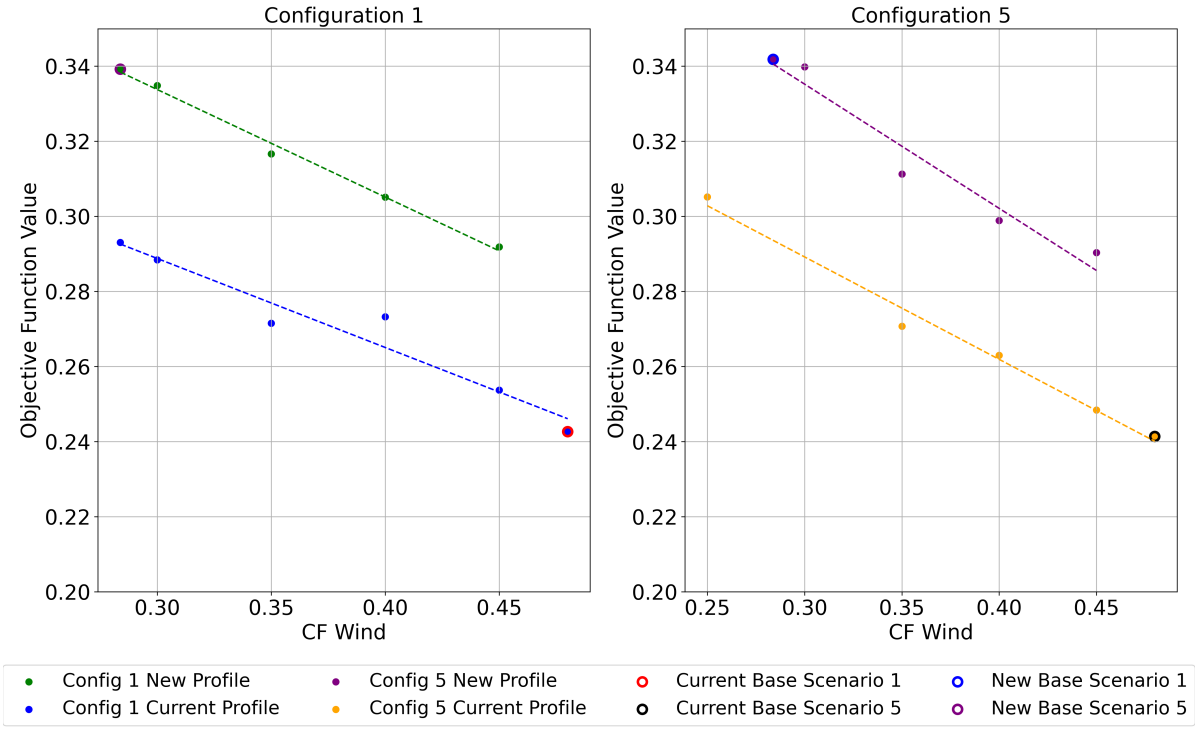

Figure 4.8: Configuration 1 and 5 with a Current and New Wind Energy Profile in a 100% Renewable Scenario

In configuration 1, comparing the current and new solutions shows a difference of 0.24 and 0.34, respectively. For configuration 5, the difference is approximately the same. This is due to the need for more installed capacity of both solar and wind because of the reduced output of the wind profile. Therefore, Figure 4.8 shows what happens to the LCOE if the capacity factor increases. This indicates a linear relationship between LCOE and the capacity factor. However, suppose the capacity factor is increased to 0.45, close to the capacity factor of the current energy profile in the model. In that case, the difference is 0.05 €/kWh. This is because the current profile operates more at its rated power, creating a more stable energy profile.

4.3.3. Technical parameters

This section analyzes the sensitivity of technical parameters used in the model for configurations 1 and 5. This analysis focuses on understanding how variations in key parameters impact the LCOE. The technical parameters that are examined include the efficiency and degradation coefficients of the batteries, electrolyzers, and fuel cells. These parameters are crucial in the model, and their values fluctuate in the literature. Thus, it is essential to investigate their influence on LCOE when varied within realistic ranges. The optimization dimensions are generally close to the optimum but do not always achieve it. This is due to the use of a step size of 1 MW(h) or kg. Additionally, because seven variables are optimized, there are multiple configurations with similar LCOE. The differences in LCOE are small, which makes the results not always immediately evident. Therefore, a trend line is used to visualize the influence of the parameters more effectively.

Efficiency Analysis

This section described the impact of changing roundtrip efficiencies of Li-ion batteries and VRFB, as well as the peak efficiency of alkaline electrolyzers and PEM fuel cells in configurations 1 and 5. The analysis considers how changes in efficiency affect LCOE and the required installed capacities for these energy storage and conversion technologies.

In configuration 1, the roundtrip efficiency of the Li-ion battery is 85%, while the VRFB in configuration 5 has a roundtrip efficiency of 75%. For Li-ion and VRFB, the efficiencies are varied from 65% to 90%.

Increased efficiency positively impacts both configurations, as indicated by a linear trendline through the data points. However, this impact is minimal. The maximum deviation from the base configuration is within a range of 0.005 €/kWh, which is approximately 2%.

The peak efficiencies for the alkaline electrolyzer vary between 50% and 80%, and for the PEM fuel cell, between 40% and 70%. The peak efficiencies of the electrolyzer and fuel cell are 72% and 60%, respectively.

The data indicates that changes in electrolyzer peak efficiency have a greater impact than changes in battery efficiency. The PEM fuel cell peak efficiency affects LCOE. An interesting result is that the capacity and the cost of the fuel cell remain the same, but the storage capacity increases due to the lower efficiency, which results in a higher cost. Higher efficiency results in reduced installed capacity, thereby lowering the overall costs. The results are shown in Figure 4.9. If the efficiency of the fuel cell decreases to 40%, the maximum increase in LCOE is within 10% relative to the base case with peak efficiency of 60%

Degradation Analysis

The sensitivity analysis also considers the degradation components of the battery, electrolyzer, and fuel cell. The degradation component of the battery is one of the main differences between Li-ion and VRFB performance in this research. Additionally, integrating an electrolyzer into a system with renewable energy can affect the performance and degradation of the electrolyzer due to frequent start-stops [129][130]. Therefore, evaluating the influence on the LCOE when the degradation coefficient increases is interesting.

For the VRFB, the model assumes a degradation coefficient of 0, so during the simulation, the usable capacity remains the same. In this analysis, the degradation increases to 40% of the initial capacity after 10,000 cycles. This increase in the VRFB degradation coefficient shows a smaller impact compared to the Li-ion battery. This is because the degradation coefficient of VRFB per cycle is still lower than that of the Li-ion battery. Moreover, such an increase in degradation for VRFB is less likely than for the Li-ion battery because the deviation from the model parameters is smaller for VRFB. An increase in the degradation coefficient of the Li-ion battery results in higher costs due to more frequent replacements.

The efficiency degradation values of the alkaline electrolyzer are 0.13% and 0.25% per 1,000 hours, while for the PEM fuel cell, it is 0.88% per 1,000 hours. Only higher degradation values are considered for the electrolyzer, reflecting a potential higher degradation due to intermittent operation mode.

As shown in Figure 4.9, even if the degradation coefficient of the alkaline electrolyzer is three times higher, the impact on LCOE remains small. This is due to two reasons: first, the electrolyzer stacks are replaced only once within the 10-year period, and even with a three times higher degradation coefficient, the performance remains acceptable due to the replacement. Second, the electrolyzer's cost share in both configurations 1 and 5 is small, thus minimally affecting LCOE. In contrast, the PEM fuel cell impacts LCOE due to its high-cost share in the storage system. When the degradation coefficient decreases, the replacement and the associated cost are excluded, which is 80% of the initial investment.

The sensitivity analysis shows that technical parameters influence LCOE, with the degradation coefficient of the PEM fuel cell having the most considerable impact. However, this coefficient is based on intermittent energy sources and is, therefore, uncertainly lower than the degradation coefficient of the alkaline electrolyzer. When analyzing the sensitivity of the technical parameters, the LCOE varies between 0.232 and 0.264, which is within a range of 10% deviation from the base case.

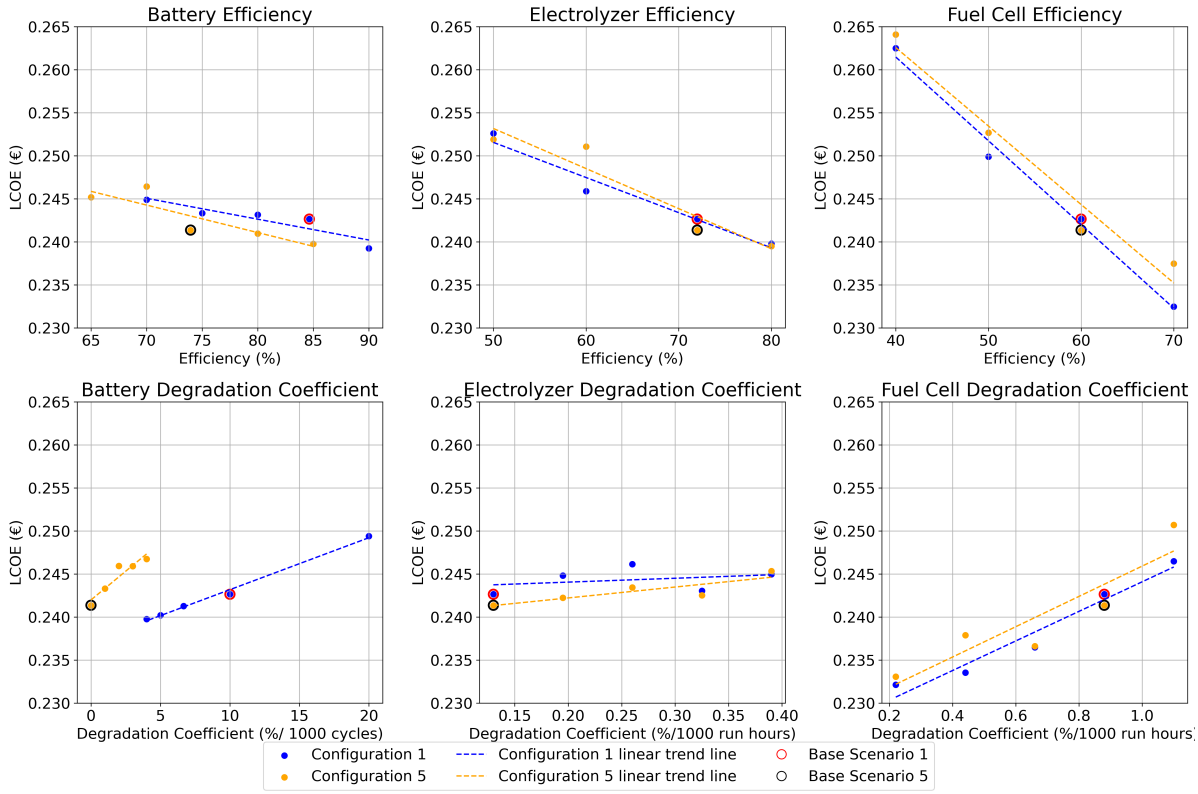

Figure 4.9: Sensitivity of Efficiency and Degradation Parameters in the Model for Configuration 1 and 5

4.3.4. Financial

This section analyzes the sensitivity of financial parameters, including the capital expenditure (CAPEX) of each asset, the annual operational expenditure (OPEX) for the connection, and the discount rate. Linear trendlines are used to make the impact more evident.

CAPEX

The CAPEX for solar and wind energy systems is analyzed, ranging from a 50% reduction to a 150% increase in price. The linear trendline in Figure 4.10 indicates that an increase in the price of wind energy has a greater impact on LCOE compared to solar energy. This is expected, as wind energy costs include a larger share of the total system cost. However, the influence of price increases is mitigated because when wind prices rise, the share of solar energy increases, and vice versa.

To analyze the effect of increasing the total energy price, the analysis considers a price increase from 0% to 200% for both solar and wind energy. This approach helps to understand the overall impact on energy costs and estimate the LCOE. In a 10-year simulation of the model, the average prices for wind and solar energy in configurations 1 and 5 are 0.05 €/kWh and 0.04 €/kWh, respectively. By doubling the investment cost of both assets, the energy price in the simulations is approximately 0.10 €/kWh. This is similar to the current PPA prices in the Dutch market [40]. This demonstrates how the LCOE is influenced when energy is purchased via a PPA for 0.10 €/kWh instead of being generated within the system. The analysis shows that a 200% increase in the price of wind and solar energy raises the LCOE from 0.24 €/kWh to 0.39 €/kWh. This emphasizes how the price of solar and wind contributes to the LCOE.

For the Li-ion battery, a price fluctuation range of -25% to 75% is considered to evaluate the impact on LCOE. Despite the low price used in this study compared to other studies, the price is sourced directly from a large-scale battery company, ensuring low uncertainty. However, it is important to examine the impact of potential price increases due to fluctuations in lithium material costs. For the VRFB in configuration 5, a range of -50% to 50% is used based on an average value from the literature. The

results indicate that the impact on LCOE is relatively low. If the price of the Li-ion battery increases by 75%, this results in an LCOE increase of 5%.

The price of the alkaline electrolyzer shows influence, especially in configuration 1, where the installed capacity and share of the electrolyzer contributes a larger portion to the total cost. In Figure 4.10, the price is varied from -25% to 75%. In configuration 1, the LCOE increases by 10% if the price of the electrolyzer increases by 75%.

The storage tank price fluctuates from -50% to 50%. In this research, an average value was used. Due to a larger storage tank in configuration 1, the influence on LCOE is greater in this configuration. The impact of a 50% price increase is an increase of 12% on the LCOE.

The impact on the LCOE of the PEM fuel cell is similar in both configurations because the installed capacity is approximately the same. If the price of the fuel cell increases by 75%, the LCOE increases by approximately 12%.

Overall, the sensitivity analysis of CAPEX indicates that energy price has a major impact on the LCOE due to its large share in the overall cost. While other assets also influence the LCOE, their impact is relatively minor. This is because a price increase in one asset typically results in a reduced installed capacity of that asset, leading to an increase in the capacity of other assets, which balances out the differences in LCOE. This interplay between assets helps to mitigate the impact of price fluctuations, maintaining a more stable LCOE.

OPEX and Discount Rate

This section examines the sensitivity of the connection price of the OPEX and the discount rate.

The annual connection cost per kW is also analyzed, as it accounts for approximately 8.7% to 10.7% of the total cost in every configuration. The connection cost is varied from -50% to 50%. The influence on LCOE is similar in both configurations because the connection size is consistent. Moreover, the connection prices of the different grid operators in the Netherlands are known. Therefore, the value is certain. If the connection cost increases by 50%, the LCOE increases by approximately 5%.

Lastly, the discount rate used in the model is 8%. The analysis varies the discount rate from 4% to 12%. The results show a major impact on LCOE, which was expected because the discount rate affects the value of money. The LCOE increases by 20% if the discount rate is increased to 12%

The sensitivity analysis of financial parameters shows that a component's influence on LCOE is directly proportional to its share of the total cost. For components with the highest price uncertainty, such as the battery, electrolyzer, storage tank, and fuel cell, the impact on LCOE is limited. Importantly, this analysis also provides insights into the LCOE when energy prices are doubled, reflecting current prices for energy purchased through a PPA. This finding underscores energy cost is the most influential financial parameter in system cost variability analysis.

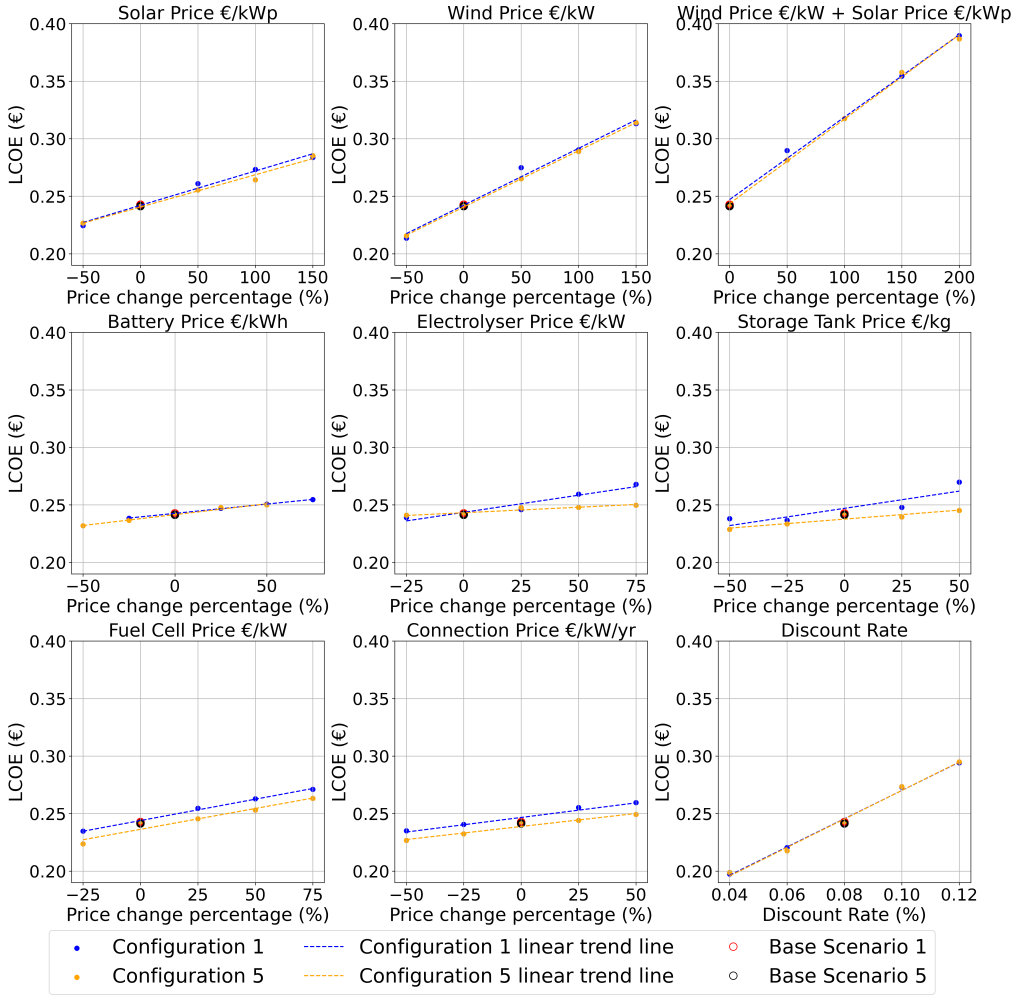

Figure 4.10: Sensitivity of CAPEX, OPEX, and Discount Rate for Configuration 1 and 5

5

Discussion

In this research, the LCOE for a data center that is 100% renewable on an hourly basis was determined. The main objective was to identify the most cost-efficient and feasible configuration for a data center in the Netherlands. A model of the energy system was developed, and a 10-year simulation was executed. During the 10-year simulation, the degradation of the components was analyzed. A cost analysis was performed based on the CAPEX, OPEX, replacement costs, and the remaining lifetime of the assets after the 10-year simulation. The cost analysis determined the LCOE of the energy systems. This analysis found that the LCOE is 0.241 €/kWh in Configuration 5 and 0.243 €/kWh in Configuration 1, making them the most cost-efficient and feasible configurations.

The environmental analysis of the two configurations with the lowest LCOE showed 0.037 kg CO_2e/kWh and 0.032 kg CO_2e/kWh, respectively. Configuration 1 requires 20 km², and Configuration 5 requires 21 km² of land. The land usage required for the on-site storage system is 0.063 km² for Configuration 1 and 0.033 km² for Configuration 5.

The sensitivity analysis showed that lowering the constraint to 80% reduces the LCOE to 0.12 €/kWh. The environmental analysis showed a 0.08 kg CO_2e/kWh, and the land usage was reduced to approximately 14 km². Additionally, using a different energy profile with a lower capacity factor has a high impact on the LCOE, potentially increasing the LCOE to 0.34 €/kWh. The CAPEX for wind and solar power and the discount rate influence the LCOE, which could increase to 0.39 €/kWh. In contrast, assets with high price uncertainty, such as batteries, electrolyzers, storage tanks, and fuel cells, had a limited impact on the LCOE. Moreover, the sensitivity of other efficiency and degradation parameters had a minor impact on the LCOE, with the fuel cell causing a maximum increase to an LCOE of 0.26 €/kWh.

5.1. Broader Perspective

The findings indicate that integrating renewable energy sources into data center operations results in an LCOE of 0.241 €/kWh. The price of 0.241 €/kWh closely aligns with the average EPEX price in 2022 of 0.242 €/kWh [124]. However, 2022 was an exceptional year for energy prices due to a rapid post-pandemic economic recovery and the Russian invasion of Ukraine in February 2022 [131]. This resulted in the highest oil prices since 2008. The price of 0.241 €/kWh was significantly higher than the prices in 2021 and 2023, which were 0.103 €/kWh and 0.096 €/kWh, respectively.

Although a data center with a capacity of 100 MW does not purchase energy at EPEX prices, it aligns closely with the LCOE when these prices increase due to global circumstances, such as in 2022. Additionally, the LCOE includes connection costs, which are additional to the EPEX price. However, this also shows that the price of a 100% renewable system is currently more than 2.5 times more expensive than the EPEX, but if 80% of the energy comes from renewable sources, the price decreases to 0.12 €/kWh, which is close to current EPEX prices.

This outcome of the 80% scenarios shows a more feasible and realistic value to implement in the

short term. Energy systems that manage 80% of the time using renewable energy for high-demand industries like data centers with a continuous load are affordable. The LCOE in this scenario suggests that other companies with continuous high energy demand, such as production companies, could also benefit from adopting similar energy systems to reduce their carbon footprint. This broader applicability highlights the potential for using more renewable energy for powering industries. However, the influence of the local energy profile and CAPEX prices of renewables needs to be considered. These factors can impact the overall LCOE.

The environmental analysis shows that the configuration emission is 0.037 kg CO_2/kWh, and for configuration 5, the emission is 0.032 kg CO_2/kWh. The average emissions on the Dutch grid were 0.27 kg CO_2/kWh in 2021 [132]. These values are much lower than the Dutch grid average, approximately 7 to 8 times less CO_2 emissions. It is important to consider that many storage components are manufactured or that the raw materials are mined in foreign countries such as South Africa and China, where the electricity grid mix results in much higher CO_2 emissions than in the Netherlands. The electricity used in manufacturing often contributes to the overall carbon emissions of these assets [93][97]. Despite this, the emissions from these configurations are still much lower than those from the Dutch energy grid and the electricity grids in these countries.

5.2. Renewable Energy Scenarios for a Data Center

Based on the research, the following scenarios could be discussed regarding the cost and feasibility of different renewable energy options compared to the current price for a data center:

Current Scenario: The current scenario uses a PPA. The price of the PPA is approximately 0.10 €/kWh, excluding the connection cost, which is an additional cost of approximately 0.01 €/kWh [40]. Because the PPA does not match hourly with renewable energy sources, only 60% of the time comes the energy directly from renewable sources [13][40]. This means that 40% of the time, energy from the grid is taken, which has high kg CO_2e/kWh. For this scenario, no additional land usage at the data center for an energy storage system is required, and no investment costs are required.

100% Renewable Scenario: For the 100% renewable scenario, configurations 1 and 5 are feasible and the most cost-effective solutions, with an LCOE of 0.243 €/kWh and 0.241 €/kWh. However, this cost is approximately 2.5 times higher than the current PPA. Moreover, for this scenario, a NPV of €1.4 bln is required over 10 years.

For both configurations, approximately 350-400 MWh of battery capacity, 80-110 MW of electrolyzer capacity, 260 tonnes of hydrogen storage, and an approximately 112 MW fuel cell are needed.

For configuration 1, the emissions are 0.037 kg CO_2e/kWh , and for configuration 5, they are 0.032 kg CO_2e/kWh. These values are 7-8 times lower than the average grid emissions, significantly reducing the data center's carbon footprint. The land usage requires more than 20 km² in addition to the size of the data centers. Onsite storage system area ranges between 33,000-63,000 m², depending on the battery type used. However, there are also some risks involved in this scenario. Implementing technologies such as alkaline electrolyzers and VRFBs in combination with intermittent energy sources poses a risk due to uncertain consequences of hydrogen systems in combination with renewables and immature VRFB technology, as discussed in section 5.4.

80% Renewable Scenario: The 80% renewable scenario aims for renewable energy usage 80% of the time. A suitable configuration for this scenario is configuration 1, with a Li-ion battery. The LCOE for this configuration is 0.12 €/kWh. This is approximately the same as the current PPA and the 0.01 €/kWh additional cost for the connection. However, for this scenario, an NPV of €725 mln over 10 years is required. In this configuration, renewable energy technologies and Li-ion battery technologies are reliable, and this will only improve, becoming cheaper and with less degradation. This configuration excludes hydrogen installation, consisting of an electrolyzer, storage tank, and fuel cell, or the VRFB, which excludes the risk of hydrogen system combined with renewables and the infancy of VRFB technology compared to the 100% renewable scenario.

Only onsite Li-ion battery installation with a capacity of 144 MWh is required. The CO_2 emissions are around 0.08 kg CO_2e/kWh, which is three times less than the emissions from the grid. Moreover, wind energy usage is reduced by 20%, but still, 12 km² is needed, and for solar PV, it is reduced by 50% to

2.4 km² compared to the 100% scenario of configuration 1. The onsite battery installation requires an additional 10,000 m², which is less than a quarter of the size of a 100 MW data center, typically around 46,000 m² [133]. For this scenario, investing in offshore wind farms is also recommended due to the higher capacity factor and a designated area to build large offshore wind farms, as further discussed in section 5.3.

Therefore, for a data center, a good option is to start with the 80% renewable scenario of configuration 1. This approach uses mature renewable sources and Li-ion battery technologies, which are reliable and exclude technologies with uncertainties and potential risks to the project. The price is approximately the same as the current PPA scenario. When prices of technologies decrease and the reliability of the hydrogen technologies and VRFB increases, transitioning to a 100% renewable scenario would become feasible and attractive for a data center. This transition is easy to implement because the system only needs to expand.

However, the scenarios are compared to the current situation. In the coming year, the current situation will change. The energy price is expected to decrease due to the increase in the availability of renewable energy sources[40]. However, in the long term, prices will increase due to the expensive storage technologies needed to stabilize the grid when conventional energy sources are excluded. This uncertainty poses a risk for the business case of the data center. Therefore, further research on the influence of a flexible grid price on the data center would be interesting.

5.3. Policy Implications

This section discusses the implications of various policies for wind energy and other key policies, such as net metering and novel grid contracts like ATR85 and ATO. These policies are evaluated for their effects on investment, stimulation of technology development, and grid management.

To power the data center, approximately 300 MW of installed capacity of onshore wind is needed, around 15km2. However, the space for onshore wind can be used double. In the Netherlands, for example, wind turbines are placed on agricultural land due to the higher windspeed and fewer people living close to the turbines. However, the required space is still challenging onshore. Due to high population density, horizon pollution, and the impact on the surrounding nature, there is much resistance from local citizens. Therefore, permits and realization of the project take longer. To avoid the long process and resistance from the surrounding people, Offshore wind is a better option for several reasons. The first reason is that wind energy is expected to grow rapidly due to technical improvements and high wind speeds at sea [134]. Second, new offshore wind farms have a high capacity factor, resulting in a more continuous energy profile because the turbines operate more often at rated capacity. Third, the energy density is between 7 and 8 W/m² [135] [123]. Fourth, many new parks are planned or have designated locations reserved in the North Sea [122]. Therefore, focusing on offshore wind would be a more feasible solution. However, offshore wind is almost twice as expensive as onshore [136]. This could have a major impact on LCOE, up to a 50% increase. However, a higher capacity factor results in less installed capacity needed for wind, and due to a more constant wind output, a smaller storage system is required, which mitigates this increase.

Moreover, the main focus should be on supporting policies that incentivize energy storage systems. By stimulating the investment in these systems, more investments will be realized, leading to an increase in storage capacity and a reduction in technology costs. This reflects the recent decrease in renewable energy prices caused by global governmental funding and support. Continuing this support is crucial for sustained progress [137].

The first policy for energy storage systems is net metering, which allows households and small businesses to offset their electricity costs by feeding excess renewable energy back into the grid annually [138]. Although this policy is only for small businesses and households, it does not apply to large consumers, such as data centers. This policy can have negative consequences on investments in battery storage and energy storage markets. By not stimulating net metering, households, and small businesses are encouraged to invest in storage systems, stimulating market growth and reducing prices for these technologies.

The second policy for energy storage systems involves special connection contracts, such as the

nonfirm ATO and ATR 85 [139][140]. These novel contracts, introduced by the grid operators, provide benefits for energy storage systems, including batteries and electrolyzers [141]. They offer a 100% discount on contract capacity (C_{Contract}), as described in subsection 3.7.5. This offer is valid when the grid operator ensures the availability of the connection for 85% of the time. Grid operators created these innovations because they need to always reserve capacity to deliver the maximum capacity to all connected off-takers. However, this simultaneous peak demand rarely occurs. When it does, a day-ahead confirmation is provided that temporary off-take is not possible. This contract organizes the grid efficiently and reduces local congestion. These contracts make investments in batteries and electrolyzers more affordable, which stimulates the development of those technologies. This results in a price decrease in the technologies in the long term, which is beneficial for investment in an energy system for the data center. Moreover, it could save operational costs for the data center if the decision tree is adjusted for this type of contract. This research shows that such costs is around 10% of total costs, as described in subsection 3.7.5. Of this 10%, approximately 45% is C_{Contract}, which amounts to more than €60 mln of NPV during the 10-year simulation.

5.4. Technology Implications

This section discusses the technological implications of the configurations analyzed in the study. The focus is on evaluating the maturity, reliability, and performance of the assets.

Both wind and solar technologies are mature and reliable renewable energy sources. They are widely deployed globally and have proven performance and efficiency. Onshore wind technology has advanced to maximize electricity production per megawatt capacity, featuring larger turbines and rotor diameters[134]. Similarly, Li-ion batteries are widely used in various applications, and their performance and degradation are well understood due to the maturity of the technology [40]. In contrast, VRFB are mostly in the pilot phase, with fewer large-scale implementations. Although promising for long-duration energy storage, VRFBs require further development and long-term validation. The larger projects have not yet researched their end-of-life, so their implementation carries certain risks. For example, a large demonstration project of 10 MW/40 MWh in China went into operation in 2017 and has an expected lifetime of 20 years [142].

Both electrolyzer technologies have been developed and used for a long period. However, integrating intermittent renewable sources like wind and solar introduces new challenges, such as partial load and start-stop cycles, which can affect performance and degradation [129]. Despite potential benefits, start-stop operations in renewable energy plants are unavoidable due to the intermittent nature of solar and wind power. This stress can lead to catalyst degradation each time the alkaline electrolyzer system cycles [129][130]. As shown in subsection 4.1.1 and Table 4.3, the average stop-start cycle is approximately 1.2 daily cycles. During the 10-year simulation, in all configurations except Configuration 2, the alkaline electrolyzer does not exceed 7,500 start-stops, and the PEM electrolyzer does not exceed 10,000 start-stops, which are their maximum limits [29]. Only in Configuration 2 does the alkaline electrolyzer reach 7,515 start-stops. However, the stacks are replaced after the 10-year simulation. The PV and wind power plants often experience power fluctuations due to changing weather conditions. Smoothing effects are methods used to stabilize these fluctuations for consistent power output [129]. This aspect is not taken into account in this research. Moreover, the literature describes the performance of the electrolyzer based on constant profiles. Therefore, the parameters used may be optimistic. However, in the sensitivity analysis, increasing the degradation coefficient of the electrolyzer to approximately 0.4%/1000h results in an LCOE difference within 0.01€/kWh for configurations 1 and 5. For fuel cells, the degradation coefficient used in this report is based on intermittent energy output, in contrast with the electrolyzer coefficient [78].

5.5. Evaluation of Results from Similar Research

This section compares different studies on energy systems, focusing on LCOE and system configurations. The findings highlight the differences in cost-effectiveness between various systems.

The study by Marocco et al. focuses on off-grid systems in remote areas, using solar energy, batteries, and hydrogen, and finds an LCOE of 0.51 €/kWh with a system consisting of a Li-ion battery and alkaline electrolyzer [29]. Their most cost-effective solution uses the same electrolyzer but a different

battery type. The second configuration is identical. This study considers data centers with continuous high energy demand and solar and wind energy input. Combining solar and wind energy with a continuous load results in a much lower LCOE. The off-grid system has a less continuous load and a more intermittent energy profile, leading to a higher LCOE.

The study by Gnibga, Blavette, and Orgerie investigates two configurations for an energy system of a data center, one with only a battery energy storage system (BESS) and one with both a battery energy storage system and a hydrogen energy storage system (HESS). The BESS shows an LCOE of 1.12 $\$_{2023}$/kWh, while the combined BESS + HESS system has an LCOE of 0.45$\$_{2023}$/kWh. Both systems are solely powered by photovoltaic (PV) energy [20]. Despite the high energy losses in the HESS, the results indicate that a system relying only on batteries is not feasible.

When comparing these results to this research, it is evident that the combination of wind and PV provides a more stable and continuous energy profile, reducing the cost of storage systems. Furthermore, the prices of PV, batteries, and electrolyzers used in this research are lower than those in Gnibga, Blavette, and Orgerie, reflecting the ongoing decrease in the cost of these assets.

5.6. Improvements and Critique of the Methodology

This section highlights potential improvements and critiques of the methodology used in this research, the use of a single weather profile, the reliance on up-to-date financial and technical data, and the optimization approach. Potential limitations and areas for improvement are discussed to provide a comprehensive evaluation of the research methods.

In this study, a weather profile from 2019 is used for both wind and solar data. The capacity factor of the onshore wind profile is high because wake effects are not considered because the energy profile of a single turbine is used. Sensitivity analysis shows that different weather profiles have a major effect on the LCOE. Since only one weather profile is used, the entire system is optimized for the longest periods without wind and solar during 2019.

Moreover, in this research, the storage system's capacity is designed for the longest period with a shortage of solar and wind energy. On April 30, 2018, there was a shortage in the market due to insufficient wind and solar production [143]. The Dutch Weather Institute (KNMI) researched the weather from 1991 to 2020 and concluded that there are, on average, 13 days per year with minimal combined wind and solar energy [144]. They advise storing five times the daily load to prevent blackouts [145]. In this system, the storage capacity is slightly over two days, which is significantly lower than their recommendation. Therefore, it is interesting to investigate the influence of different weather profiles on the model's outcome. During periods without wind and solar, the grid operator buys energy from neighboring countries because weather events are local [143]. However, in systems like this, this is not feasible.

Regarding the difference in the advised storage capacity and the results from this research, the advice assumes annual production equals annual consumption. However, in this research, energy production is much higher than annual consumption. Therefore, the combination of solar and wind energy often provides a consistent baseload to power the data center due to the over-dimensioned installed capacity, resulting in a direct usage rate of over 80%. This reduces the needed storage capacity, making the difference in the advised storage capacity less critical.

Besides, due to over-dimensioning, 30-40% of the energy is curtailed. This is because the total generation exceeds the connection or storage capacities of batteries, or hydrogen storage is full. Consequently, renewable energy sources are curtailed. However, this energy could be sold and delivered back to the grid or to other industries, which is not considered. This could make the LCOE even lower.

Moreover, most of the financial and technical data for Li-ion batteries, alkaline and PEM electrolyzers, storage tanks, and PEM fuel cells are provided by the company Repowered [40]. Therefore, the prices of these assets are up-to-date, and their parameters are better known because these technologies are currently in use. In contrast, the data for other technologies are taken from existing literature, which may be more outdated. Although the sensitivity analysis showed that the parameters have a minor influence on the LCOE, it is important for the VRFB to further research technical parameters such as

degradation, efficiency, and cost components. This will ensure accurate performance evaluation of the model and decrease the chance of additional costs associated with unexpected failures. Additionally, CAPEX prices do not account for land costs. However, compared to the overall prices, this represents a minimal share. At the end of 2023, the average price for a hectare of land in the Netherlands was €93,100 [146]. This means the additional cost of onsite storage assets for a configuration requiring 6.3 hectares is approximately € 0.5 mln. This amount is negligible relative to the total cost. For wind and solar projects, the land can be double used, so that cost is not considered.

Furthermore, the optimization used in this study is designed to optimize the dimensions based on a step size of 10 kW/kWp or kWh, to save computation time. However, this approach does not always identify the most cost-effective option. This is due to two reasons. First, the objective function has multiple local minima where the optimization converges. However, the local minima are close to each other. Otherwise, it wouldn't converge because a swarm of 100 particles is used. Second, the termination criterion of a 0.0001 €/kWh difference between the objective function's new and old best outcomes is reached before finding the most cost-effective solution. Therefore, this approach sometimes results in the optimization converging to a local minimum close to the global minimum or stopping too soon. Multiple optimizations are run to mitigate this, and the results are compared. The multiple runs showed a significance of 0.001 as a result of the step size and the termination criteria. If multiple optimizations are close to the same minimum, the one with the lowest LCOE is chosen. Moreover, the variables are manually checked to see if they are close to the constraints, enhancing the robustness and significance of the optimization.

Lastly, in this research, the capacity density of the storage tank is self-determined based on simple assumptions and existing tanks. However, this could make the results less certain, but interesting for further investigation. Also, the capacity density of the wind chosen is much higher than in most literature. Often, the energy density onshore is around 2 W/m², considering a capacity factor of 0.33 [147][148][149]. This results in a capacity density of 6 W/m². However, Enevoldsen and Jacobson provides a more accurate method for determining the onshore capacity density [150].

5.7. Further Research

Based on the aspects discussed and the shortcomings identified in the literature, several recommendations can be made to improve and extend the research. These recommendations focus on areas where further research and development are needed.

Investigate the Impact of Intermittent Renewable Energy Input on Electrolyzer Performance: Research how intermittent energy inputs from renewable sources affect electrolyzer performance. Current literature mainly focuses on scenarios where electrolyzers operate under continuous load. However, the energy input is highly variable in systems where renewables are integrated. Understanding the effects of frequent on/off cycles and partial loads on electrolyzer performance and efficiency is crucial for optimizing their use in renewable energy systems.

In-Depth Research on Vanadium Redox Flow Batteries: A study on VRFB is essential. This research should focus on their technical parameters, limitations, degradation mechanisms, and cost components. Such research will help assess the reliability and feasibility of VRFBs for large-scale energy storage. This provides valuable and reliable data for potential investors and stakeholders interested in implementing this technology in their energy storage system.

Perform an Environmental Analysis of 300 Bar Storage Tanks: A detailed life cycle assessment of 300 bar storage tanks has not been conducted. Consequently, there is insufficient information on the emissions generated during their manufacturing. Despite positive outcomes from prior research, understanding the environmental impact of these tanks throughout their lifecycle is important for assessing hydrogen systems. Moreover, large-scale on-land hydrogen storage is not well described in the literature. It is interesting to investigate how a large-scale storage system should be set up, considering land usage, safety, and transport of hydrogen to and from the electrolyzer and fuel cells.

Optimize Electrolyzer Utilization and Explore Hydrogen Production for Grid Stability:

From this research, it can be concluded that the electrolyzer only operates 30% of the time. The rest of the time, the electrolyzer is turned off. An interesting research topic should be investigating the

potential for using the inactive hours of the electrolyzers to produce hydrogen. During these hours, additional hydrogen can be produced and transported to the future hydrogen backbone or surrounding industry [116]. This would allow continuous operations and may improve performance and reduce degradation. Additionally, producing hydrogen during inactive hours can reduce system costs and increase economic feasibility. Moreover, examining the effects of large-scale energy storage systems on local grids, focusing on congestion management, is important. Assess how these systems influence grid stability, curtailment, and overall performance.

Test Different Types of Fuel Cells for Cost and Performance Optimization: The PEM fuel cells significantly contribute to energy storage costs. Therefore, evaluating the performance of different types of fuel cells is crucial. In this research, the choice of a PEM fuel cell was fixed. However, there are many different types of fuel cells. An LCOE analysis can provide valuable insights for optimizing the assets of energy storage systems, potentially leading to cost reductions and performance improvements.

Investigate the Impact of Data Center Location on LCOE:

In this research, the Netherlands was chosen as a case study to evaluate the influence of weather conditions on the LCOE for data centers. It is recommended to further investigate how different geographic locations affect the LCOE, particularly in the context of a 100% renewable energy scenario. From the sensitivity analyses, it can be concluded that the influence of the weather profile has a major impact on the LCOE.

Explore the Impact of Battolyser Technology on Energy Systems: Investigate the potential benefits of Battolyser technology, which combines battery storage and electrolyzer functions. This dual-function technology could improve efficiency and cost-effectiveness within energy systems. Analyzing its impact on performance and LCOE can reveal significant advantages for energy storage solutions [151].

6

Conclusion

The main research question addressed in this thesis is: *What is the most feasible and cost-effective configuration for an energy system that enables a data center to utilize 100% renewable energy on an hourly basis, and what are the associated environmental impacts in terms of CO_2 emissions from production and land use requirements?*

To answer this question, eight configurations consisting of different combinations of storage technologies, electrolyzers, and renewable energy sources were investigated. The study examined Li-ion, lead-acid, VRFB, and zinc-bromide batteries, as well as alkaline and PEM electrolyzers, storage tanks, and PEM fuel cells, with solar and wind power as renewable sources. A model was developed to simulate the energy flow, performance, and financial and technical parameters of these components, optimizing their dimensions based on LCOE.

The findings indicate that configurations 5 and 1, which include VRFB or Li-ion batteries with an alkaline electrolyzer, storage tank, and PEM fuel cell, offer the most cost-effective solutions for a 100% renewable energy use on an hourly basis, with LCOEs of 0.241 and €0.243 €/kWh, respectively. Key insights from the research are summarized below:

- **Performance of the Assets**:
  - Curtailment ranged from 33% to 45%, with renewable energy use consistently exceeding 80%. Oversizing energy sources is more cost-effective than expanding energy storage.
  - Lead-acid batteries were unsuitable due to high degradation and costs. VRFBs outperformed zinc-bromide batteries.
  - Electrolyzers operated 2800-4300 hours per year, with no replacements needed except in configuration 4, with the lead-acid battery and the PEM electrolyzer. Moreover, Configurations Alkaline electrolyzers had a lower LCOE than PEM electrolyzers.
  - One fuel cell replacement was needed in every scenario, with configura requiring two. Fuel cells had the largest cost share among energy storage components.
- **Cost**:
  - The NPV of the total cost ranged from €1.4 bln to €1.6 bln over the 10-year simulation.
  - In configuration 1, the NPV of the total cost is €1.43 bln. The shares are: wind + solar 45.1%, battery 8.3%, electrolyzer 6.4%, storage tank 10.4%, fuel cell 19.1%, and connection 10.7%. Solar power dominated the energy share.
  - In configuration 5, the NPV of the total cost is €1.42 bln. The shares are: wind + solar 47.4%, battery 9.5%, electrolyzer 4.5%, storage tank 10.2%, fuel cell 18.9%, and connection 9.6%.
  - The CAPEX of VRFB is nearly double that of Li-ion batteries, but their overall cost per usable capacity is lower due to their longer lifespan and full capacity utilization.

- **Environmental Impact**:
  - Configurations 1 and 5 had CO_2 emissions of 0.038 kg and 0.033 kg per kWh, respectively, 7-8 times lower than the Dutch grid average.
  - Configuration 1 requires 20 km² and configuration 5 requires 21 km² of land. Onsite land usage is around 0.063 km² in Configuration 1 and 0.033 km² in Configuration 5 for the storage system.
- **Scenarios for the Data Center**:
  - The 80% renewable scenario, Only the Li-ion battery and renewable energy sources, has an LCOE of 0.12 €/kWh. However, it requires an NPV of €725 mln over 10 years.
  - It utilizes reliable, mature technologies like renewable energy and Li-ion batteries, making it more reliable with fewer potential risks compared to the 100% scenario. This is because hydrogen installation, when integrated with intermittent renewable sources, raises challenges such as partial load and start-stop cycles, which could affect performance. Moreover, VRFBs are promising for long-duration energy storage. However, they require further development and long-term validation.
  - CO_2 emissions are three times lower than grid emissions at around 0.08 kg CO_2/kWh.
  - The on-site land usage is reduced by 83%, and the total land usage required is 15 km², which is a reduction of 20% compared to the 100% renewable scenario.
- **Broader Applicability**:
  - The findings suggest that other high-energy-demand industries could also reduce their carbon footprint, indicating broader applicability for renewable energy technologies.
  - Expanding the use of renewable energy and storage technologies beyond the studied scenarios could provide significant environmental and economic benefits across various sectors.
- **Policy Implications**:
  - Supporting policies that incentivize energy storage systems are crucial for reducing the cost of these technologies.
  - Offshore wind is recommended. Despite this technology having a high cost that significantly influences the LCOE, its higher capacity factor and more constant wind supply reduce the need for extensive storage systems, partially offsetting the cost. Additionally, offshore designated locations make implementation more feasible by excluding the problems associated with permitting and realization.

In conclusion, the most cost-effective configuration for a data center to use 100% renewable energy on an hourly basis is a combination of Li-ion or VRFB batteries with an Alkaline Electrolyzer. Different energy profiles, CAPEX of wind and solar, and the discount rate are sensitive factors affecting the LCOE. However, the costs and technical parameters of other storage assets have a limited impact, showing the robustness of the energy system.

It is recommended first to implement the 80% renewable scenario with Li-ion batteries to reduce risks and uncertainties. This approach has a positive impact on CO_2 emissions and achieves an LCOE approximately the same as the current PPA. As technology prices decrease and reliability improves, transitioning to the 100% renewable scenario is advised. This approach balances cost, environmental impact, and technological reliability while paving the way for broader applications in other high-energy-demand industries.

References

[1] UNFCCC. *The Paris Agreement*. 2023. URL: https://unfccc.int/process-and-meetings/the-paris-agreement (visited on 12/12/2023).

[2] *Executive Summary – CO2 Emissions in 2023 – Analysis*. IEA. URL: https://www.iea.org/reports/co2-emissions-in-2023/executive-summary (visited on 04/03/2024).

[3] World Meteorological Organization (WMO). *United in Science Report: Climate Change Has Not Stopped for COVID19*. 2020. URL: https://www.unep.org/news-and-stories/press-release/united-science-report-climate-change-has-not-stopped-covid19 (visited on 12/12/2023).

[4] IEA. *Data Centres & Networks*. URL: https://www.iea.org/energy-system/buildings/data-centres-and-data-transmission-networks#tracking (visited on 11/30/2023).

[5] Martijn Koot and Fons Wijnhoven. "Usage Impact on Data Center Electricity Needs: A System Dynamic Forecasting Model". In: *Applied Energy* 291 (June 1, 2021), p. 116798. ISSN: 0306-2619. DOI: 10.1016/J.APENERGY.2021.116798.

[6] CBS and Rutger Woolthuis. *Elektriciteit Geleverd Aan Datacenters, 2017-2021*. 2022. URL: https://www.cbs.nl/nl-nl/maatwerk/2022/49/elektriciteit-geleverd-aan-datacenters-2017-2021 (visited on 12/12/2023).

[7] Chia Ming Wu, Ruay Shiung Chang, and Hsin Yu Chan. "A Green Energy-Efficient Scheduling Algorithm Using the DVFS Technique for Cloud Datacenters". In: *Future Generation Computer Systems* 37 (July 1, 2014), pp. 141–147. ISSN: 0167-739X. DOI: 10.1016/J.FUTURE.2013.06.009.

[8] Íñigo Goiri et al. "Matching Renewable Energy Supply and Demand in Green Datacenters". In: *Ad Hoc Networks* 25 (PB Feb. 1, 2015), pp. 520–534. ISSN: 1570-8705. DOI: 10.1016/J.ADHOC.2014.11.012.

[9] Sebastian Crisan et al. *Data Center Optimization Methodology to Maximize the Usage of Locally Produced Renewable Energy*. Apr. 14, 2015. DOI: 10.1109/SustainIT.2015.7101363.

[10] Urs Hölzl. *Meeting Our Match: Buying 100 Percent Renewable Energy*. Apr. 4, 2018. URL: https://blog.google/outreach-initiatives/environment/meeting-our-match-buying-100-percent-renewable-energy/ (visited on 12/28/2023).

[11] Vincent Xia. *When 100% Renewable Energy Doesn't Mean Zero Carbon | Stanford Doerr School of Sustainability*. May 19, 2019. URL: https://sustainability.stanford.edu/news/when-100-renewable-energy-doesnt-mean-zero-carbon (visited on 12/28/2023).

[12] Blake Matich. "24/7 Hourly Matching – a New Granular Phase of Renewable Energy Sourcing – Pv Magazine International". In: (Dec. 18, 2021). URL: https://www.pv-magazine.com/2021/12/18/the-weekend-read-24-7-hourly-matching-a-new-granular-phase-of-renewable-energy-sourcing/ (visited on 12/28/2023).

[13] Alix de Monts Diego et al. *Decarbonizing the Grid with 24/7 Clean Power Purchase Agreements | McKinsey*. May 11, 2022. URL: https://www.mckinsey.com/industries/electric-power-and-natural-gas/our-insights/decarbonizing-the-grid-with-24-7-clean-power-purchase-agreements (visited on 12/28/2023).

[14] Jean Marc Pierson et al. "Datazero: Datacenter with Zero Emission and Robust Management Using Renewable Energy". In: *IEEE Access* 7 (2019), pp. 103209–103230. ISSN: 21693536. DOI: 10.1109/ACCESS.2019.2930368.

[15] Maroua Haddad, Jean-Marc Nicod, and Marie-Cécile Marion-Péra. *Hydrogen Infrastructure: Data-Center Supply-Refueling Station Synergy*. Dec. 11, 2017. DOI: 10.1109/VPPC.2017.8330978.

[16] Maroua Haddad et al. *Stand-Alone Renewable Power System Scheduling for a Green Data-Center Using Integer Linear Programming Version 1*. Research Report. FEMTO-ST, Mar. 2019. URL: https://hal.science/hal-02081951 (visited on 03/12/2024).

[17] G. Rostirolla et al. "A Survey of Challenges and Solutions for the Integration of Renewable Energy in Datacenters". In: *Renewable and Sustainable Energy Reviews* 155 (Mar. 1, 2022), p. 111787. ISSN: 1364-0321. DOI: 10.1016/j.rser.2021.111787. URL: https://www.sciencedirect.com/science/article/pii/S136403212101056X (visited on 03/13/2024).

[18] Zachariah Iverson et al. "Optimal Design of Hybrid Renewable Energy Systems (HRES) Using Hydrogen Storage Technology for Data Center Applications". In: *Renewable Energy* 52 (Apr. 1, 2013), pp. 79–87. ISSN: 0960-1481. DOI: 10.1016/j.renene.2012.10.038. URL: https://www.sciencedirect.com/science/article/pii/S0960148112006830 (visited on 03/13/2024).

[19] Miguel Vasconcelos et al. "Optimal Sizing of a Globally Distributed Low Carbon Cloud Federation". In: *2023 IEEE/ACM 23rd International Symposium on Cluster, Cloud and Internet Computing (CCGrid)*. 2023 IEEE/ACM 23rd International Symposium on Cluster, Cloud and Internet Computing (CCGrid). Bangalore, India: IEEE, May 2023, pp. 203–215. ISBN: 9798350301199. DOI: 10.1109/CCGrid57682.2023.00028. URL: https://ieeexplore.ieee.org/document/10171555/ (visited on 03/13/2024).

[20] Wedan Gnibga, Anne Blavette, and Anne-Cecile Orgerie. "Renewable Energy in Data Centers: The Dilemma of Electrical Grid Dependency and Autonomy Costs". In: *IEEE Transactions on Sustainable Computing* PP (Jan. 1, 2023), pp. 1–13. DOI: 10.1109/TSUSC.2023.3307790.

[21] *Tariefbladen | Enexis Netbeheer*. URL: https://www.enexis.nl/zakelijk/aansluitingen/tarieven/tariefbladen (visited on 03/15/2024).

[22] *Tarieven grootzakelijk | Liander*. URL: https://www.liander.nl/grootzakelijk/tarieven (visited on 03/15/2024).

[23] *Tarieven Stedin*. Stedin. URL: https://www.stedin.net/zakelijk/betalingen-en-facturen/tarieven (visited on 03/15/2024).

[24] Abraham Alem Kebede et al. "Techno-Economic Analysis of Lithium-Ion and Lead-Acid Batteries in Stationary Energy Storage Application". In: *Journal of Energy Storage* 40 (Aug. 1, 2021), p. 102748. ISSN: 2352-152X. DOI: 10.1016/J.EST.2021.102748.

[25] K Mongird et al. "Energy Storage Technology and Cost Characterization Report". In: (). URL: https://www.energy.gov/sites/default/files/2019/07/f65/Storage%20Cost%20and%20Performance%20Characterization%20Report_Final.pdf.

[26] *What Is the Energy Content of Hydrogen?* Enapter. URL: https://www.enapter.com/kb_post/what-is-the-energy-content-of-hydrogen (visited on 03/16/2024).

[27] Tubagus Aryandi Gunawan et al. "At What Cost Can Renewable Hydrogen Offset Fossil Fuel Use in Ireland's Gas Network?" In: *Energies* 13.7 (7 Jan. 2020), p. 1798. ISSN: 1996-1073. DOI: 10.3390/en13071798. URL: https://www.mdpi.com/1996-1073/13/7/1798 (visited on 05/08/2024).

[28] Maider Santos and Iker Marino. "Energy Analysis of the Raggovidda Integrated System". In: (). URL: https://www.haeolus.eu/wp-content/uploads/2019/01/D5.1.pdf.

[29] Paolo Marocco et al. "Optimal Design of Stand-Alone Solutions Based on RES + Hydrogen Storage Feeding off-Grid Communities". In: *Energy Conversion and Management* 238 (June 2021), p. 114147. ISSN: 01968904. DOI: 10.1016/j.enconman.2021.114147. URL: https://linkinghub.elsevier.com/retrieve/pii/S019689042100323X (visited on 02/07/2024).

[30] Antoine Perrigot et al. "Technical Economic Analysis of PV-driven Electricity and Cold Cogeneration Systems Using Particle Swarm Optimization Algorithm". In: *Energy* 211 (Nov. 15, 2020), p. 119009. ISSN: 0360-5442. DOI: 10.1016/j.energy.2020.119009. URL: https://www.sciencedirect.com/science/article/pii/S0360544220321162 (visited on 02/07/2024).

[31] A. H. Elsheikh and M. Abd Elaziz. "Review on Applications of Particle Swarm Optimization in Solar Energy Systems". In: *International Journal of Environmental Science and Technology* 16.2 (Feb. 1, 2019), pp. 1159–1170. ISSN: 1735-2630. DOI: 10.1007/s13762-018-1970-x. URL: https://doi.org/10.1007/s13762-018-1970-x (visited on 02/19/2024).

[32] F. Fodhil, A. Hamidat, and O. Nadjemi. “Potential, Optimization and Sensitivity Analysis of Photovoltaic-Diesel-Battery Hybrid Energy System for Rural Electrification in Algeria”. In: *Energy* 169 (Feb. 15, 2019), pp. 613–624. ISSN: 0360-5442. DOI: 10.1016/J.ENERGY.2018.12.049.

[33] Shakti Singh, Prachi Chauhan, and Nirbhow Jap Singh. “Capacity Optimization of Grid Connected Solar/Fuel Cell Energy System Using Hybrid ABC-PSO Algorithm”. In: *International Journal of Hydrogen Energy* 45.16 (Mar. 20, 2020), pp. 10070–10088. ISSN: 0360-3199. DOI: 10.1016/J.IJHYDENE.2020.02.018.

[34] Dongshu Wang, Dapei Tan, and Lei Liu. “Particle Swarm Optimization Algorithm: An Overview”. In: *Soft Computing* 22.2 (Jan. 1, 2018), pp. 387–408. ISSN: 1433-7479. DOI: 10.1007/s00500-016-2474-6. URL: https://doi.org/10.1007/s00500-016-2474-6 (visited on 03/20/2024).

[35] C. Caballero L. Miranda J. Santillan and V. Bernabe-Loranca. *PySwarms: A Research Toolkit for Particle Swarm Optimization in Python*. manual. 2018. URL: https://pyswarms.readthedocs.io/en/latest/.

[36] Kenneth Hansen. “Decision-Making Based on Energy Costs: Comparing Levelized Cost of Energy and Energy System Costs”. In: *Energy Strategy Reviews* 24 (Apr. 1, 2019), pp. 68–82. ISSN: 2211-467X. DOI: 10.1016/J.ESR.2019.02.003.

[37] Vilayanur Viswanathan et al. “2022 Grid Energy Storage Technology Cost and Performance Assessment”. In: (2022). URL: https://www.pnnl.gov/sites/default/files/media/file/ESGC%20Cost%20Performance%20Report%202022%20PNNL-33283.pdf.

[38] Eurostat. *HICP - Annual Data (Average Index and Rate of Change)*. Apr. 17, 2024. DOI: 10.2908/PRC_HICP_AIND. URL: https://ec.europa.eu/eurostat/databrowser/view/prc_hicp_aind/default/table?lang=en&category=prc.prc_hicp.

[39] Board of Governors of the Federal Reserve System (US). *U.S. Dollars to Euro Spot Exchange Rate*. FRED, Federal Reserve Bank of St. Louis. Jan. 1, 1999. URL: https://fred.stlouisfed.org/series/AEXUSEU (visited on 04/18/2024).

[40] Jeroen Janssen. *Expert Judgment on Renewable Energy Projects*. Consultancy on Hydrogen, Batteries, and PV at Depowered and Repowered. 2024.

[41] N. Belmonte et al. “A Comparison of Energy Storage from Renewable Sources through Batteries and Fuel Cells: A Case Study in Turin, Italy”. In: *International Journal of Hydrogen Energy* 41.46 (Dec. 14, 2016), pp. 21427–21438. ISSN: 0360-3199. DOI: 10.1016/j.ijhydene.2016.07.260. URL: https://www.sciencedirect.com/science/article/pii/S0360319916323151 (visited on 05/30/2024).

[42] Md Mustafizur Rahman et al. “Assessment of Energy Storage Technologies: A Review”. In: *Energy Conversion and Management* 223 (Nov. 1, 2020), p. 113295. ISSN: 0196-8904. DOI: 10.1016/j.enconman.2020.113295. URL: https://www.sciencedirect.com/science/article/pii/S0196890420308347 (visited on 05/10/2024).

[43] *Classification of Energy Storage Technologies: An Overview*. Emerging Technology News. Oct. 21, 2020. URL: https://etn.news/energy-storage/classification-of-energy-storage-technologies-an-overview (visited on 05/10/2024).

[44] Léonard Wagner. “Chapter 27 - Overview of Energy Storage Technologies”. In: *Future Energy (Second Edition)*. Ed. by Trevor M. Letcher. Boston: Elsevier, Jan. 1, 2014, pp. 613–631. ISBN: 978-0-08-099424-6. DOI: 10.1016/B978-0-08-099424-6.00027-2. URL: https://www.sciencedirect.com/science/article/pii/B9780080994246000272 (visited on 03/15/2024).

[45] Andreas Poullikkas. “A Comparative Overview of Large-Scale Battery Systems for Electricity Storage”. In: *Renewable and Sustainable Energy Reviews* 27 (Nov. 1, 2013), pp. 778–788. ISSN: 1364-0321. DOI: 10.1016/j.rser.2013.07.017. URL: https://www.sciencedirect.com/science/article/pii/S1364032113004620 (visited on 05/16/2024).

[46] Ababay Ketema Worku et al. “Energy Storage Technologies; Recent Advances, Challenges, and Prospectives”. In: *Planning of Hybrid Renewable Energy Systems, Electric Vehicles and Microgrid: Modeling, Control and Optimization*. Ed. by Aashish Kumar Bohre et al. Singapore: Springer Nature, 2022, pp. 125–150. ISBN: 978-981-19097-9-5. DOI: 10.1007/978-981-19-0979-5_7. URL: https://doi.org/10.1007/978-981-19-0979-5_7 (visited on 05/10/2024).

[47] Abraham Alem Kebede et al. “A Comprehensive Review of Stationary Energy Storage Devices for Large Scale Renewable Energy Sources Grid Integration”. In: *Renewable and Sustainable Energy Reviews* 159 (May 1, 2022), p. 112213. ISSN: 1364-0321. DOI: 10.1016/j.rser.2022.112213. URL: https://www.sciencedirect.com/science/article/pii/S1364032122001368 (visited on 05/11/2024).

[48] “Chapter 2 - Technologies of Energy Storage Systems”. In: *Grid-Scale Energy Storage Systems and Applications*. Ed. by Fu-Bao Wu, Bo Yang, and Ji-Lei Ye. Academic Press, Jan. 1, 2019, pp. 17–56. ISBN: 978-0-12-815292-8. DOI: 10.1016/B978-0-12-815292-8.00002-2. URL: https://www.sciencedirect.com/science/article/pii/B9780128152928000022 (visited on 05/14/2024).

[49] Nikolaos Ntavarinos et al. “Assessment of Energy Storage Technologies for Case Studies with Increased Renewable Energy Penetration”. In: *Annals of Limnology and Oceanography* 4.1 (Sept. 30, 2019), pp. 001–014. DOI: 10.17352/alo.000007. URL: https://www.agriscigroup.us/articles/ALO-4-107.php (visited on 05/24/2024).

[50] M. Wagemaker. *Energy Storage in Batteries*. Lecture Slides for Course CH3222. Delft, Netherlands: Delft University of Technology, 2023.

[51] Xiayue Fan et al. “Battery Technologies for Grid-Level Large-Scale Electrical Energy Storage”. In: *Transactions of Tianjin University* 26 (Jan. 8, 2020). DOI: 10.1007/s12209-019-00231-w.

[52] Ghassan Zubi et al. “The Lithium-Ion Battery: State of the Art and Future Perspectives”. In: *Renewable and Sustainable Energy Reviews* 89 (June 1, 2018), pp. 292–308. ISSN: 1364-0321. DOI: 10.1016/J.RSER.2018.03.002.

[53] S. Ould Amrouche et al. “Overview of Energy Storage in Renewable Energy Systems”. In: *International Journal of Hydrogen Energy* 41.45 (Dec. 7, 2016), pp. 20914–20927. ISSN: 0360-3199. DOI: 10.1016/j.ijhydene.2016.06.243. URL: https://www.sciencedirect.com/science/article/pii/S0360319916309478 (visited on 05/10/2024).

[54] Christian Doetsch and Astrid Pohlig. “The Use of Flow Batteries in Storing Electricity for National Grids”. In: *Future Energy: Improved, Sustainable and Clean Options for Our Planet* (Jan. 1, 2020), pp. 263–277. DOI: 10.1016/B978-0-08-102886-5.00013-X.

[55] Bin Li and Jun Liu. “Progress and Directions in Low-Cost Redox-Flow Batteries for Large-Scale Energy Storage”. In: *National Science Review* 4.1 (Jan. 1, 2017), pp. 91–105. ISSN: 2053714X. DOI: 10.1093/NSR/NWW098.

[56] Petr Vanýsek and Vítězslav Novák. “Redox Flow Batteries as the Means for Energy Storage”. In: *Journal of Energy Storage* 13 (Oct. 1, 2017), pp. 435–441. ISSN: 2352-152X. DOI: 10.1016/J.EST.2017.07.028.

[57] Puiki Leung et al. “Progress in Redox Flow Batteries, Remaining Challenges and Their Applications in Energy Storage”. In: *RSC Advances* 2.27 (Oct. 8, 2012), pp. 10125–10156. ISSN: 2046-2069. DOI: 10.1039/C2RA21342G. URL: https://pubs.rsc.org/en/content/articlehtml/2012/ra/c2ra21342g (visited on 12/04/2023).

[58] Tianyu Li, Changkun Zhang, and Xianfeng Li. “Machine Learning for Flow Batteries: Opportunities and Challenges”. In: *Chemical Science* 13.17 (May 4, 2022), pp. 4740–4752. ISSN: 20416539. DOI: 10.1039/D2SC00291D. URL: https://pubs.rsc.org/en/content/articlehtml/2022/sc/d2sc00291d (visited on 12/18/2023).

[59] Zebo Huang et al. “Comprehensive Analysis of Critical Issues in All-Vanadium Redox Flow Battery”. In: *ACS Sustainable Chemistry and Engineering* 10.24 (June 20, 2022), pp. 7786–7810. ISSN: 21680485. DOI: 10.1021/ACSSUSCHEMENG.2C01372/ASSET/IMAGES/LARGE/SC2C01372_0006.JPEG. URL: https://pubs.acs.org/doi/full/10.1021/acssuschemeng.2c01372 (visited on 12/18/2023).

[60] Huamin Zhang, Wenjing Lu, and Xianfeng Li. “Progress and Perspectives of Flow Battery Technologies”. In: *Electrochemical Energy Reviews* 2.3 (Sept. 1, 2019), pp. 492–506. ISSN: 25208136. DOI: 10.1007/S41918-019-00047-1/FIGURES/13. URL: https://link.springer.com/article/10.1007/s41918-019-00047-1 (visited on 01/16/2024).

[61] Xiaoqiang Guo, Hengyi Zhu, and Shiqi Zhang. “Overview of Electrolyser and Hydrogen Production Power Supply from Industrial Perspective”. In: *International Journal of Hydrogen Energy* 49 (Jan. 2, 2024), pp. 1048–1059. ISSN: 0360-3199. DOI: 10.1016/j.ijhydene.2023.10.325. URL: https://www.sciencedirect.com/science/article/pii/S0360319923055362 (visited on 02/15/2024).

[62] Dishant Rathee. “Types of Electrolysers”. In: *CEF Explains* (July 2023). URL: https://www.ceew.in/cef/quick-reads/explains/types-of-electrolysers.

[63] Tom Smolinka, Emile Tabu Ojong, and Jürgen Garche. “Hydrogen Production from Renewable Energies—Electrolyzer Technologies”. In: *Electrochemical Energy Storage for Renewable Sources and Grid Balancing* (Jan. 1, 2015), pp. 103–128. DOI: 10.1016/B978-0-444-62616-5.00008-5.

[64] V. A. Martinez Lopez et al. “Dynamic Operation of Water Electrolyzers: A Review for Applications in Photovoltaic Systems Integration”. In: *Renewable and Sustainable Energy Reviews* 182 (Aug. 1, 2023), p. 113407. ISSN: 1364-0321. DOI: 10.1016/j.rser.2023.113407. URL: https://www.sciencedirect.com/science/article/pii/S1364032123002642 (visited on 06/20/2024).

[65] *Types of Fuel Cells*. Energy.gov. URL: https://www.energy.gov/eere/fuelcells/types-fuel-cells (visited on 06/20/2024).

[66] John Roach. “Hydrogen Fuel Cells Could Provide Emission-Free Backup Power at Datacenters, Microsoft Says”. In: *Microsoft News* (2024). URL: https://news.microsoft.com/source/features/sustainability/hydrogen-fuel-cells-could-provide-emission-free-backup-power-at-datacenters-microsoft-says/.

[67] M. A. Aminudin et al. “An Overview: Current Progress on Hydrogen Fuel Cell Vehicles”. In: *International Journal of Hydrogen Energy* 48.11 (Feb. 5, 2023), pp. 4371–4388. ISSN: 0360-3199. DOI: 10.1016/j.ijhydene.2022.10.156. URL: https://www.sciencedirect.com/science/article/pii/S0360319922048534 (visited on 06/20/2024).

[68] *Comparison of Fuel Cell Technologies*. Energy.gov. URL: https://www.energy.gov/eere/fuelcells/comparison-fuel-cell-technologies (visited on 06/20/2024).

[69] Kendall Mongird et al. “2020 Grid Energy Storage Technology Cost and Performance Assessment”. In: (2020). URL: https://www.pnnl.gov/sites/default/files/media/file/Final%20-%20ESGC%20Cost%20Performance%20Report%2012-11-2020.pdf.

[70] *Lead Acid Battery Downsides & Maintenance*. URL: https://www.powertechsystems.eu/home/tech-corner/lead-acid-battery-downsides/ (visited on 04/16/2024).

[71] *Lead Acid Battery Specification*. manual. 2024. URL: https://docs.rs-online.com/2fd3/0900766b80f593a4.pdf.

[72] *Technical Manual: Sealed Lead-Acid Batteries*. manual. 2024. URL: https://www.power-sonic.com/wp-content/uploads/2018/12/Technical-Manual.pdf.

[73] Michael Dieterle et al. “Life Cycle Assessment (LCA) for Flow Batteries: A Review of Methodological Decisions”. In: *Sustainable Energy Technologies and Assessments* 53 (Oct. 2022), p. 102457. ISSN: 22131388. DOI: 10.1016/j.seta.2022.102457. URL: https://linkinghub.elsevier.com/retrieve/pii/S2213138822005094 (visited on 05/14/2024).

[74] *E22 250kW Vanadium Redox Flow Battery Datasheet*. manual. 2024. URL: https://energystoragesolutions.com/documents/Datasheet-E22-250kW.pdf.

[75] Øystein Ulleberg. “Modeling of Advanced Alkaline Electrolyzers: A System Simulation Approach”. In: *International Journal of Hydrogen Energy* 28.1 (Jan. 1, 2003), pp. 21–33. ISSN: 0360-3199. DOI: 10.1016/S0360-3199(02)00033-2. URL: https://www.sciencedirect.com/science/article/pii/S0360319902000332 (visited on 02/14/2024).

[76] Philipp Lettenmeier. *Efficiency Electrolysis*. Siemenens Energy Globak GmbH & Co. KG, 2020.

[77] Joakim Andersson and Stefan Grönkvist. “Large-Scale Storage of Hydrogen”. In: *International Journal of Hydrogen Energy* 44.23 (May 3, 2019), pp. 11901–11919. ISSN: 0360-3199. DOI: 10.1016/j.ijhydene.2019.03.063. URL: https://www.sciencedirect.com/science/article/pii/S0360319919310195 (visited on 06/15/2024).

[78] Rok Stropnik et al. “The Influence of Degradation Effects in Proton Exchange Membrane Fuel Cells on Life Cycle Assessment Modelling and Environmental Impact Indicators”. In: *International Journal of Hydrogen Energy*. Hydrogen Society 47.57 (July 5, 2022), pp. 24223–24241. ISSN: 0360-3199. DOI: 10.1016/j.ijhydene.2022.04.011. URL: https://www.sciencedirect.com/science/article/pii/S0360319922014768 (visited on 04/15/2024).

[79] IRENA. “Renewable Power Generation Costs in 2022”. In: (2022). URL: https://www.irena.org/-/media/Files/IRENA/Agency/Publication/2023/Aug/IRENA_Renewable_power_generation_costs_in_2022.pdf?rev=cccb713bf8294cc5bec3f870e1fa15c2.

[80] Paul Fabianek and Reinhard Madlener. “Techno-Economic Analysis and Optimal Sizing of Hybrid PV-wind Systems for Hydrogen Production by PEM Electrolysis in California and Northern Germany”. In: *International Journal of Hydrogen Energy* (Dec. 19, 2023). ISSN: 0360-3199. DOI: 10.1016/j.ijhydene.2023.11.196. URL: https://www.sciencedirect.com/science/article/pii/S0360319923059414 (visited on 03/22/2024).

[81] Stephanie Weckend, Andreas Wade, and Garvin Heath. *End of Life Management: Solar Photovoltaic Panels*. NREL/TP–6A20-73852, T12-06:2016, 1561525. June 1, 2016, NREL/TP–6A20-73852, T12–06:2016, 1561525. DOI: 10.2172/1561525. URL: https://www.osti.gov/servlets/purl/1561525/ (visited on 05/06/2024).

[82] *Turbine Lifetime Limits Require a Reality Check | News+ | IJGlobal*. URL: https://www.ijglobal.com/articles/157132/turbine-lifetime-limits-require-a-reality-check (visited on 05/06/2024).

[83] “Electricity Storage and Renewables: Costs and Markets to 2030”. In: (2030). URL: https://www.irena.org/-/media/Files/IRENA/Agency/Publication/2017/Oct/IRENA_Electricity_Storage_Costs_2017.pdf?rev=a264707cb8034a52b6f6123d5f1b1148.

[84] L. Tang et al. “Capital Cost Evaluation of Conventional and Emerging Redox Flow Batteries for Grid Storage Applications”. In: *Electrochimica Acta* 437 (Jan. 1, 2023), p. 141460. ISSN: 0013-4686. DOI: 10.1016/j.electacta.2022.141460. URL: https://www.sciencedirect.com/science/article/pii/S0013468622016176 (visited on 04/29/2024).

[85] S. Shiva Kumar and Hankwon Lim. “An Overview of Water Electrolysis Technologies for Green Hydrogen Production”. In: *Energy Reports* 8 (Nov. 1, 2022), pp. 13793–13813. ISSN: 2352-4847. DOI: 10.1016/J.EGYR.2022.10.127.

[86] Aliaksei Patonia and Rahmatallah Poudineh. *Cost-Competitive Green Hydrogen: How to Lower the Cost of Electrolysers?* Working Paper 47. OIES Paper: EL, 2022. URL: https://www.econstor.eu/handle/10419/253279 (visited on 05/07/2024).

[87] Junye Wang, Hualin Wang, and Yi Fan. “Techno-Economic Challenges of Fuel Cell Commercialization”. In: *Engineering* 4 (May 1, 2018), pp. 352–360. DOI: 10.1016/j.eng.2018.05.007.

[88] Davide Trapani et al. “The Potential of Hydrogen-Battery Storage Systems for a Sustainable Renewable-Based Electrification of Remote Islands in Norway”. In: *Journal of Energy Storage* 75 (Jan. 1, 2024), p. 109482. ISSN: 2352-152X. DOI: 10.1016/j.est.2023.109482. URL: https://www.sciencedirect.com/science/article/pii/S2352152X23028803 (visited on 02/08/2024).

[89] Romain Besseau et al. “Past, Present and Future Environmental Footprint of the Danish Wind Turbine Fleet with LCA_WIND_DK, an Online Interactive Platform”. In: *Renewable and Sustainable Energy Reviews* 108 (July 1, 2019), pp. 274–288. ISSN: 1364-0321. DOI: 10.1016/j.rser.2019.03.030. URL: https://www.sciencedirect.com/science/article/pii/S1364032119301704 (visited on 06/05/2024).

[90] Bastian Burger, Christian Bauer, and Paul Scherrer. “Ecoinvent Report No. 6-XIII”. In: (). URL: https://ecolo.org/documents/documents_in_english/Life-cycle-analysis-PSI-05.pdf.

[91] Amelie Müller et al. “A Comparative Life Cycle Assessment of Silicon PV Modules: Impact of Module Design, Manufacturing Location and Inventory”. In: *Solar Energy Materials and Solar Cells* 230 (Sept. 15, 2021), p. 111277. ISSN: 0927-0248. DOI: 10.1016/j.solmat.2021.111277. URL: https://www.sciencedirect.com/science/article/pii/S0927024821003202 (visited on 06/07/2024).

[92] Xin Lai et al. “Critical Review of Life Cycle Assessment of Lithium-Ion Batteries for Electric Vehicles: A Lifespan Perspective”. In: *eTransportation* 12 (May 2022), p. 100169. ISSN: 25901168. DOI: 10.1016/j.etran.2022.100169. URL: https://linkinghub.elsevier.com/retrieve/pii/S2590116822000157 (visited on 05/30/2024).

[93] *China - Countries & Regions*. IEA. URL: https://www.iea.org/countries/china (visited on 05/31/2024).

[94] Enoch Zhao et al. “Assessing the Life Cycle Cumulative Energy Demand and Greenhouse Gas Emissions of Lithium-Ion Batteries”. In: *Journal of Energy Storage* 43 (Nov. 2021), p. 103193. ISSN: 2352152X. DOI: 10.1016/j.est.2021.103193. URL: https://linkinghub.elsevier.com/retrieve/pii/S2352152X21008926 (visited on 05/30/2024).

[95] H. Bewi Komesse et al. “A Comprehensive Cradle-to-Grave Life Cycle Assessment of Three Representative Lithium-Ion Stationary Batteries Targeting a 20-Year Bi-Daily Charge–Discharge Service”. In: *The International Journal of Life Cycle Assessment* (Apr. 24, 2024). ISSN: 1614-7502. DOI: 10.1007/s11367-024-02303-z. URL: https://doi.org/10.1007/s11367-024-02303-z (visited on 06/12/2024).

[96] Thomas Le Varlet et al. “Comparative Life Cycle Assessment of Lithium-Ion Battery Chemistries for Residential Storage”. In: *Journal of Energy Storage* 28 (Apr. 1, 2020), p. 101230. ISSN: 2352-152X. DOI: 10.1016/j.est.2020.101230. URL: https://www.sciencedirect.com/science/article/pii/S2352152X19309880 (visited on 05/30/2024).

[97] Nick Blume et al. “Life Cycle Assessment of an Industrial□scale Vanadium Flow Battery”. In: *Journal of Industrial Ecology* 26 (Sept. 27, 2022). DOI: 10.1111/jiec.13328.

[98] Selina Weber et al. “Life Cycle Assessment of a Vanadium Redox Flow Battery”. In: *Environmental Science & Technology* 52.18 (Sept. 18, 2018), pp. 10864–10873. ISSN: 0013-936X. DOI: 10.1021/acs.est.8b02073. URL: https://doi.org/10.1021/acs.est.8b02073 (visited on 06/09/2024).

[99] “Front Matter”. In: *Flow Batteries*. Ed. by Christina Roth, Jens Noack, and Maria Skyllas□Kazacos. 1st ed. Wiley, Jan. 24, 2023. ISBN: 978-3-527-34922-7 978-3-527-83276-7. DOI: 10.1002/9783527832767.fmatter. URL: https://onlinelibrary.wiley.com/doi/10.1002/9783527832767.fmatter (visited on 06/13/2024).

[100] Haoyang He et al. “Flow Battery Production: Materials Selection and Environmental Impact”. In: *Journal of Cleaner Production* 269 (Oct. 2020), p. 121740. ISSN: 09596526. DOI: 10.1016/j.jclepro.2020.121740. URL: https://linkinghub.elsevier.com/retrieve/pii/S095965262031787X (visited on 06/13/2024).

[101] Muhammad Haider Ali Khan et al. “Strategies for Life Cycle Impact Reduction of Green Hydrogen Production – Influence of Electrolyser Value Chain Design”. In: *International Journal of Hydrogen Energy* 62 (Apr. 2024), pp. 769–782. ISSN: 03603199. DOI: 10.1016/j.ijhydene.2024.01.081. URL: https://linkinghub.elsevier.com/retrieve/pii/S0360319924000922 (visited on 06/07/2024).

[102] Amit Kumar Tripathi and K.A. Subramanian. “Comparative Life Cycle Energy and GHG Emissions Assessment of Green Hydrogen Production with Different Electrolysers and Solar Photovoltaics System”. In: *2022 IEEE North Karnataka Subsection Flagship International Conference (NKCon)*. 2022 IEEE North Karnataka Subsection Flagship International Conference (NKCon). Nov. 2022, pp. 1–9. DOI: 10.1109/NKCon56289.2022.10127022. URL: https://ieeexplore.ieee.org/abstract/document/10127022?casa_token=I8I0EMpyT94AAAAA:i9oh5N51bqGsB4qs5N1zt7MNu5NDMsHnL9PP2I6C2YcIIbPfUVUVgkKLzUHuVPKpOkIr17brpQ (visited on 06/14/2024).

[103] David Bionaz et al. “Life Cycle Environmental Analysis of a Hydrogen-Based Energy Storage System for Remote Applications”. In: *Energy Reports* 8 (Nov. 1, 2022), pp. 5080–5092. ISSN: 2352-4847. DOI: 10.1016/j.egyr.2022.03.181. URL: https://www.sciencedirect.com/science/article/pii/S2352484722007363 (visited on 06/18/2024).

[104] Mitja Mori et al. “Life-Cycle Assessment of a Hydrogen-Based Uninterruptible Power Supply System Using Renewable Energy”. In: *The International Journal of Life Cycle Assessment* 19.11 (Nov. 1, 2014), pp. 1810–1822. ISSN: 1614-7502. DOI: 10.1007/s11367-014-0790-6. URL: https://doi.org/10.1007/s11367-014-0790-6 (visited on 06/17/2024).

[105] Qian Cheng et al. “Review of Common Hydrogen Storage Tanks and Current Manufacturing Methods for Aluminium Alloy Tank Liners”. In: *International Journal of Lightweight Materials and Manufacture* 7.2 (Mar. 1, 2024), pp. 269–284. ISSN: 2588-8404. DOI: 10.1016/j.ijlmm.2023.08.002. URL: https://www.sciencedirect.com/science/article/pii/S2588840423000434 (visited on 06/17/2024).

[106] G. Kubilay Karayel, Nader Javani, and Ibrahim Dincer. “A Comprehensive Assessment of Energy Storage Options for Green Hydrogen”. In: *Energy Conversion and Management* 291 (Sept. 2023), p. 117311. ISSN: 01968904. DOI: 10.1016/j.enconman.2023.117311. URL: https://linkinghub.elsevier.com/retrieve/pii/S019689042300657X (visited on 06/08/2024).

[107] Alessandro Agostini et al. “Role of Hydrogen Tanks in the Life Cycle Assessment of Fuel Cell-Based Auxiliary Power Units”. In: *Applied Energy* 215 (Apr. 1, 2018), pp. 1–12. ISSN: 0306-2619. DOI: 10.1016/j.apenergy.2018.01.095. URL: https://www.sciencedirect.com/science/article/pii/S0306261918301090 (visited on 06/17/2024).

[108] Mitja Mori et al. “Life Cycle Sustainability Assessment of a Proton Exchange Membrane Fuel Cell Technology for Ecodesign Purposes”. In: *International Journal of Hydrogen Energy* 48.99 (Dec. 2023), pp. 39673–39689. ISSN: 03603199. DOI: 10.1016/j.ijhydene.2023.05.255. URL: https://linkinghub.elsevier.com/retrieve/pii/S0360319923026459 (visited on 06/08/2024).

[109] Rok Stropnik et al. “Life Cycle Assessment of 1kW PEMFC System with the Focus on Critical Materials”. In: *2019 7th International Youth Conference on Energy (IYCE)*. 2019 7th International Youth Conference on Energy (IYCE). July 2019, pp. 1–7. DOI: 10.1109/IYCE45807.2019.8991589. URL: https://ieeexplore.ieee.org/document/8991589 (visited on 06/08/2024).

[110] Peter Enevoldsen and Mark Z. Jacobson. “Data Investigation of Installed and Output Power Densities of Onshore and Offshore Wind Turbines Worldwide”. In: *Energy for Sustainable Development* 60 (Feb. 1, 2021), pp. 40–51. ISSN: 0973-0826. DOI: 10.1016/j.esd.2020.11.004. URL: https://www.sciencedirect.com/science/article/pii/S0973082620303367 (visited on 06/15/2024).

[111] *Zonnepark Fluitenberg - PowerField*. URL: https://www.powerfield.nl/locatie/zonnepark-fluitenberg/ (visited on 06/01/2024).

[112] *Omvang*. Zonnevelden Bunnik. URL: https://www.zonneveldenbunnik.nl/zonnevelden/omvang/ (visited on 06/01/2024).

[113] David Reber, Sam Jarvis, and Michael Marshak. “Beyond Energy Density: Flow Battery Design Driven by Safety and Location”. In: *Energy Advances* 2 (July 2023). DOI: 10.1039/D3YA00208J.

[114] RWE Benelux. *RWE Geeft Groen Licht Voor Grootschalig Batterijopslagproject in Eemshaven*. 2023. URL: https://benelux.rwe.com/pers/2023-09-21-rwe-geeft-groen-licht-voor-grootschalig-batterijopslagproject-in-eemshaven/#:~:text=Essen%20%2F%20Eemshaven%2C%2021%20september%202023&text=In%20totaal%20worden%20110%20kasten,miljoen%20euro%20in%20te%20investeren.

[115] Sinohyenergy. *100MW Green Hydrogen Plant*. 2024. URL: https://www.sinohyenergy.com/100mw-green-hydrogen-plant/.

[116] Gasunie. *Hydrogen Network*. 2024. URL: https://www.gasunie.nl/en/expertise/hydrogen/hydrogen-network.

[117] Port of Rotterdam. *Port of Rotterdam Authority Offers Site for Green Hydrogen Plant with a Capacity of up to 1 GW*. 2023. URL: https://www.portofrotterdam.com/en/news-and-press-releases/port-of-rotterdam-authority-site-green-hydrogen-plant-1GW.

[118] Arthur D. Little. *1 GW Electrolyzer: Analysis of Technology, Economic, and Market Developments*. 2020. URL: https://www.smartdeltaresources.com/sites/default/files/inline-files/ADL-1%20GW-Electrolyzer-FINALReport-EXTERNAL.pdf.

[119] ISPT. *Public Report Gigawatt Advanced Green Electrolyser Design*. 2021. URL: https://ispt.eu/media/Public-report-gigawatt-advanced-green-electrolyser-design.pdf.

[120] Sofoklis S. Makridis. "Hydrogen Storage and Compression". In: *Methane and Hydrogen for Energy Storage*. Ed. by Rupp Carriveau and David S-K. Ting. Institution of Engineering and Technology, July 27, 2016, pp. 1–28. ISBN: 978-1-78561-193-3 978-1-78561-194-0. DOI: 10.1049/PBPO101E_ch1. URL: https://digital-library.theiet.org/content/books/10.1049/pbpo101e_ch1 (visited on 06/01/2024).

[121] Container Container. *Shipping Container Dimensions*. 2024. URL: https://www.containercontainer.com/shipping-container-dimensions/#:~:text=Shipping%20containers%20and%20storage%20containers,foot%20to%20be%209ft%206%E2%80%9D.

[122] Rijksoverheid. *Waar Staan En Komen de Windparken Op Zee?* 2024. URL: https://windopzee.nl/onderwerpen/wind-zee/waar/.

[123] Wind op zee. *Windenergiegebied Hollandse Kust (West)*. June 2024. URL: https://windopzee.nl/imagemaps/kaart-waar-wanneer/hollandse-kust-west/.

[124] Jan Willem Zwang. *Terugblik 2023 En Verwachtingen 2024*. Dec. 30, 2023. URL: https://www.stratergy.nl/post/terugblik-2023-en-verwachtingen-2024 (visited on 06/08/2024).

[125] CO2emissiefactoren. *Jaarlijst 2023*. CO2emissiefactoren, 2023. URL: https://www.co2emissiefactoren.nl/wp-content/uploads/2023/04/Jaarlijst-2023-0304.pdf.

[126] CE Delft. *Emissiefactor Elektriciteit Fossiele Bronnen*. CE Delft, 2021. URL: https://www.rvo.nl/sites/default/files/2022-05/CE_Delft_210338_Emissiefactor_Elektriciteit_Fossiele_Bronnen_DEF.pdf.

[127] WindEurope. *The EU Built a Record 17 GW of New Wind Energy in 2023 - Wind Now 19 Percent of Electricity Production*. 2023. URL: https://windeurope.org/newsroom/press-releases/the-eu-built-a-record-17-gw-of-new-wind-energy-in-2023-wind-now-19-percent-of-electricity-production/#:~:text=The%20%E2%80%9Ccapacity%20factor%E2%80%9D%20of%20new,varies%20between%20different%20renewable%20technologies.

[128] Kuichao Ma et al. "Research on Evaluation Method of Wind Farm Wake Energy Efficiency Loss Based on SCADA Data Analysis". In: *Sustainability* 16.5 (5 Jan. 2024), p. 1813. ISSN: 2071-1050. DOI: 10.3390/su16051813. URL: https://www.mdpi.com/2071-1050/16/5/1813 (visited on 06/18/2024).

[129] Hirokazu Kojima et al. "Influence of Renewable Energy Power Fluctuations on Water Electrolysis for Green Hydrogen Production". In: *International Journal of Hydrogen Energy* 48.12 (Feb. 8, 2023), pp. 4572–4593. ISSN: 0360-3199. DOI: 10.1016/j.ijhydene.2022.11.018. URL: https://www.sciencedirect.com/science/article/pii/S0360319922052028 (visited on 06/18/2024).

[130] Ilham Ait-oujallal, Jamal Mabrouki, and Younes Abrouki. "The Effect of Renewable Energy Power Fluctuations on Water Electrolysis for Green Hydrogen Production". In: *Technical and Technological Solutions Towards a Sustainable Society and Circular Economy*. Ed. by Jamal Mabrouki and Azrour Mourade. Cham: Springer Nature Switzerland, 2024, pp. 413–425. ISBN: 978-3-031-56292-1. DOI: 10.1007/978-3-031-56292-1_33. URL: https://doi.org/10.1007/978-3-031-56292-1_33 (visited on 06/18/2024).

[131] International Energy Agency. *Global Energy Crisis*. 2024. URL: https://www.iea.org/topics/global-energy-crisis.

[132] *Rapportage CO2-uitstoot*. URL: https://klimaatmonitor.databank.nl/content/co2-uitstoot (visited on 06/09/2024).

[133] Research and Markets. *Global Data Centre Trends 2022 to 2026*. Accessed: 2024-07-01. 2022. URL: https://www.researchandmarkets.com/reports/5647291/global-data-centre-trends-2022-to-2026.

[134] International Energy Agency. *Wind Energy*. 2024. URL: https://www.iea.org/energy-system/renewables/wind.

[135] Noordzeeloket. *Hollandse Kust (Zuid) Wind Farm Zone Including Offshore Wind Farm Luchterduinen (LUD)*. June 2024. URL: https://www.noordzeeloket.nl/en/functions-and-use/offshore-wind-energy/free-passage-shared-use/full-tekst-video-shared-use-hollandse-kust-zuid/full-tekst-video-shared-use-hollandse-kust-zuid/.

[136] Statista. *Weighted Average Installed Cost for Offshore Wind Power Worldwide from 2010 to 2021*. Statista, 2024. URL: https://www.statista.com/statistics/506756/weighted-average-installed-cost-for-offshore-wind-power-worldwide/.

[137] Max Roser. "Why did renewables become so cheap so fast?" In: *Our World in Data* (Dec. 2020). URL: https://ourworldindata.org/cheap-renewables-growth.

[138] *Afbouw salderingsregeling voor kleinverbruikers (35.594)*. URL: https://www.eerstekamer.nl/wetsvoorstel/35594_afbouw_salderingsregeling?start_docList=50 (visited on 06/09/2024).

[139] Energy Storage NL. *ACM opent de deur voor Non-Firm ATO's (NFA 1.0)*. [Accessed: 26-Jun-2024]. 2024. URL: https://www.energystoragenl.nl/acm-opent-de-deur-voor-non-firm-atos-nfa-1-0/.

[140] Topsector Energie. *De ins- en outs van netcongestie en transportschaarste: Waar zit de ruimte voor innovatieve oplossingen?* [] 2024. URL: https://topsectorenergie.nl/nl/kennisbank/faq-de-ins-en-outs-van-netcongestie-en-transportschaarste-waar-zit-de-ruimte-voor-innovatieve-oplossingen/.

[141] Peter Oortmann. *Consultatie nieuwe alternatieve transportrechten (ATR85) geopend*. Energy Storage NL. Mar. 15, 2024. URL: https://www.energystoragenl.nl/consultatie-nieuwe-alternatieve-transportrechten-atr85-geopend/ (visited on 06/09/2024).

[142] Anuoluwapo Aluko and Andy Knight. "A Review on Vanadium Redox Flow Battery Storage Systems for Large-Scale Power Systems Application". In: *IEEE access : practical innovations, open solutions* 11 (2023), pp. 13773–13793. DOI: 10.1109/ACCESS.2023.3243800.

[143] NOS News. *Netbeheerder moest groot inkopen om stroomtekort op te vangen*. 2024. URL: https://nos.nl/artikel/2229787-netbeheerder-moest-groot-inkopen-om-stroomtekort-op-te-vangen.

[144] KNMI. *Dagen met weinig wind en zon*. Accessed: 2024-06-30. 2024. URL: https://www.knmi.nl/over-het-knmi/nieuws/dagen-met-weinig-wind-en-zon.

[145] Solar Magazine. *Klimaatscenario's KNMI: Mogelijk 13 dagen per jaar te weinig wind- en zonne-energie*. Accessed: 2024-06-30. 2024. URL: https://solarmagazine.nl/nieuws-zonne-energie/i24045/klimaatscenario-s-knmi-mogelijk-13-dagen-per-jaar-te-weinig-wind-en-zonne-energie.

[146] Kadaster. *Kwartaalbericht Agrarische Grondmarkt 2023-4*. 2023. URL: https://www.kadaster.nl/-/kwartaalbericht-agrarische-grondmarkt-2023-4#:~:text=De%20gemiddelde%20prijs%20van%20bouwland,(%E2%82%AC%2084.500%20per%20ha)..

[147] A.H.M. (Arno) Smets. *Wind Energy Potential - Sustainable Energy - TU Delft*. Lecture. Delft, Netherlands: Delft University of Technology, 2023.

[148] Lee M. Miller et al. "Two Methods for Estimating Limits to Large-Scale Wind Power Generation". In: *Proceedings of the National Academy of Sciences* 112.36 (Sept. 8, 2015), pp. 11169–11174. DOI: 10.1073/pnas.1408251112. URL: https://www.pnas.org/doi/abs/10.1073/pnas.1408251112 (visited on 06/15/2024).

[149] David J. C. MacKay. *Sustainable Energy - without the Hot Air*. Bloomsbury Publishing, 2016.

[150] Peter Enevoldsen and Mark Z. Jacobson. “Data Investigation of Installed and Output Power Densities of Onshore and Offshore Wind Turbines Worldwide”. In: *Energy for Sustainable Development* 60 (Feb. 1, 2021), pp. 40–51. ISSN: 0973-0826. DOI: 10.1016/j.esd.2020.11.004. URL: https://www.sciencedirect.com/science/article/pii/S0973082620303367 (visited on 06/01/2024).

[151] F. M. Mulder et al. “Efficient Electricity Storage with a Battolyser, an Integrated Ni–Fe Battery and Electrolyser”. In: *Energy & Environmental Science* 10.3 (Mar. 15, 2017), pp. 756–764. ISSN: 1754-5706. DOI: 10.1039/C6EE02923J. URL: https://pubs.rsc.org/en/content/articlehtml/2017/ee/c6ee02923j (visited on 12/28/2023).

Note: The author acknowledges the use of Grammarly and OpenAI for writing assistance and spelling correction. These tools were never used for content generation.

A

Cost overview

Table A.1: Costs for Configurations 1 to 4, Represented as the NPV of the 10-Year Simulation

Configuration	**1**	**2**	**3**	**4**
Solar CAPEX	€ 244,089,000	€ 260,948,000	€ 283,671,000	€ 296,132,000
Solar OPEX	€ 32,757,141	€ 35,019,646	€ 38,069,110	€ 39,741,396
Solar Replacement	€ -	€ -	€ -	€ -
Solar Residual Replacement	€ -98,602,361	€ -105,412,735	€ -114,591,933	€ -119,625,687
Solar Residual	€ -	€ -	€ -	€ -
Wind Capex	€ 482,160,000	€ 593,680,000	€ 501,840,000	€ 647,800,000
Wind OPEX	€ 161,766,642	€ 199,182,056	€ 168,369,362	€ 217,339,537
Wind Residual Replacement	€ -	€ -	€ -	€ -
Wind Replacement	€ -179,077,969	€ -220,497,363	€ -186,387,274	€ -240,597,952
Wind Residual	€ -	€ -	€ -	€ -
Battery CAPEX	€ 98,490,000	€ 0	€ 107,310,000	-
Battery OPEX	€ 26,974,527	€ 0	€ 29,390,157	-
Battery Replacement	€ 26,605,541	€ -	€ 24,852,647	-
Battery Residual	€ -15,589,164	€ -0	€ -16,985,209	-
Battery Residual Replacement	€ -18,349,459	€ -0	€ -24,852,647	-
Electrolyzer CAPEX	€ 87,210,000	€ 91,035,000	€ 126,100,000	€ 144,300,000
Electrolyzer OPEX	€ 11,703,724	€ 12,217,045	€ 16,922,825	€ 19,365,295
Electrolyzer Replacement	€ -	€ -	€ -	€ 54,807,833
Electrolyzer Residual	€ -7,730,098	€ -8,069,137	€ -7,185,356	€ -8,222,417
Electrolyzer Residual	€ -	€ -	€ -	€ -54,807,833
Storage Tank CAPEX	€ 186,200,000	€ 198,100,000	€ 175,700,000	€ 168,000,000
Storage Tank OPEX	€ 37,482,515	€ 39,878,014	€ 35,368,839	€ 33,818,810
Storage Replacement	€ -	€ -	€ -	€ -
Storage Residual	€ -75,217,481	€ -80,024,613	€ -70,975,893	€ -67,865,396
Storage Residual	€ -	€ -	€ -	€ -
Fuel Cell Capex	€ 226,000,000	€ 224,000,000	€ 226,000,000	€ 224,000,000
Fuel Cell OPEX	€ 30,329,568	€ 30,061,165	€ 30,329,568	€ 30,061,165
Fuel Replacement	€ 97,680,614	€ 204,964,782	€ 90,445,013	€ 112,926,397
Fuelcell Residual	€ -14,308,665	€ -14,182,040	€ -14,308,665	€ -14,182,040
Fuel Residual Replacement	€ -67,368,914	€ -83,004,273	€ -77,039,077	€ -32,018,699
Connection Cost	€ 153,006,946	€ 156,211,681	€ 150,122,685	€ 151,084,105
Total	€ 1,426,212,107	€ 1,534,107,230	€ 1,492,165,152	€ 1,602,056,513

Table A.2: Costs for Configurations 5 to 8, Represented as the NPV of the 10-Year Simulation

Configuration	**5**	**6**	**7**	**8**
Solar CAPEX	€ 265,346,000	€ 319,588,000	€ 318,122,000	€ 277,807,000
Solar OPEX	€ 35,609,865	€ 42,889,230	€ 42,692,490	€ 37,282,152
Solar Replacement	€ -	€ -	€ -	€ -
Solar Residual	€ -107,189,354	€ -129,100,989	€ -128,508,783	€ -112,223,108
Solar Residual replacement	€ -	€ -	€ -	€ -
Wind CAPEX	€ 495,280,000	€ 508,400,000	€ 487,080,000	€ 537,920,000
Wind OPEX	€ 166,168,456	€ 170,570,269	€ 163,417,322	€ 180,474,349
Wind Residual	€ -183,950,839	€ -188,823,709	€ -180,905,295	€ -199,787,666
Wind Replacement	€ -	€ -	€ -	€ -
Battery CAPEX	€ 161,820,000	€ 89,040,000	€ 186,465,000	€ 173,040,000
Battery OPEX	€ 24,518,637	€ 11,309,171	€ 28,252,798	€ 21,978,201
Battery Replacement	€ -	€ -	€ -	€ -
Battery Residual	€ -51,226,287	€ -28,186,804	€ -59,027,992	€ -54,778,129
Battery Residual Replacement	€ -	€ -	€ -	€ -
Electrolyzer CAPEX	€ 61,200,000	€ 71,910,000	€ 97,500,000	€ 102,700,000
Electrolyzer OPEX	€ 8,213,140	€ 9,650,439	€ 13,084,659	€ 13,782,507
Electrolyzer Replacement	€ -	€ -	€ -	€ -
Electrolyzer Residual	€ -5,424,630	€ -6,373,941	€ -5,555,687	€ -5,851,991
Electrolyzer Residual Replacement	€ -	€ -	€ -	€ -
Storage Tank CAPEX	€ 182,000,000	€ 175,700,000	€ 167,300,000	€ 170,800,000
Storage Tank OPEX	€ 36,637,044	€ 35,368,839	€ 33,677,899	€ 34,382,457
Storage Replacement	€ -	€ -	€ -	€ -
Storage Residual	€ -73,520,846	€ -70,975,894	€ -67,582,624	€ -68,996,486
Storage Residual Replacement	€ -	€ -	€ -	€ -
Fuel Cell CAPEX	€ 222,000,000	€ 230,000,000	€ 230,000,000	€ 230,000,000
Fuel Cell OPEX	€ 29,792,761	€ 30,866,374	€ 30,866,374	€ 30,866,374
Fuel Replacement	€ 95,951,754	€ 115,951,211	€ 92,045,810	€ 99,409,475
Fuel Cell Residual	€ -14,055,414	€ -14,561,916	€ -14,561,916	€ -14,561,916
Fuel Residual Replacement	€ -66,176,544	€ -32,876,343	€ -78,402,600	€ -68,561,284
Connection Cost	€ 135,701,378	€ 140,188,007	€ 144,193,925	€ 130,573,802
Total	€ 723,679,268	€ 1,480,531,945	€ 1,500,153,380	€ 1,516,255,737

B

Model validation

This chapter explains the steps to validate the model during its coding process. First, it explains the process of building and testing the assets. Then, it elaborates on how the assets were combined. This is followed by graphs and an explanation of how the degradation of components and their replacement were tested. Finally, the economic model and optimization validation are discussed.

Step 1: Validation of functions, Assets, and the energy flows

- The first step was to model all the assets separately. The different operations were first identified to model the assets. These are described in section 2.4.
- For the battery, these two operation modes were the discharge and charge operations. The two operations were modeled according to the formulas. After the operation modes were modeled, they were tested with different energy inputs and loads. The outcome of the model was checked using the formulas that are described.
- The same validation process was applied to the electrolyzer, hydrogen tank, and fuel cell. For the electrolyzer, there are three operational modes: off, partial load, and maximum load. The hydrogen storage tank has two modes: storing hydrogen and using hydrogen. The fuel cell also has three modes: off, partial load, and maximum load. Each of these modes is a separate function in the modeled class. These modes were checked using different inputs and loads to ensure the outcomes matched the formulas for different time steps.
- Once the assets were validated, they were combined into an energy system. Within this energy system, there is a decision tree. Using an input and an output, the sequence and order of the asset's usage were tested and validated.
- After testing the modes of each asset and their combinations within the energy system, the code was reviewed by employees of the company to ensure no mistakes were made.

Step 2: Validation of the Degradation and Replacement of the Assets

The second step involved validating degradation of the battery, electrolyzer, and fuel cell. The performance of these assets is modeled dynamically and decreases over time. Therefore, the model includes degradation parameters and replacement when the state of health (SOH) falls below a certain threshold.

Inputs and loads were applied to test the battery, electrolyzer, and fuel cell degradation. This time, instead of testing formulas at specific time steps, the performance was evaluated over a 10-year simulation period. Figures are made to show how the degradation coefficients (cycles/runtimes) influence the degradation of the assets and when replacements occur. The 10-year simulation results of the ”normal” degradation coefficient are displayed on the left, while the results with the degradation

coefficient multiplied by a factor of three are shown on the right.

Battery Degradation and Replacement:

Figures B.1, B.2, and B.3 show the cycles, replacement, and SOH of the battery. Under normal conditions, the battery is replaced after 2000 cycles when its SOH reaches 80%. The graph shows that this is in year 7. By increasing the degradation coefficient by 3, the battery lasts approximately 667 cycles, leading to three replacements over 10 years. This is shown in the figures and validates the dynamic model of battery degradation.

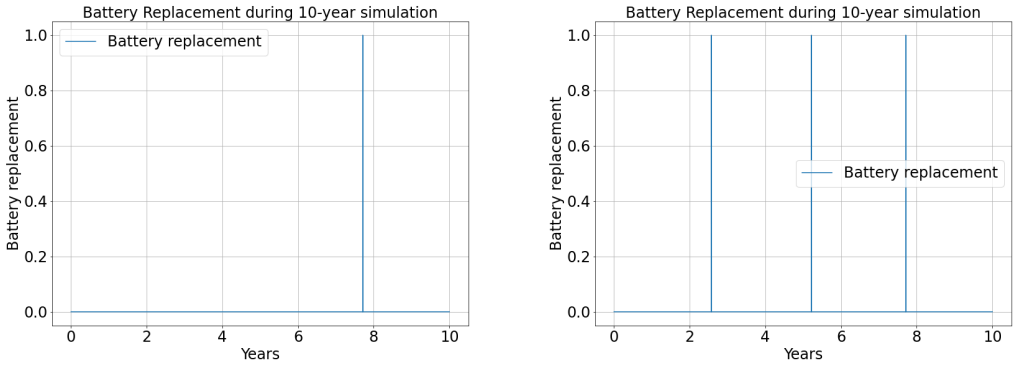

(a) Battery Replacement (normal) **(b)** Battery Replacement (degradation x 3)

Figure B.1: Comparison of Battery Replacement

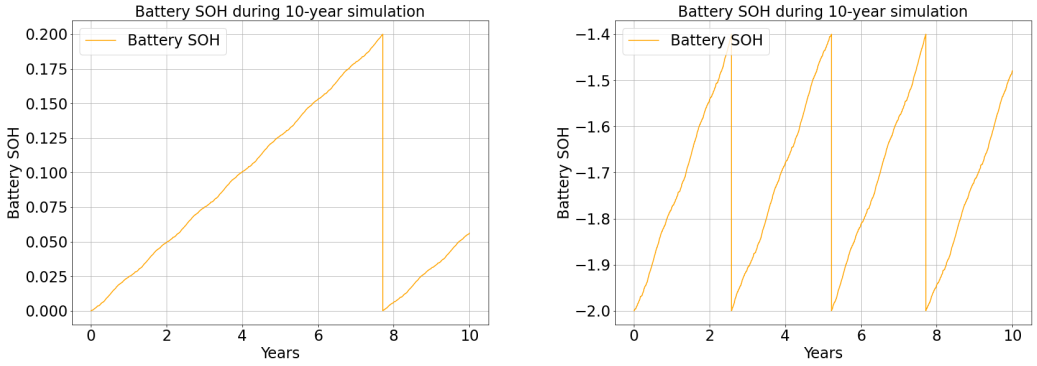

(a) Battery SOH (Normal) **(b)** Battery SOH (degradation x 3)

Figure B.2: Comparison of Battery SOH

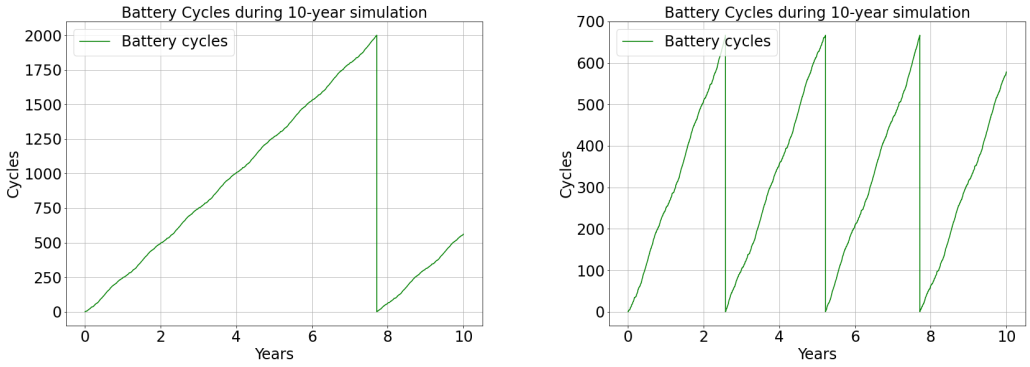

(a) Battery Cycles (Normal) **(b)** Battery Cycles (degradation x 3)

Figure B.3: Comparison of Battery Cycles

Electrolyzer Degradation and Replacement:

Similar to the battery, the electrolyzer's degradation was analyzed. Figures B.4, B.5, and B.6 show the degradation when the coefficient is increased from 0.13%/1000h to 0.39%/1000h, and the replacement occurs when SOH reaches 90%. In the standard case, the electrolyzer is not replaced within 10 years as it does not exceed 76,923 run hours. With increased degradation, it is replaced after 25,641 run hours, as shown in the figures.

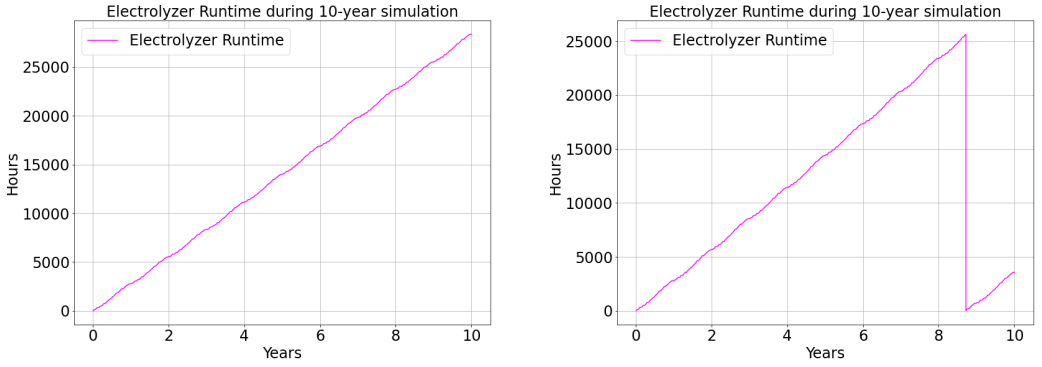

(a) Electrolyzer Runtime (Normal) **(b)** Electrolyzer Runtime (degradation x 3)

Figure B.4: Comparison of Electrolyzer Runtime

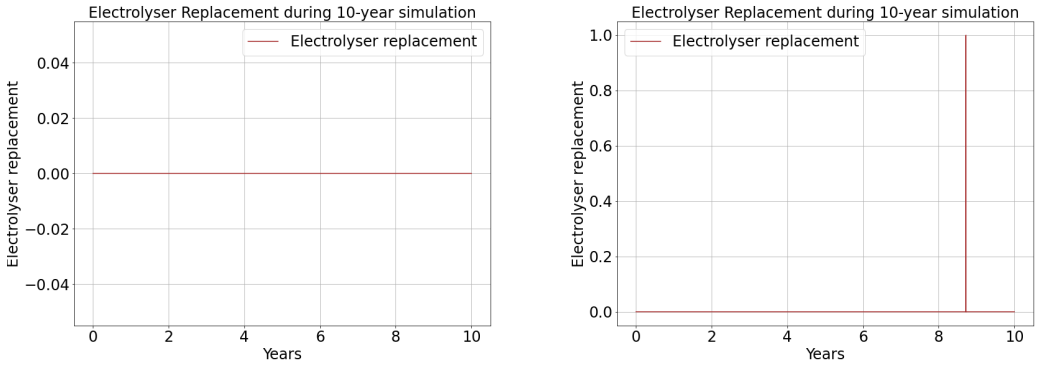

(a) Electrolyzer Replacement (Normal) **(b)** Electrolyzer Replacement (degradation x 3)

Figure B.5: Comparison of Electrolyzer Replacement

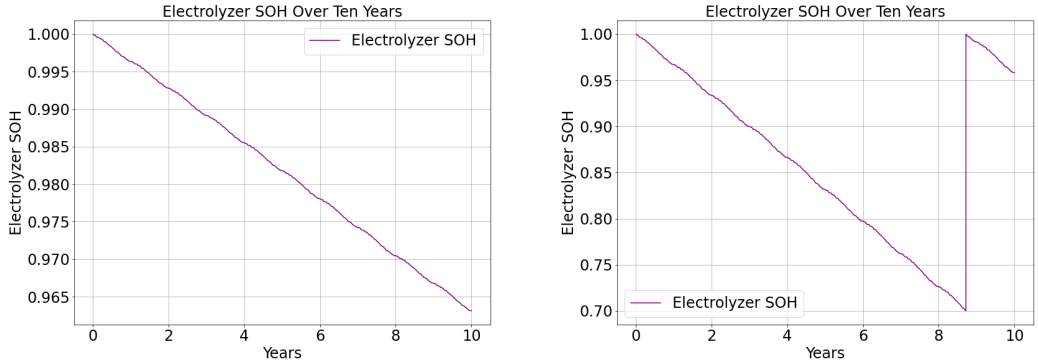

(a) Electrolyzer SOH (Normal) **(b)** Electrolyzer SOH (degradation x 3)

Figure B.6: Comparison of Electrolyzer SOH

Fuel Cell Degradation and Replacement:

The same method was applied to the fuel cell. The model uses a degradation coefficient of 0.88% per 1000 hours. Figures B.7, B.8, and B.9 show that the fuel cell is replaced after 11,363 run hours, occurring at the end of year 6. During the 10-year simulation, the fuel cell is replaced once. By increasing the degradation coefficient to 2.64% per 1000 hours, the fuel cell is replaced after 3787 hours. This validation confirms the dynamic model's accuracy for fuel cell degradation over time.

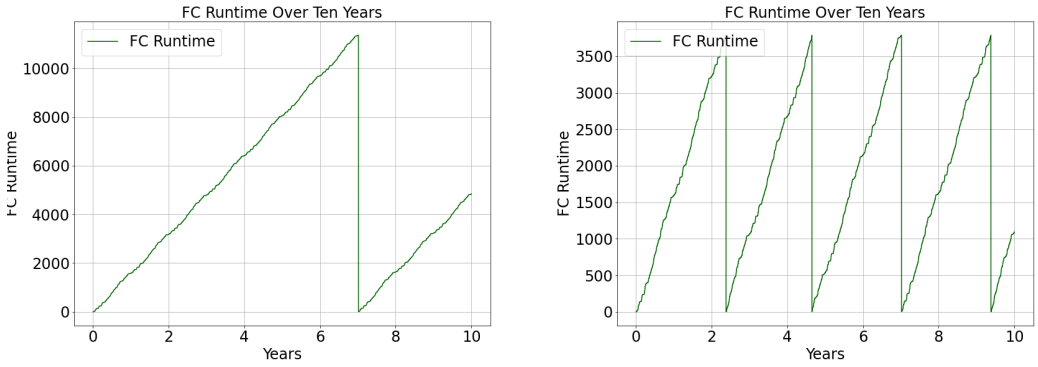

(a) FC Runtime (Normal) **(b)** FC Runtime (degradation x 3)

Figure B.7: Comparison of FC Runtime

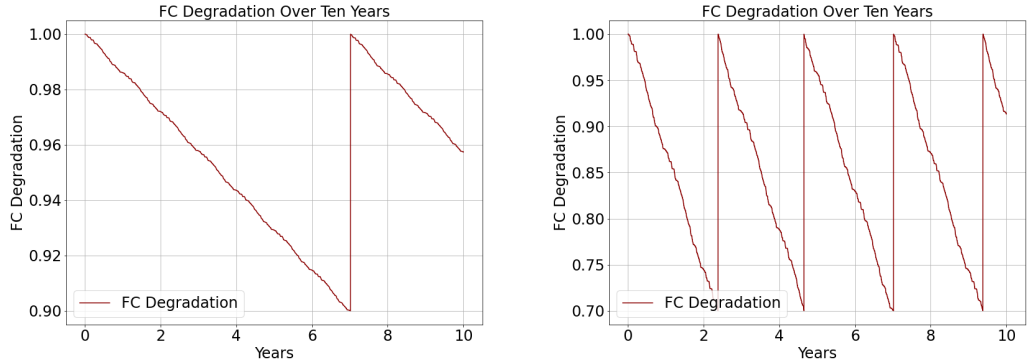

(a) FC Degradation (Normal) **(b)** FC Degradation (degradation x 3)

Figure B.8: Comparison of FC Degradation

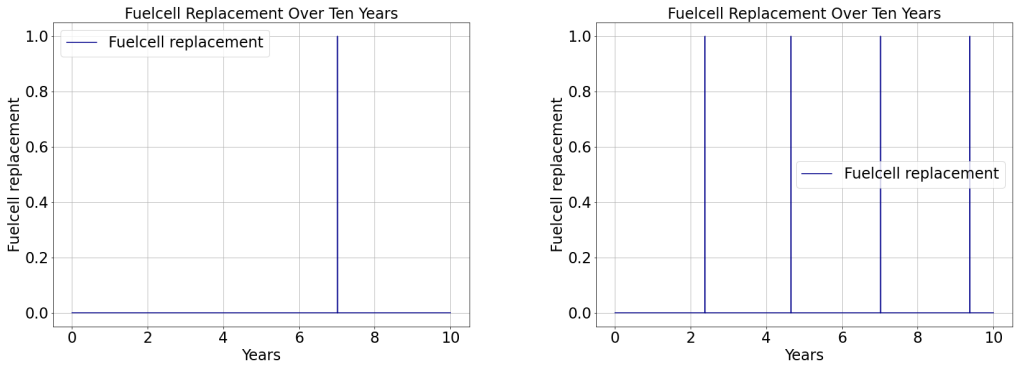

(a) Fuel Cell Replacement (Normal) **(b)** Fuel Cell Replacement (degradation x 3)

Figure B.9: Comparison of Fuel Cell Replacement

Step 3: Validation of the Economic Model

- First, the formulas for cost calculation were determined, as described in subsection 2.5.3.
- An Excel sheet was then created to calculate the costs based on these formulas. The Excel calculations were used to develop a Python class that performs the cost calculations.
- The economic model created in Python provides an overview based on the capacities and input parameters of CAPEX, OPEX, replacement costs, and lifetime.
- In Table B.1, the CAPEX costs assigned to year 0 and the discounted OPEX costs distributed across years 1 to 10 are shown. These outputs for CAPEX and OPEX costs are generated in Python.
- The discounted replacement costs of the assets in the respective years are shown in Table B.2. At the end of the period, the discounted residual values of the assets and the replaced components are calculated based on their remaining lifetime.
- Finally, Table B.3 provides a summary of the values in these tables. Based on these values, the total cost is determined, and by dividing this by the discounted total energy usage of the data center, the LCOE is calculated.
- The output files generated by Python matched the Excel sheet calculations, validating the model.

Table B.1: Discounted CAPEX and OPEX of Configuration 1 Over a 10-Year Simulation

Asset	Solar	Wind	Battery	Electrolyzer	Storage	Fuel Cell	Connection
Year 0	€ 244,089,000	€ 482,160,000	€ 98,490,000	€ 87,210,000	€ 186,200,000	€ 226,000,000	-
Year 1	€ 4,520,167	€ 22,322,222	€ 3,722,222	€ 1,615,000	€ 5,172,222	€ 4,185,185	€ 21,113,469
Year 2	€ 4,185,340	€ 20,668,724	€ 3,446,502	€ 1,495,370	€ 4,789,095	€ 3,875,171	€ 19,549,509
Year 3	€ 3,875,314	€ 19,137,708	€ 3,191,206	€ 1,384,602	€ 4,434,347	€ 3,588,122	€ 18,101,397
Year 4	€ 3,588,254	€ 17,720,100	€ 2,954,820	€ 1,282,039	€ 4,105,877	€ 3,322,335	€ 16,760,553
Year 5	€ 3,322,457	€ 16,407,500	€ 2,735,944	€ 1,187,073	€ 3,801,738	€ 3,076,236	€ 15,519,030
Year 6	€ 3,076,349	€ 15,192,129	€ 2,533,282	€ 1,099,142	€ 3,520,128	€ 2,848,367	€ 14,369,473
Year 7	€ 2,848,472	€ 14,066,786	€ 2,345,631	€ 1,017,724	€ 3,259,377	€ 2,637,377	€ 13,305,067
Year 8	€ 2,637,474	€ 13,024,802	€ 2,171,881	€ 942,337	€ 3,017,942	€ 2,442,015	€ 12,319,507
Year 9	€ 2,442,105	€ 12,060,002	€ 2,011,001	€ 872,534	€ 2,794,391	€ 2,261,125	€ 11,406,951
Year 10	€ 2,261,209	€ 11,166,669	€ 1,862,038	€ 807,902	€ 2,587,399	€ 2,093,635	€ 10,561,991
Residual System	-98,602,361	-179,077,969	-15,589,164	-7,730,098	-75,217,481	-14,308,665	-

Table B.2: Discounted Replacement and Residuals of Configuration 1 Over a 10-Year Simulation

Asset	Solar	Wind	Battery	Electrolyser	Storage	Fuel Cell	Connection
Year 0	-	-	-	-	-	-	-
Year 1	-	-	-	-	-	-	-
Year 2	-	-	-	-	-	-	-
Year 3	-	-	-	-	-	-	-
Year 4	-	-	-	-	-	-	-
Year 5	-	-	-	-	-	-	-
Year 6	-	-	-	-	-	-	-
Year 7	-	-	-	-	-	-	-
Year 8	-	-	€ 26,605,541	-	-	€ 97,680,614	-
Year 9	-	-	-	-	-	-	-
Year 10	-	-	-	-	-	-	-
Residual replacement	-	-	-18,349,459	-	-	-67,368,914	-

Table B.3: Summary of Discounted CAPEX, OPEX, Replacement Costs, Residual System Values, and Total Costs Over a 10-Year Simulation for Configuration 1

	CAPEX	OPEX	Replacement	Residual System	Residual Replacement	Total
Solar	€ 244,089,000	€ 32,757,141	-	-98,602,361	-	€ 178,243,780
Wind	€ 482,160,000	€ 161,766,642	-	-179,077,969	-	€ 464,848,673
Battery	€ 98,490,000	€ 26,974,527	€ 26,605,541	-15,589,164	-18,349,459	€ 118,131,445
Electrolyzer	€ 87,210,000	€ 11,703,724	-	-7,730,098	-	€ 91,183,626
Storage	€ 186,200,000	€ 37,482,515	-	-75,217,481	-	€ 148,465,034
Fuel Cell	€ 226,000,000	€ 30,329,568	€ 97,680,614	-14,308,665	-67,368,914	€ 272,332,603
Connection	-	€ 153,006,946	-	-	-	€ 153,006,946
Total cost						€ 1,426,212,107

Step 4: Validation of the Optimization

- The objective function is the LCOE, which is calculated after simulating 10 years of the energy model. The optimization executes a few hundred to a thousand iterations until the objective function value is found and the termination criteria are met, as described in section 2.5. The results of these optimizations were then validated by inputting the outcome of the optimization, the most cost-effective dimensions of the assets, into the energy model to ensure the same input and parameters were used. If the outcomes of the optimization and the model matched, the optimization results were considered valid.
- Additionally, the outcome of the optimization value needs to be tested. By performing multiple runs, the outcomes were compared. The results consistently fell within a 0.001 range of each other, demonstrating the reliability of the optimization process.
- Moreover, the optimization needs to be tested to determine if it finds the optimal solution or is close to the most cost-effective solution. By lowering the optimized dimensions one by one, it was checked whether the LCOE was lower than the optimization outcome and if the constraint of 100% renewable energy was met. If the constraint was not met or the LCOE was within the significance range, it indicated that the optimization had found the feasible boundary of the problem. This is shown in Figure B.10. The heatmap shows the effect on the LCOE when the parameters are decremented. In most cases, the LCOE is higher or equal to the optimized value. Moreover, Figure B.11 shows if the constraint of 100% renewable is met if the variables are decremented.

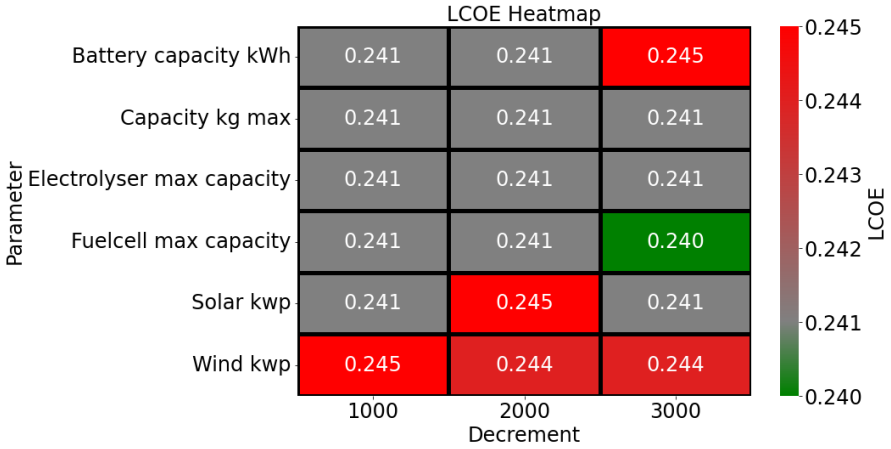

Figure B.10: Heatmap of the LCOE for Configuration 5 When the Variables Are Decremented

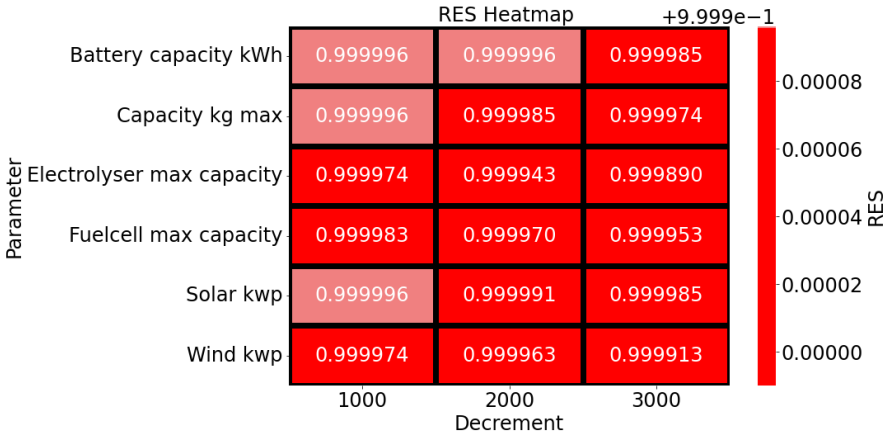

Figure B.11: Heatmap of the Percentage of Renewable Energy for Configuration 5 When the Variables Are Incremented